QA tests of the EGSnrc system and comparisons with EGS4 (Draft)

B.R.B. Walters, J. Treurniet, D.W.O. Rogers and I. Kawrakow
Ionizing Radiation Standards
National Research Council of Canada
Ottawa, K1A OR6

Printed: June 15, 2015
(last edited: 2001-04-04 14:38:49-04)
THIS IS STILL A DRAFT

NRCC Report PIRS-703

Abstract

The EGSnrc code system for Monte Carlo simulation of electron and photon transport in materials is benchmarked against a variety of calculations done using the EGS4 system. The purpose is two fold: (i) to ensure that EGSnrc is behaving as expected; (ii) to highlight some of the differences to be expected between the two codes.

This is an incomplete draft, and work is ongoing since a small change was made in the EGSnrc system after most of this work was done. There may be some small refinements still, but they should not be significant and we are releasing this draft now to avoid delaying the release of EGSnrc.

Contents

List of Figures

1 Introduction

This report compares results calculated with the EGSnrc code[**?**, **?**, **?**, **?**] to those calculated with EGS4/PRESTA[**?**, **?**, **?**]. In both cases a variety options is used to both demonstrate their effects and to explain why the various diffrences exist.

The first set of calculations is for a broad paralel beams of electrons on lead and water phatoms. Following this is a comparison of dose deposition from pencil beams of electrons on the same phantoms. This is followed by a study of bremsstrahlung emmision from lead and beryllium targets.

The report concludes with a few compariosns of calculated stopping-power ratios for water to air in electron beams incident on water phantoms.

In all cases, a broad range of energeis is used to explore how the changes affect different energy regions.

2 Introduction of SPIN option

In the middle of these QA tests, both multiple scattering and spin correction options were added to the code. To avoid re-running all of these calculations, a few spot-checks were performed to make sure the new version of EGSnrc with these options turned off produced the same data as the old version. 100 keV, 10MeV and 10GeV broad parallel beams were run for both water and lead phantoms. Figures **??** to **??** show that the SPIN=Off option is equivalent to the previous version of the EGSnrc code.

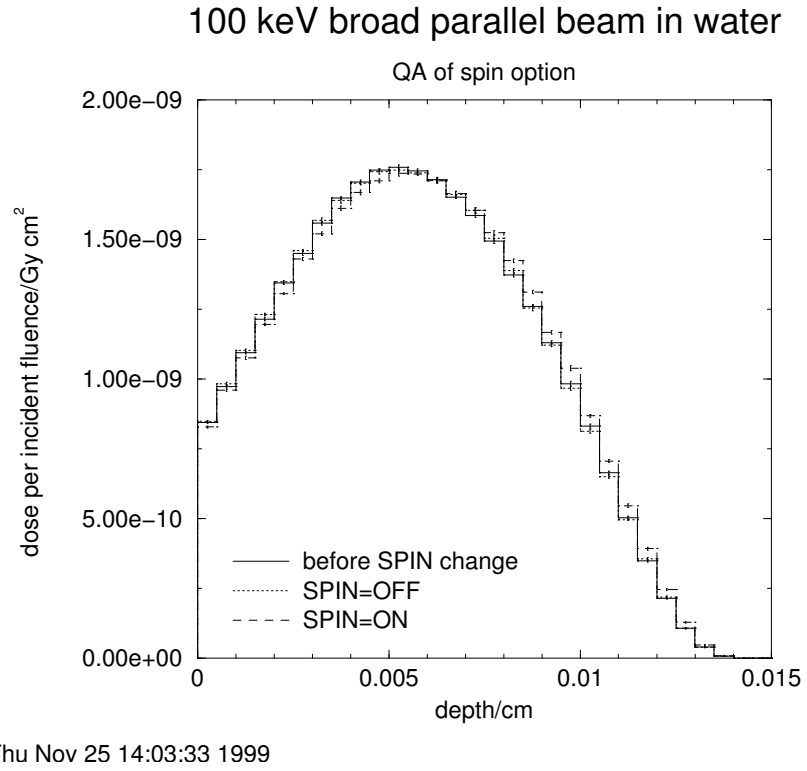

Figure 1: Depth-dose histogram for a 100 keV broad parallel beam in a water phantom.

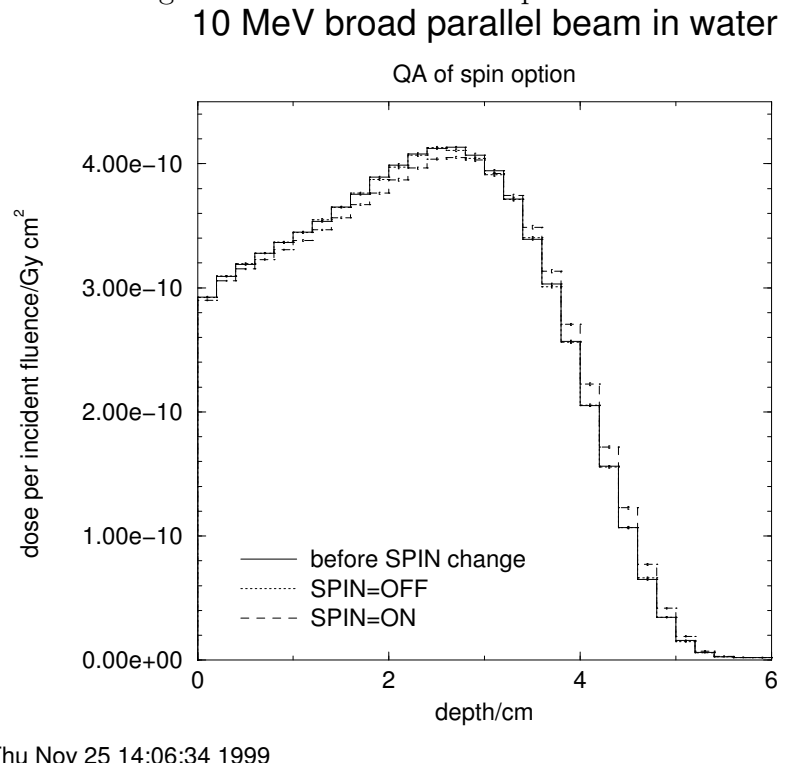

Figure 2: Depth-dose histogram for a 10 MeV broad parallel beam in a water phantom.

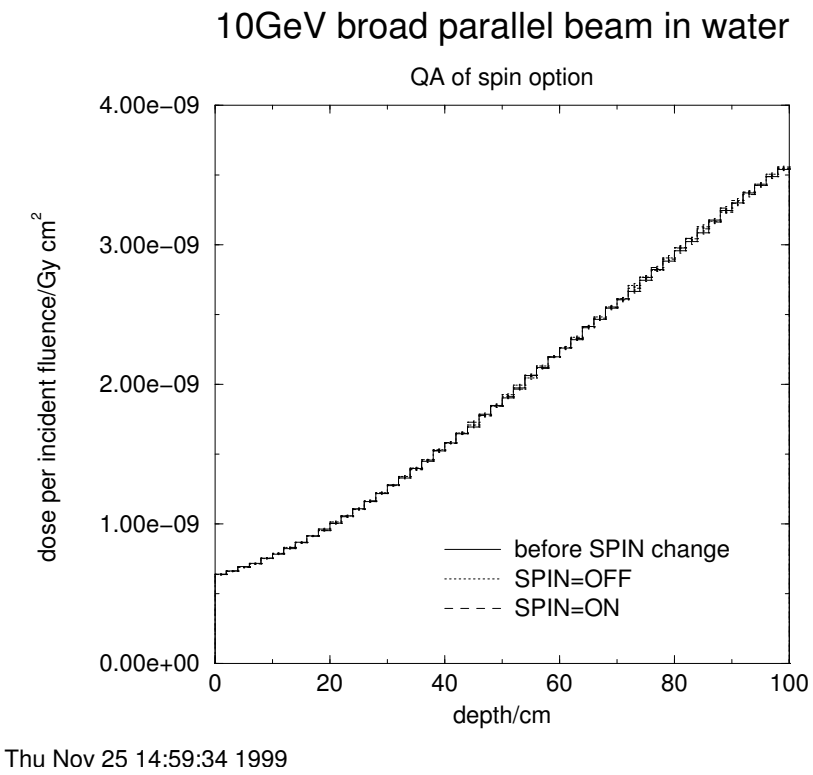

Figure 3: Depth-dose histogram for a 10 GeV broad parallel beam in a water phantom.

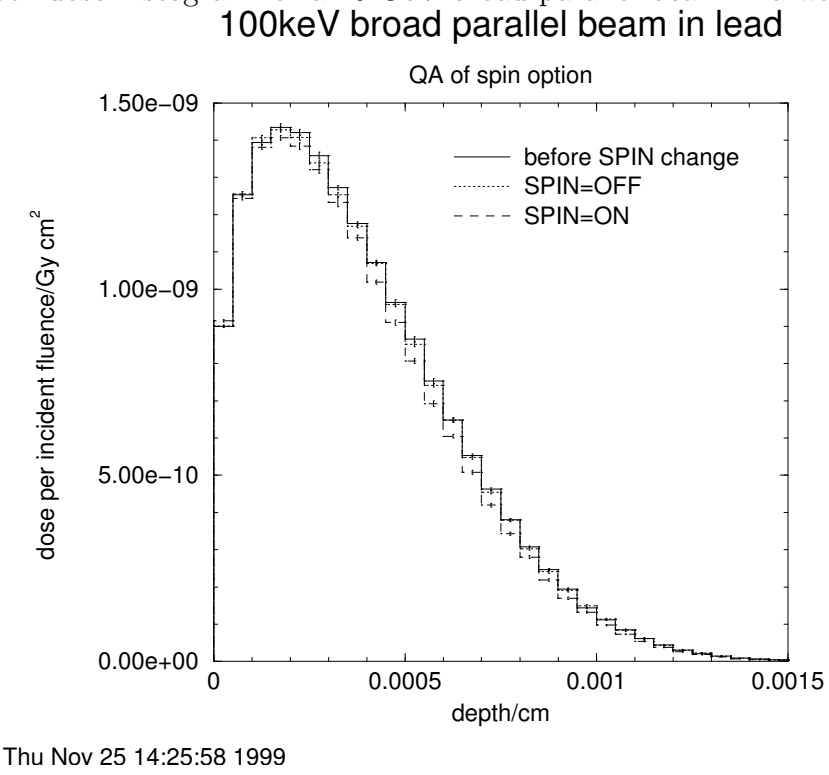

Figure 4: Depth-dose histogram for a 100 keV broad parallel beam in a lead phantom.

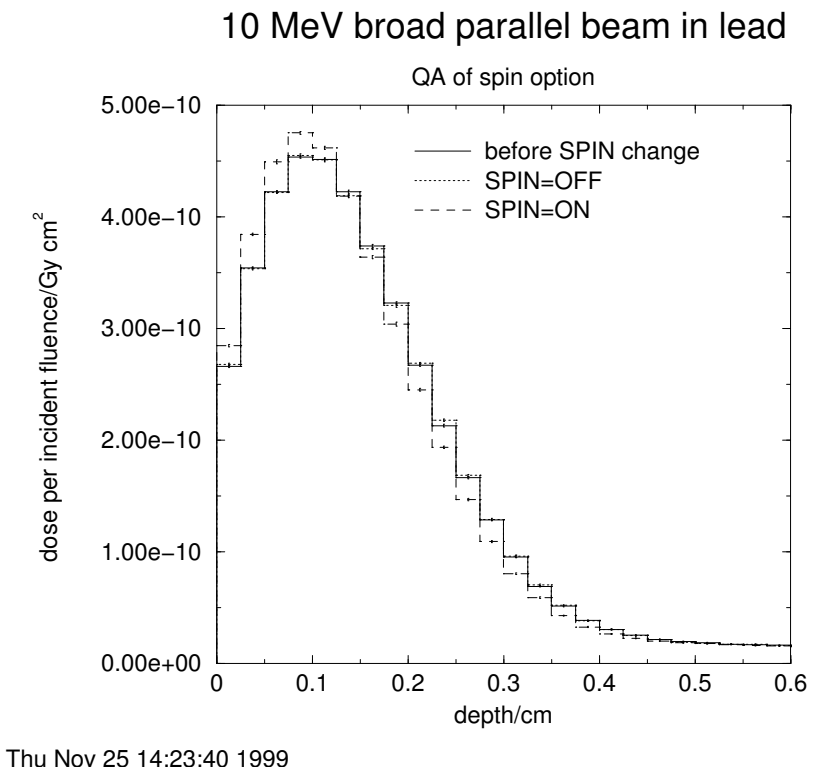

Figure 5: Depth-dose histogram for a 10 MeV broad parallel beam in a lead phantom.

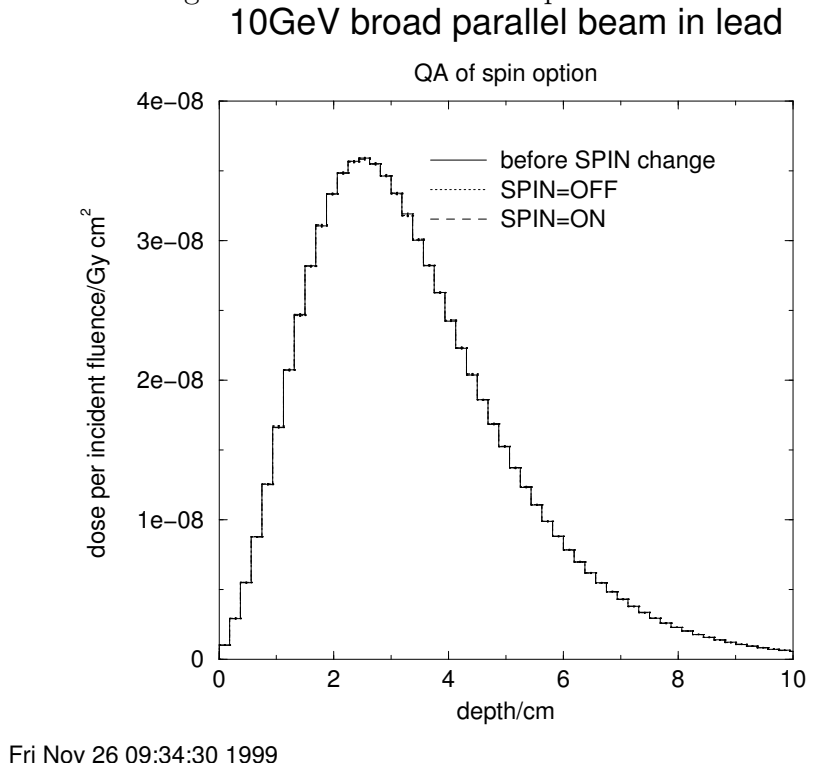

Figure 6: Depth-dose histogram for a 10 GeV broad parallel beam in a lead phantom.

3 Depth-dose curves for broad parallel beams

This section presents comparisons for broad parallel beams of electrons incident on water and then lead phantoms.

The calculations with DOSRZ are both done using PRESTA, in one case the default value of ESTEPE, and in the other case, a value thought to be close to optimum (1% for water, 0.3% for lead).

In the water case, the EGS4/PRESTA results are usually quite similar to each other and to the EGSnrc results with the SPIN=Off option. The SPIN=On case produces a slightly greater value of R_{50} for a given energy beam at lower energies but this becomes a negligible effect at higher energies. This is discussed further below in section **??**.

In the lead case, the same things hold true except that here the effect of the spin option is to decrease the value of R_{50} for a given energy.

3.1 Water phantom

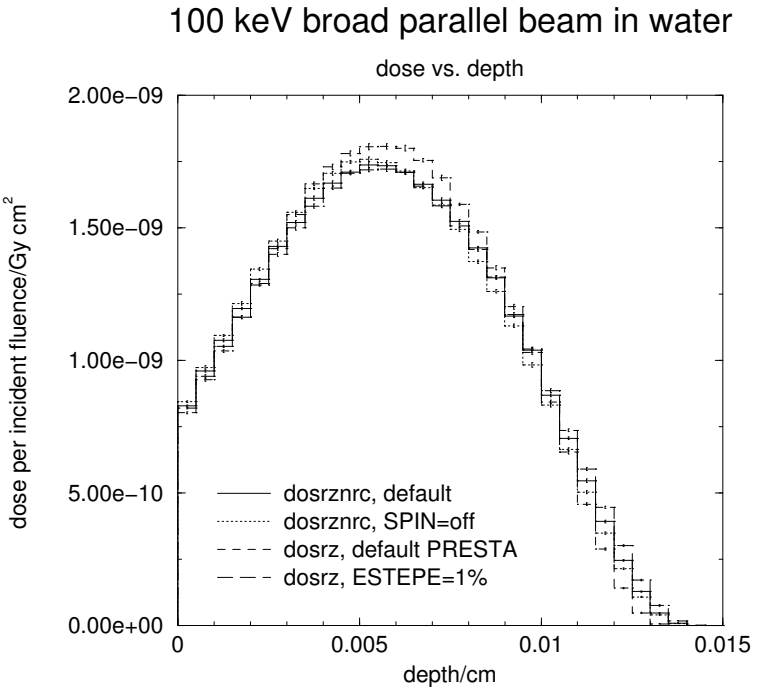

Figure 7: Depth-dose histogram for a 100 keV broad parallel beam in a water phantom.

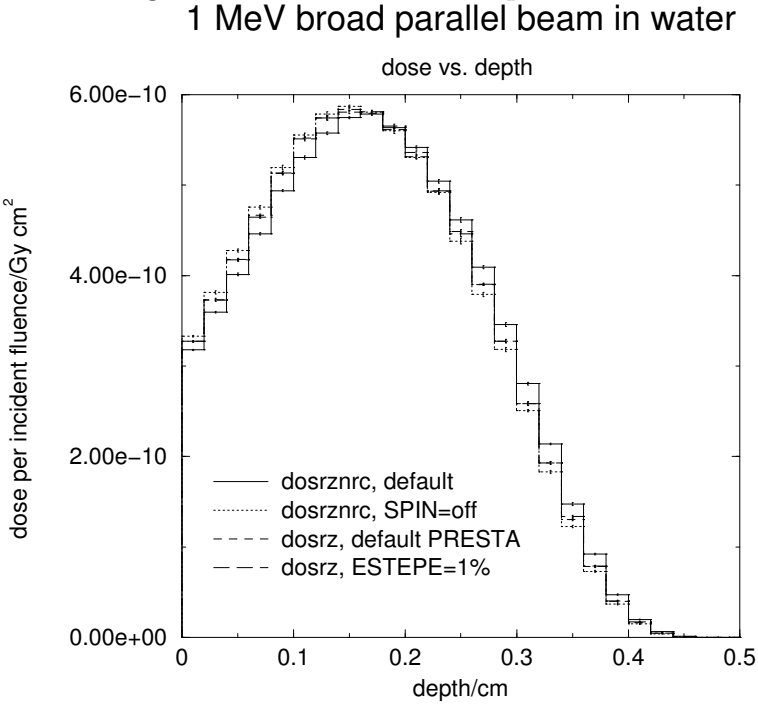

Figure 8: Depth-dose histogram for a 1 MeV broad parallel beam in a water phantom.

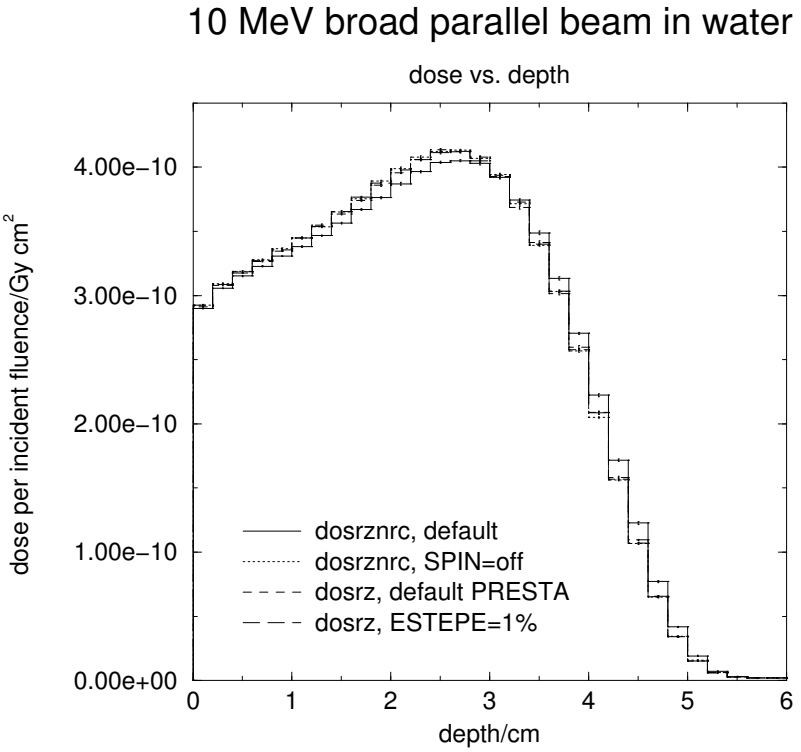

Figure 9: Depth-dose histogram for a 10 MeV broad parallel beam in a water phantom.

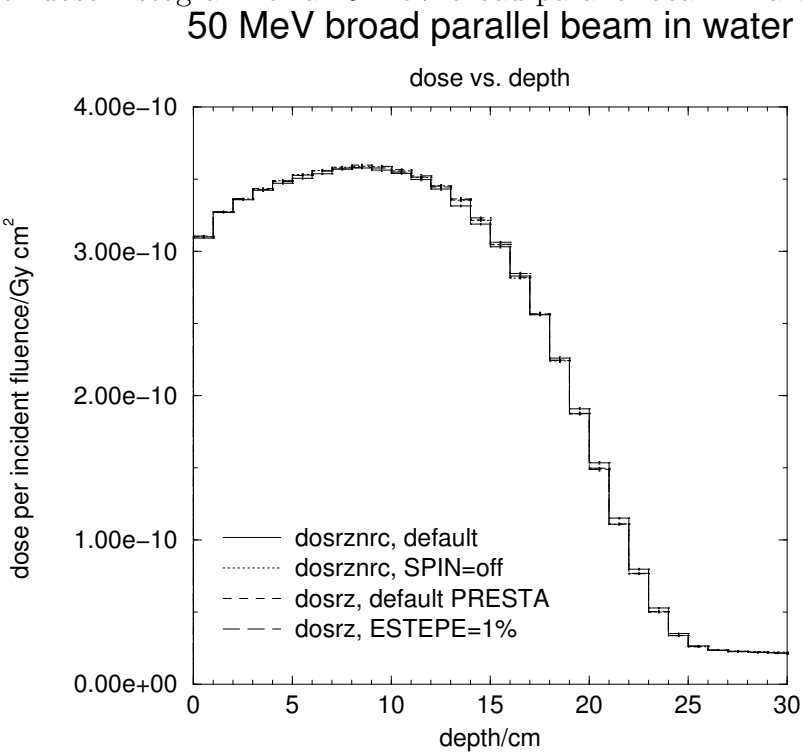

Figure 10: Depth-dose histogram for a 50 MeV broad parallel beam in a water phantom.

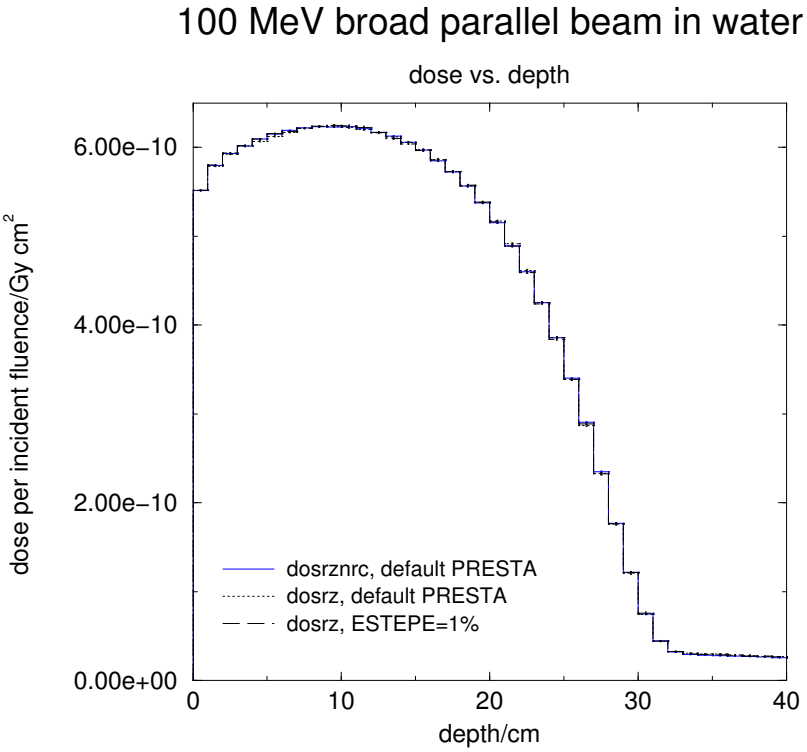

Figure 11: Depth-dose histogram for a 100 MeV broad parallel beam in a water phantom.

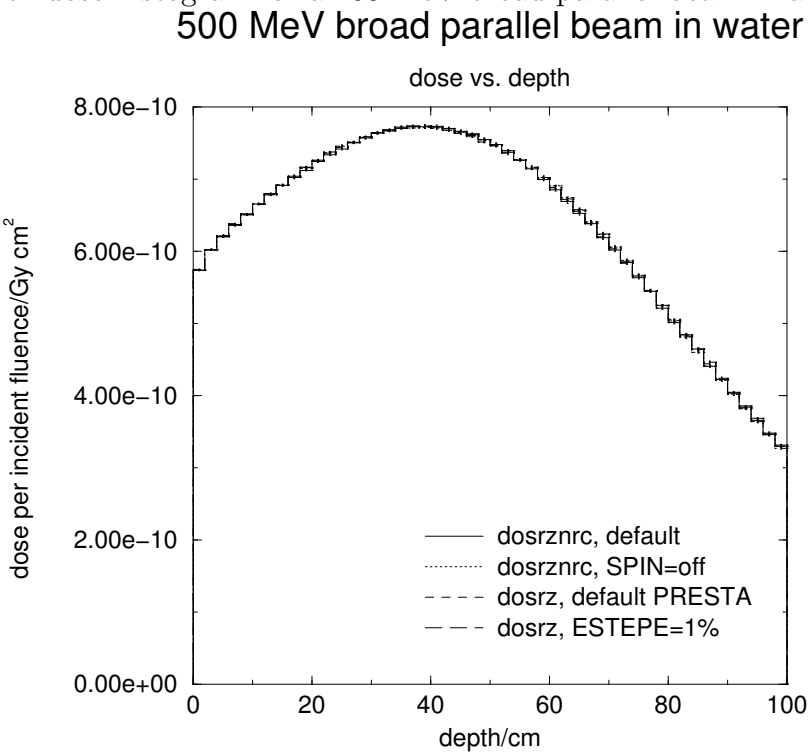

Figure 12: Depth-dose histogram for a 500 MeV broad parallel beam in a water phantom.

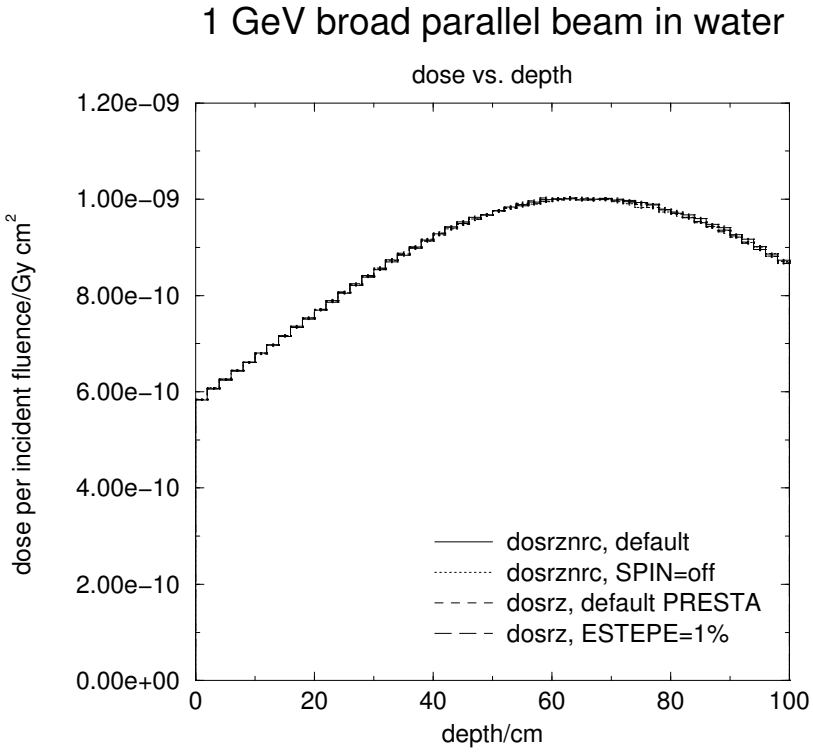

Figure 13: Depth-dose histogram for a 1 GeV broad parallel beam in a water phantom.

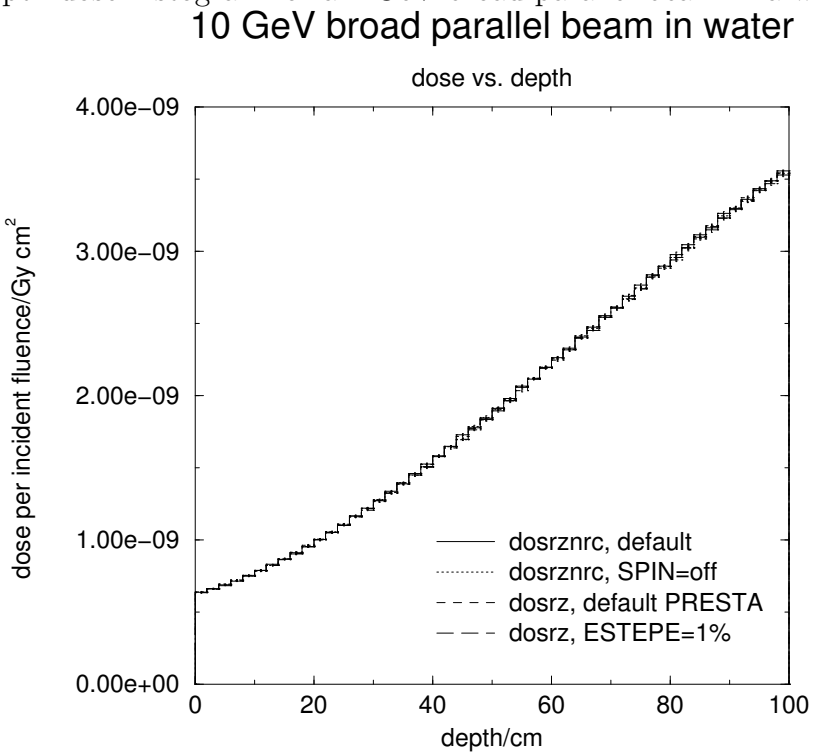

Figure 14: Depth-dose histogram for a 10 GeV broad parallel beam in a water phantom.

3.2 Lead phantom

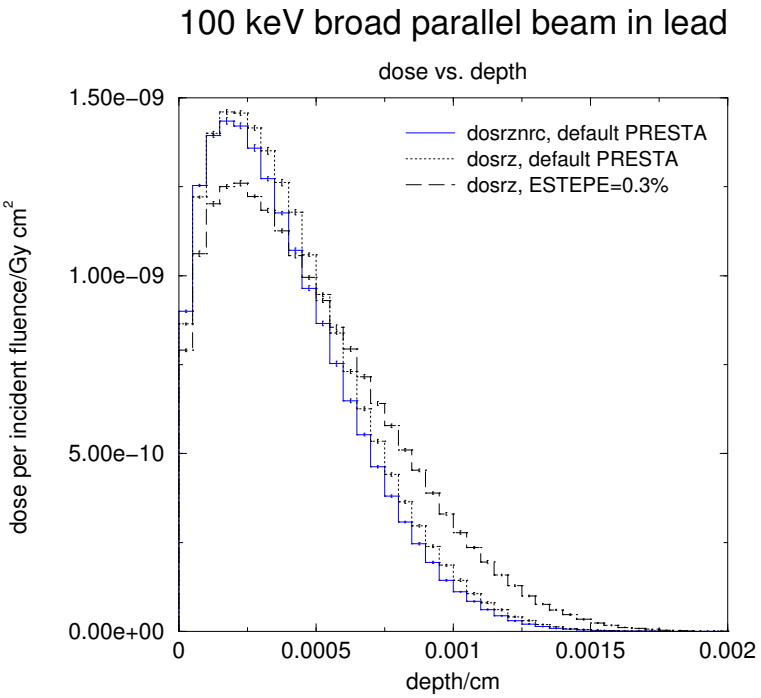

Figure 15: Depth-dose histogram for a 100 keV broad parallel beam in a lead phantom.

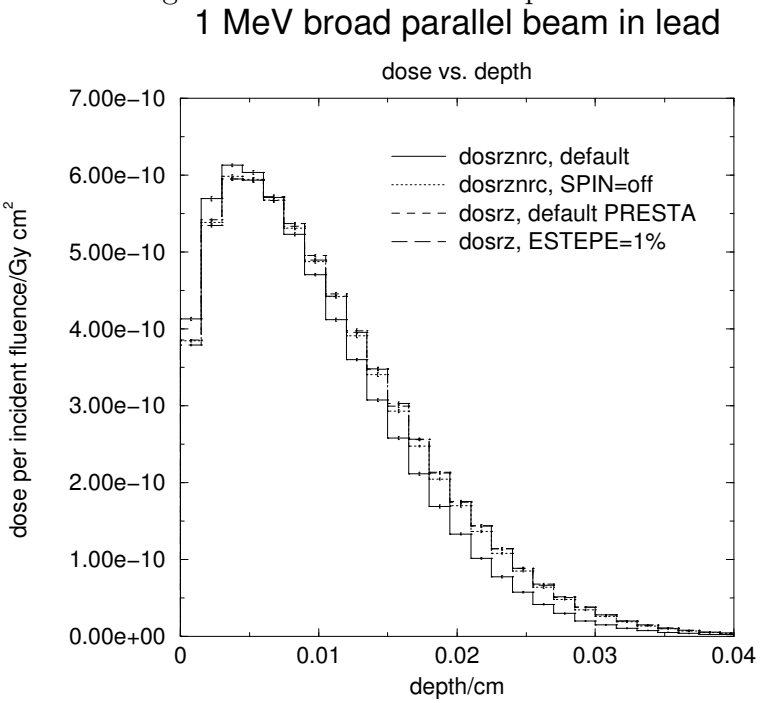

Figure 16: Depth-dose histogram for a 1 MeV broad parallel beam in a lead phantom.

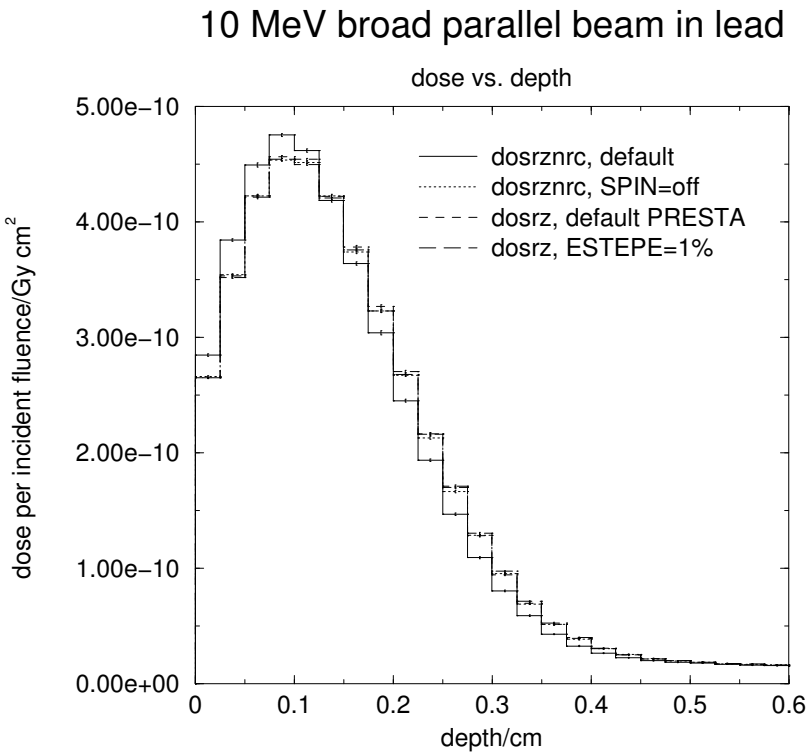

Figure 17: Depth-dose histogram for a 10 MeV broad parallel beam in a lead phantom.

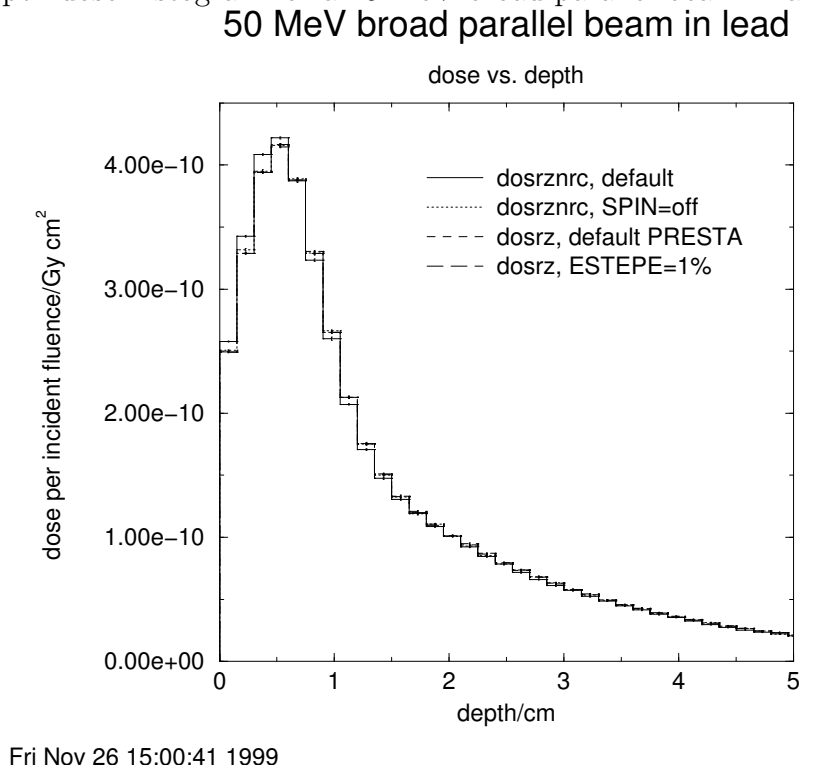

Figure 18: Depth-dose histogram for a 50 MeV broad parallel beam in a lead phantom.

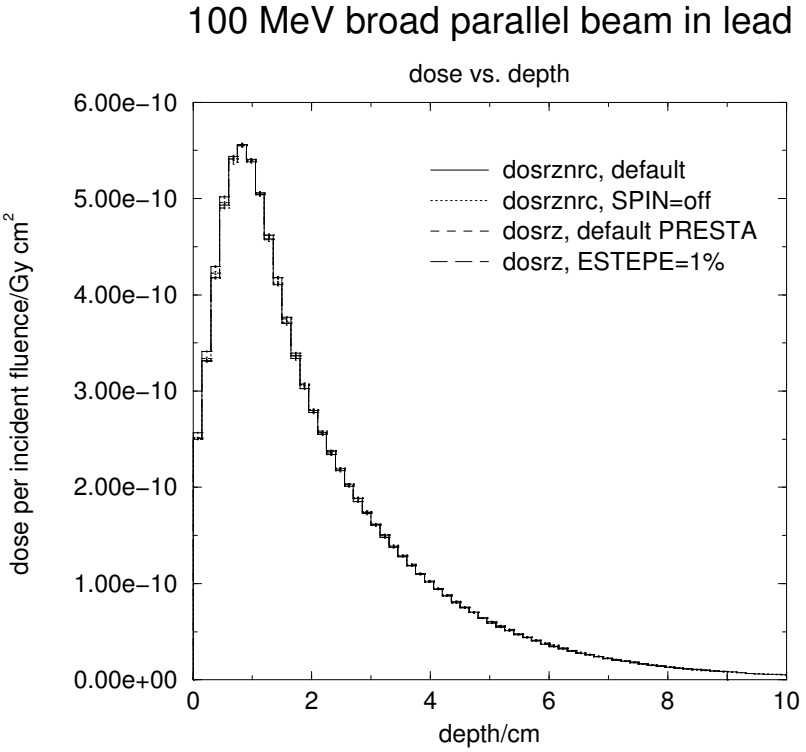

Figure 19: Depth-dose histogram for a 100 MeV broad parallel beam in a lead phantom.

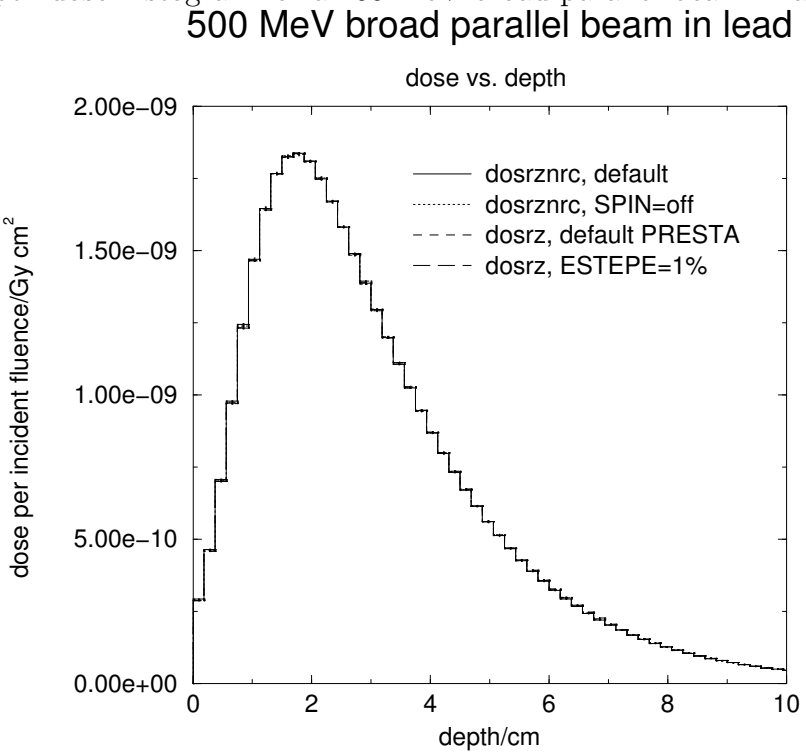

Figure 20: Depth-dose histogram for a 500 MeV broad parallel beam in a lead phantom.

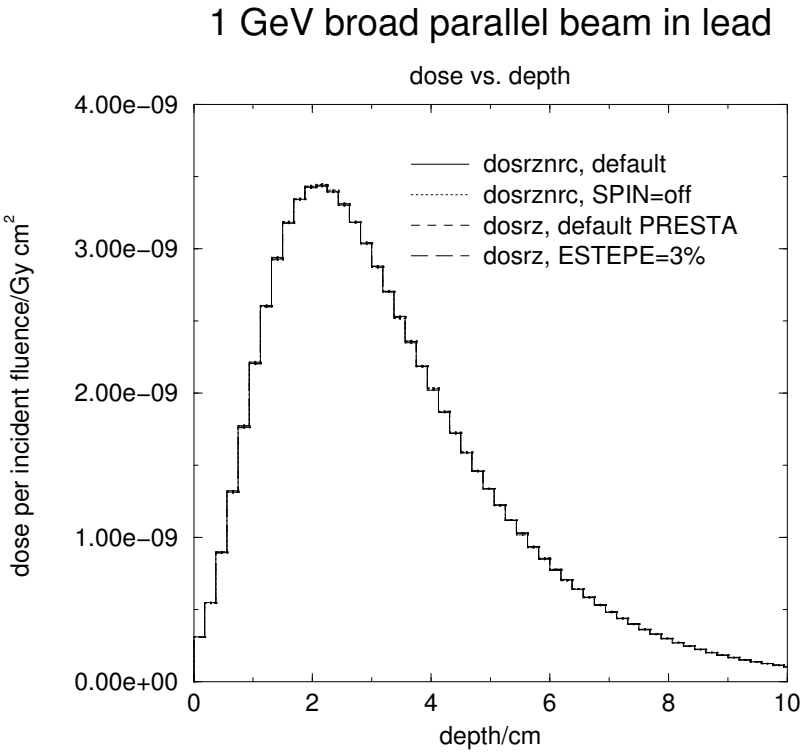

Figure 21: Depth-dose histogram for a 1 GeV broad parallel beam in a lead phantom.

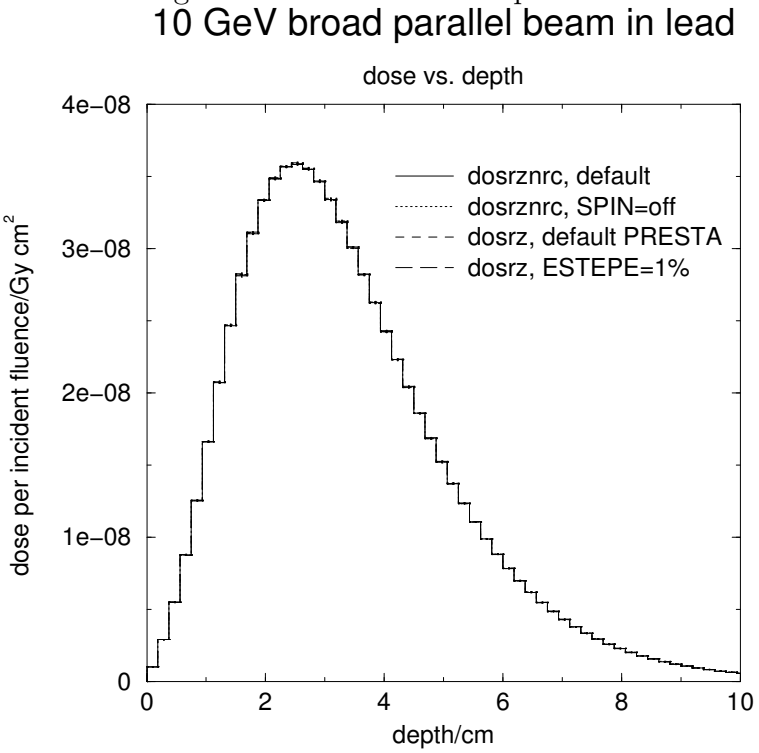

Figure 22: Depth-dose histogram for a 10 GeV broad parallel beam in a lead phantom.

4 Results for a pencil beam

Results for a broad parallel beam are often quite insensitive to the details of electron transport so in this section we consider the case of the central axis depth-dose curve for a pencil beam incident on the phantom.

In the water case the lower energy beams show differences comparable to the broad beam case but now we can see some small but clear differences at higher energies as well. For the lead case, these differences at higher energies are not so obvious.

4.1 Water phantom

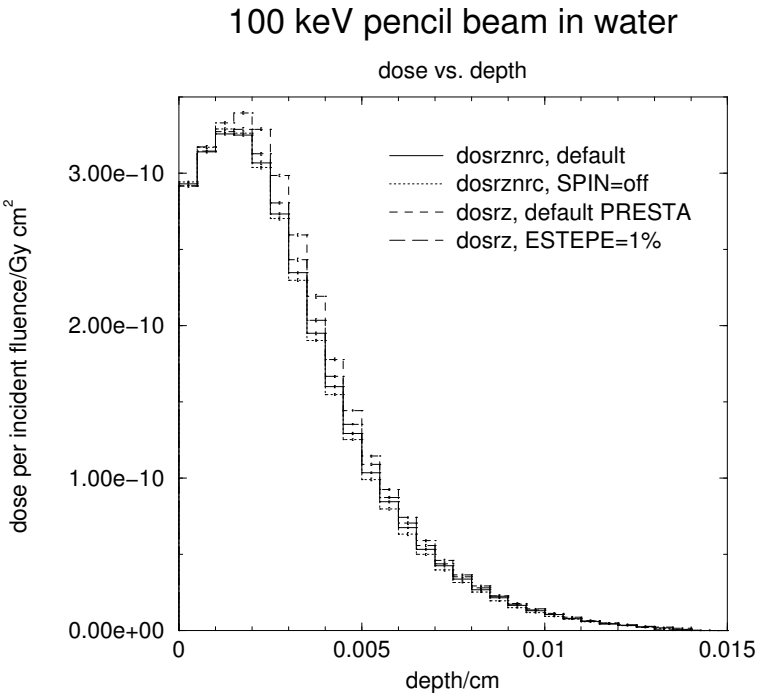

Figure 23: Depth-dose histogram for a 100 keV pencil beam in the 0.0015 cm central radius of a water phantom.

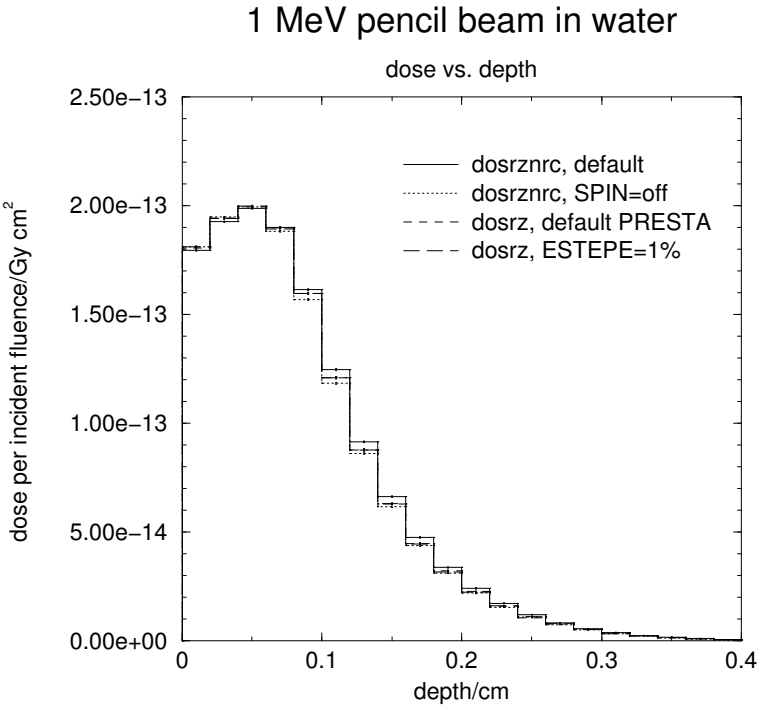

Figure 24: Depth-dose histogram for a 1 MeV pencil beam in the 0.04 cm central radius of a water phantom.

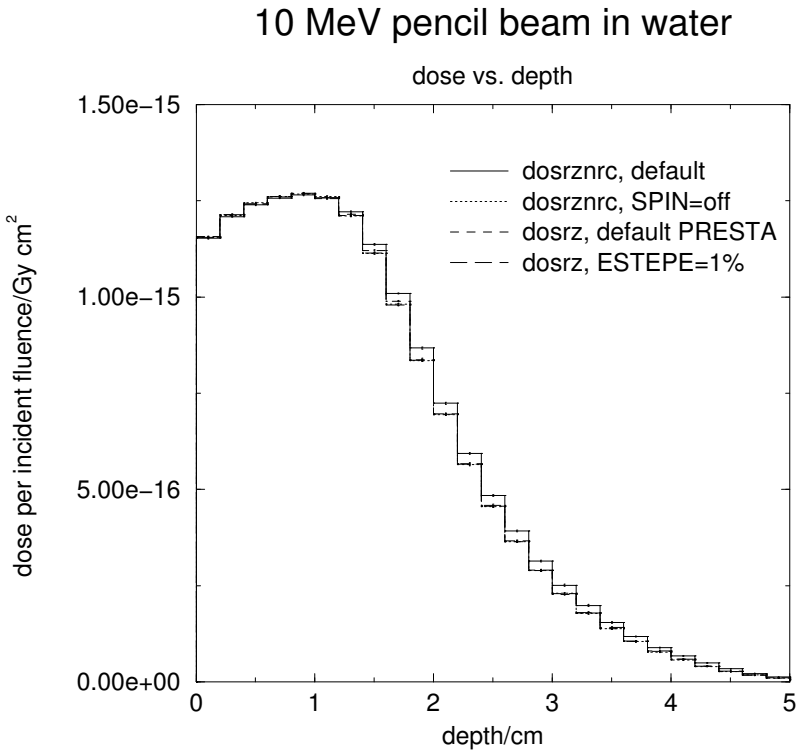

Figure 25: Depth-dose histogram for a 10 MeV pencil beam in the 0.5 cm central radius of a water phantom.

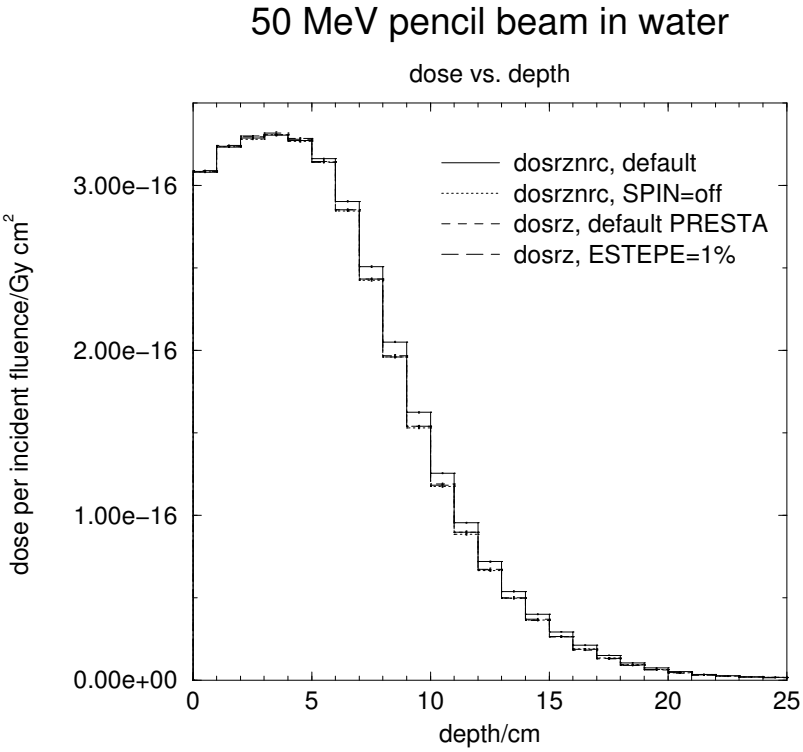

Figure 26: Depth-dose histogram for a 50 MeV pencil beam in the 1 cm central radius of a water phantom.

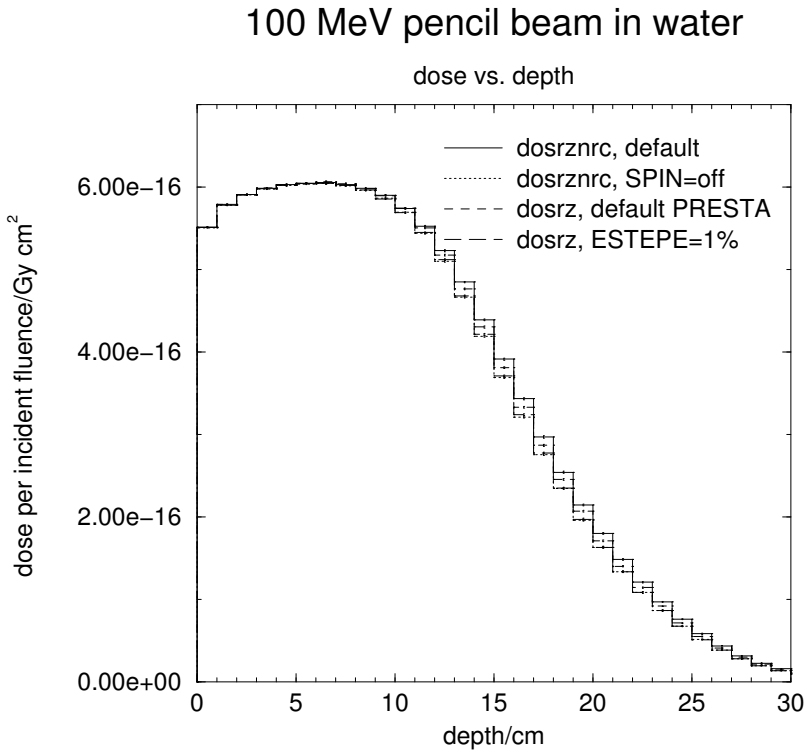

Figure 27: Depth-dose histogram for a 100 MeV pencil beam in the 1 cm central radius of a water phantom.

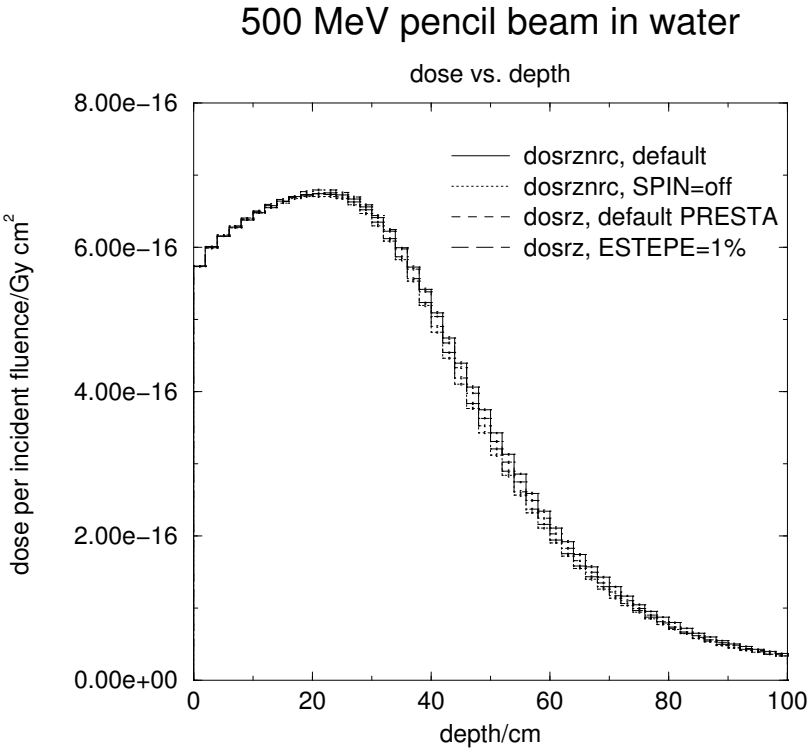

Figure 28: Depth-dose histogram for a 500 MeV pencil beam in the 1 cm central radius of a water phantom.

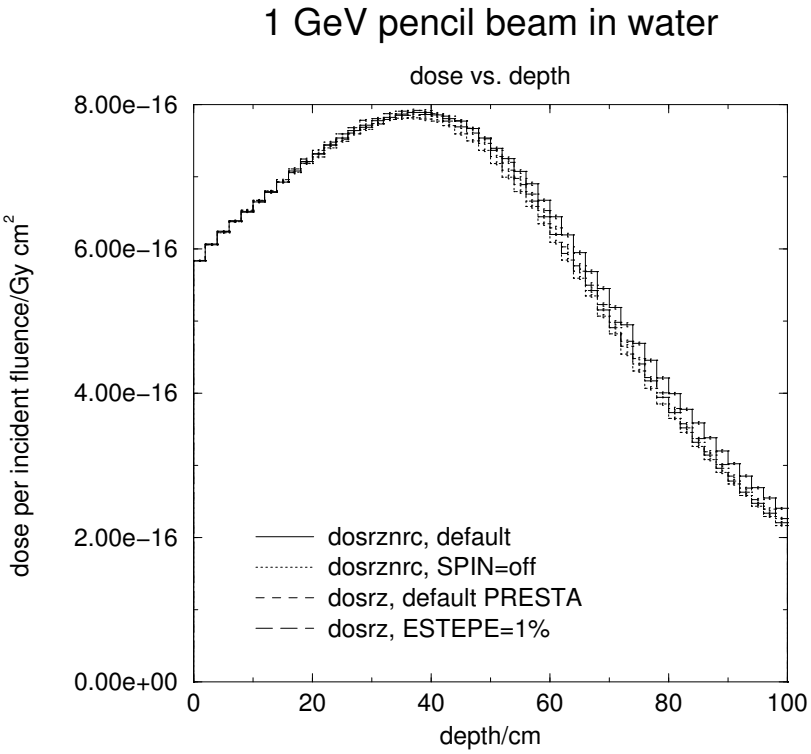

Figure 29: Depth-dose histogram for a 1 GeV pencil beam in the 1 cm central radius of a water phantom.

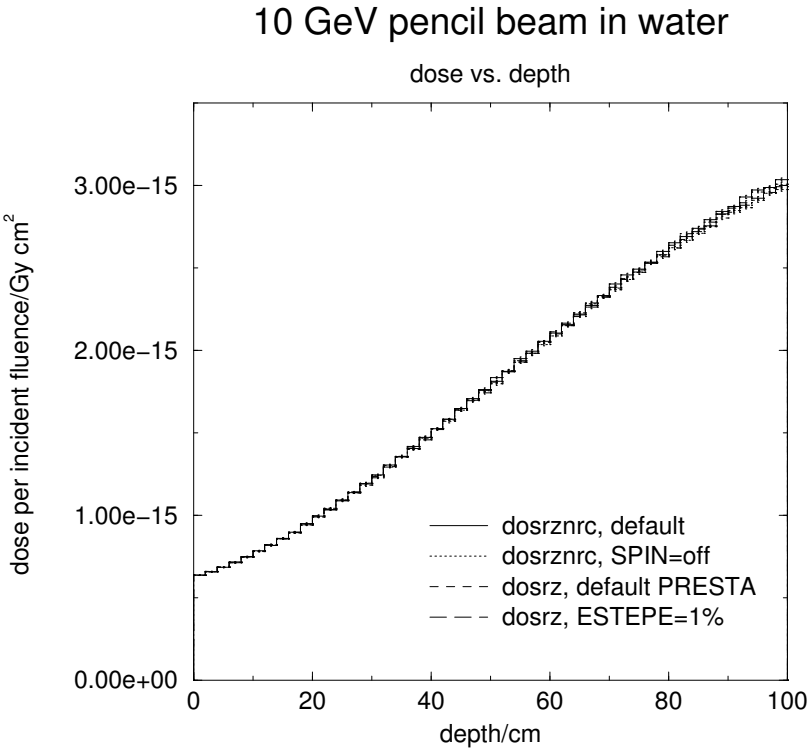

Figure 30: Depth-dose histogram for a 10 GeV pencil beam in the 1 cm central radius of a water phantom.

4.2 Lead phantom

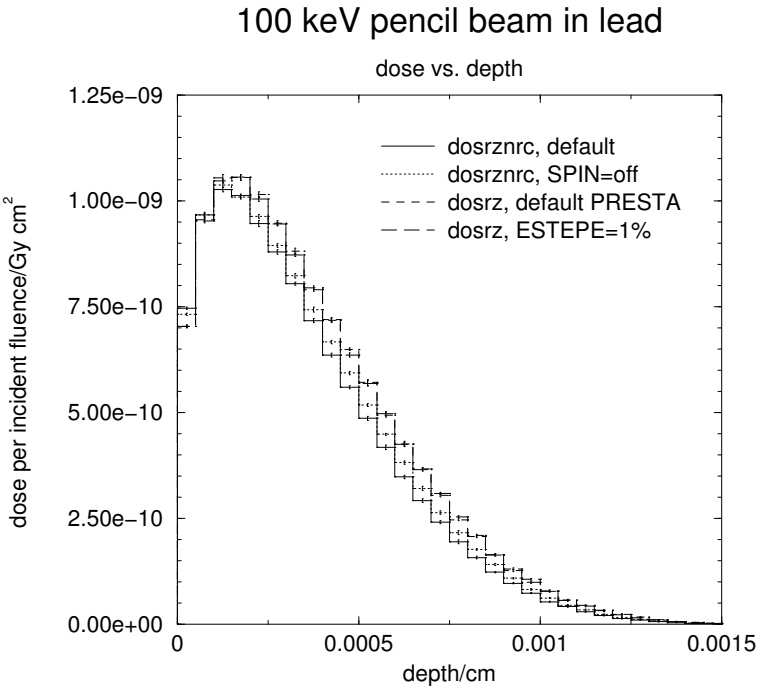

Figure 31: Depth-dose histogram for a 100 keV pencil beam in the 0.001 cm central radius of a lead phantom.

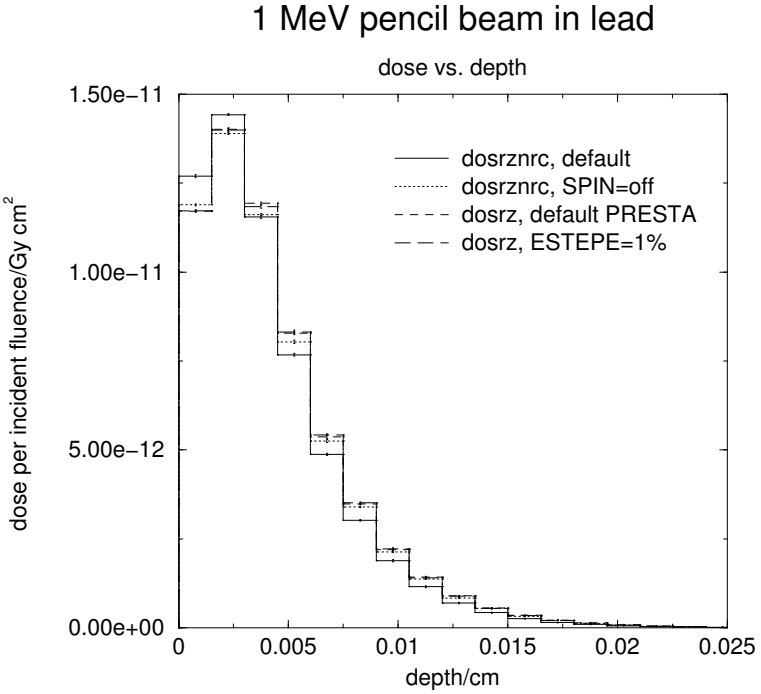

Figure 32: Depth-dose histogram for a 1 MeV pencil beam in the 0.004 cm central radius of a lead phantom.

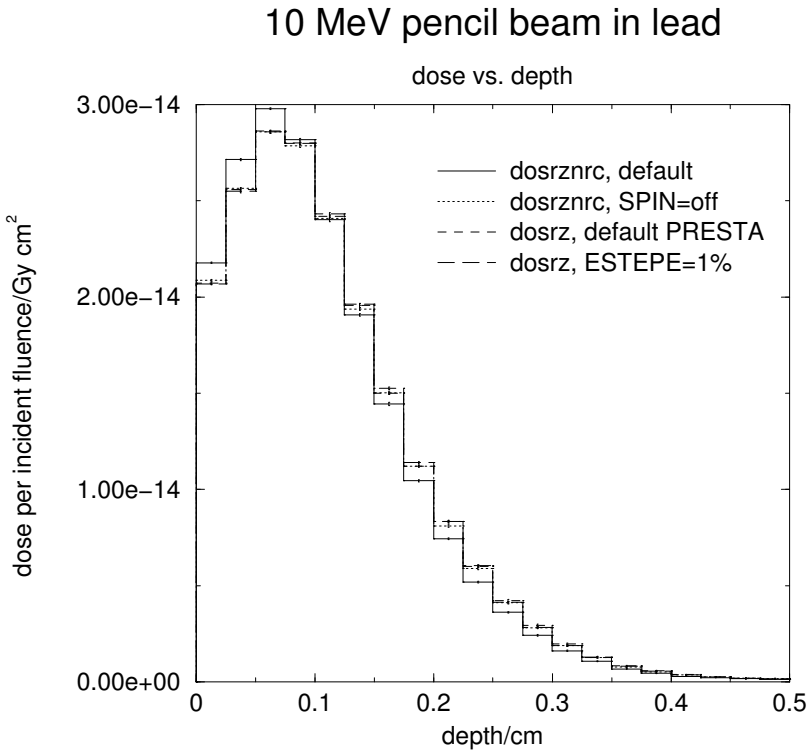

Figure 33: Depth-dose histogram for a 10 MeV pencil beam in the 0.1 cm central radius of a lead phantom.

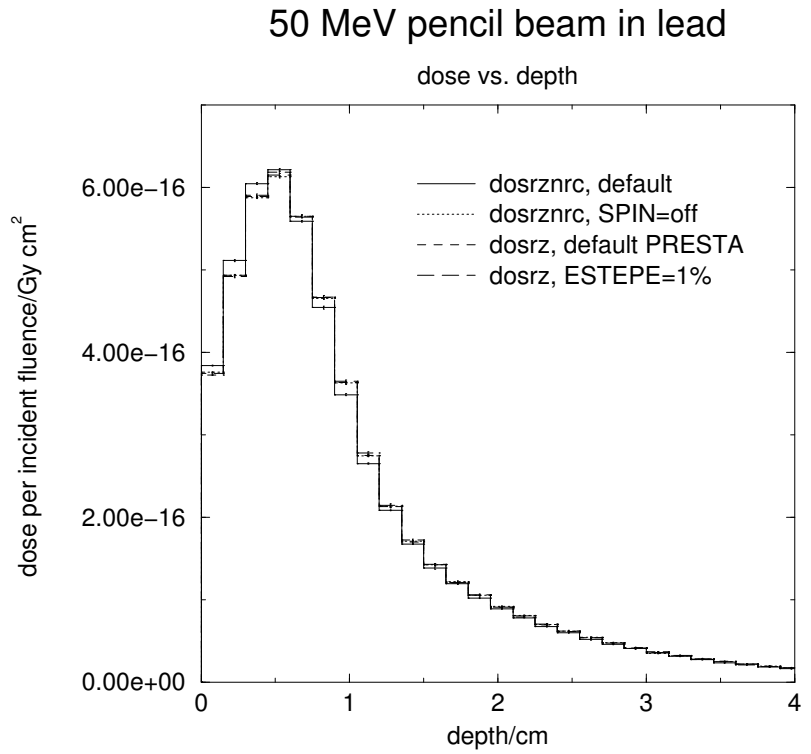

Figure 34: Depth-dose histogram for a 50 MeV pencil beam in the 0.8 cm central radius of a lead phantom.

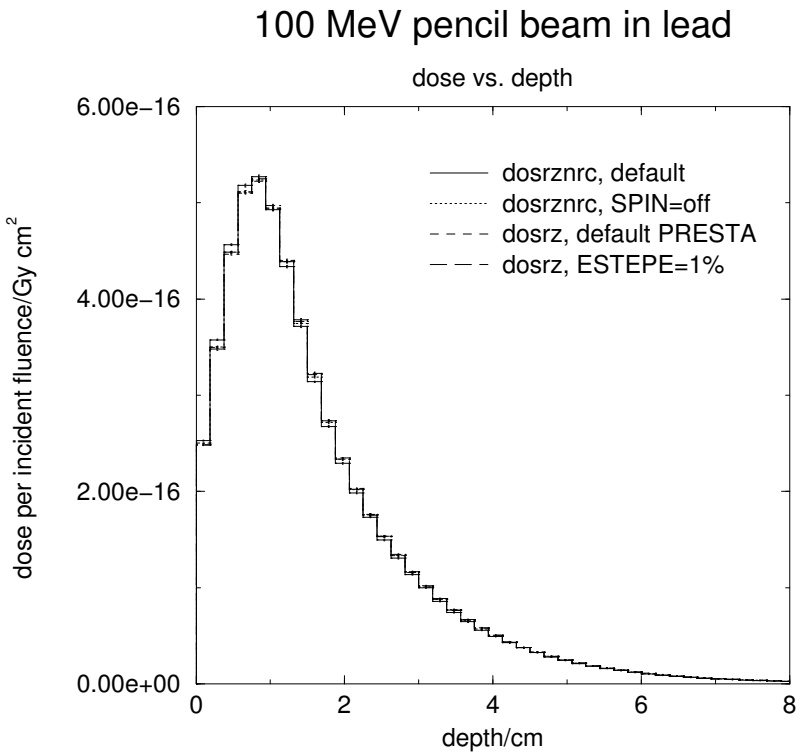

Figure 35: Depth-dose histogram for a 100 MeV pencil beam in the 1 cm central radius of a lead phantom.

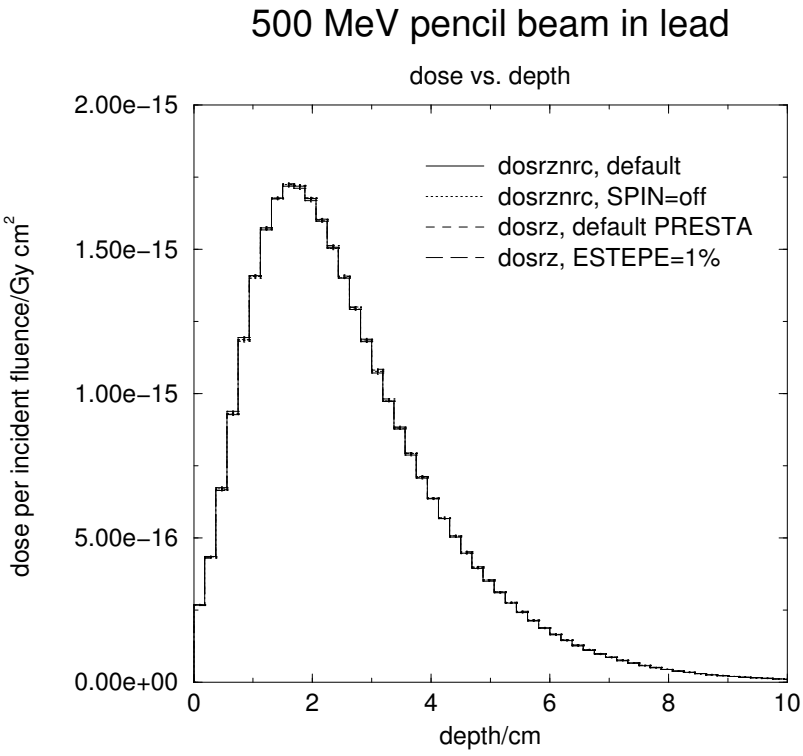

Figure 36: Depth-dose histogram for a 500 MeV pencil beam in the 1 cm central radius of a lead phantom.

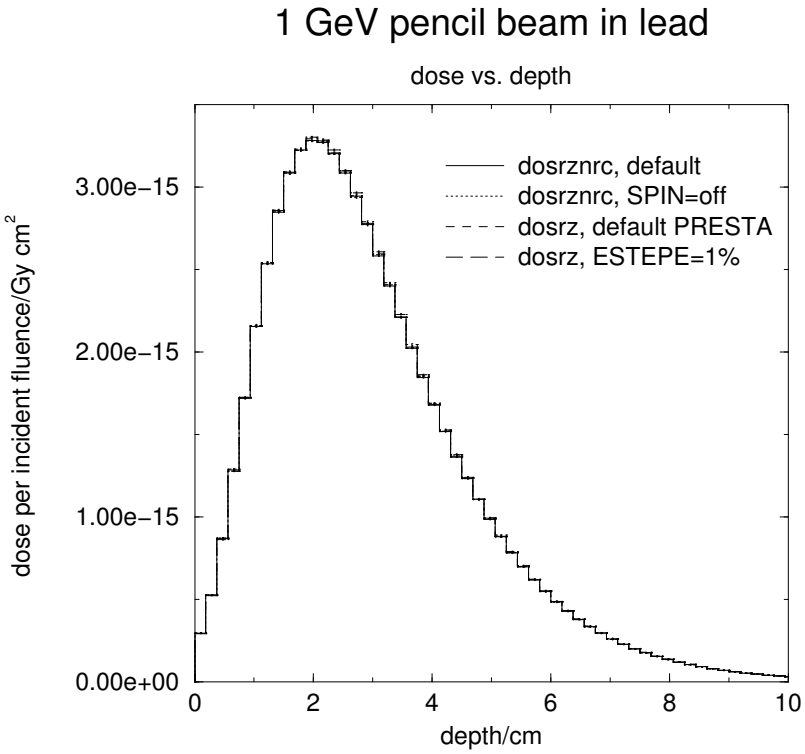

Figure 37: Depth-dose histogram for a 1 GeV pencil beam in the 1 cm central radius of a lead phantom.

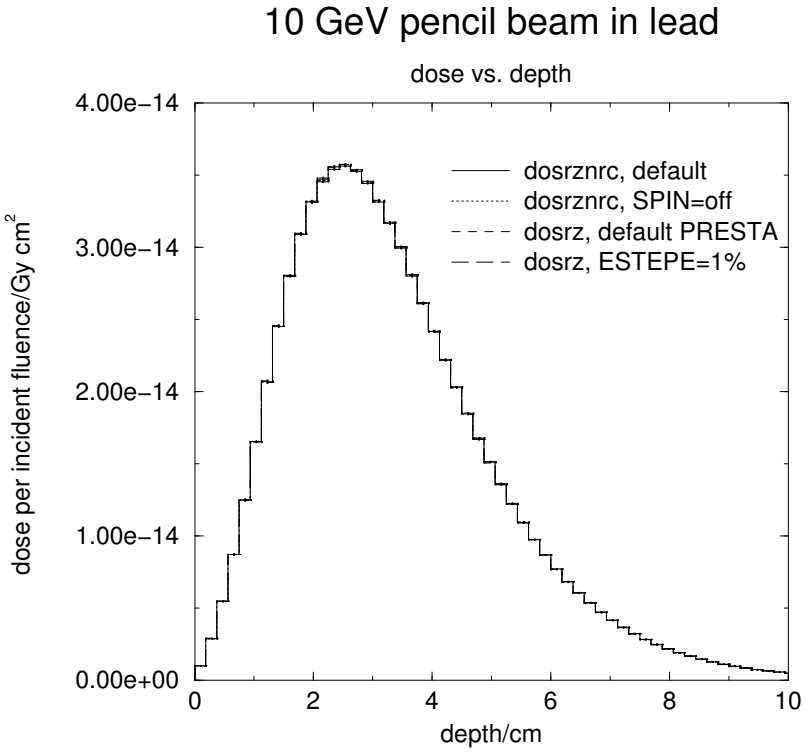

Figure 38: Depth-dose histogram for a 10 GeV pencil beam in the 1 cm central radius of a lead phantom.

4.3 Depth-dose curves in Be

Using default PRESTA values, DOSRZ crashes for beam energies greater than or equal to 500 MeV due to "too many negative ustep errors". By setting ESTEPE=0.3%, the number of ustep errors decreases to about 3 per batch for a 500 MeV beam. The simulation completes in this case.

A log file with IWATCH=steps for 100 histories with ESTEPE=0 is stored in `/usr/people/egsnrc/doc/pirs703/be_bug_dosrz/dosrz_egs4_bug_Be_500MeV.egs4log.gz`. The corresponding input file is `old_Be_500MeV.bug.egs4inp`.

Since this problem does not occur with EGSnrc, we have not pursued it further.

5 How closely an EGSnrc mimic EGS4?

In PIRS-701 there is a discussion of how to make the electron transport algorithm in EGSnrc mimic as closely as possible that of either EGS4 or EGS4/PRESTA (currently sections 3.4.2.i and ii). This can never be a perfect emulation because, eg, EGSnrc always uses the new multiple scattering theory, uses corrected bremsstrahlung sampling routines, has fixed up the ficticious cross section problem and handles energy loss more accurately. EGSnrc also has new options such as bound Compton scattering, new bremsstrahlung sampling routines and atomic relaxation but these can be turned off.

To emulate EGS4/PRESTA calculations using EGSnrc,we set `BOUNDARY CROSSING ALGORITHM` and the `ELECTRON-STEP ALGORITHM` to "PRESTA-I", `SKINDEPTH FOR BCA` to 20. `ESTEPE` used in the DOSRZnrc calculations was 0.25 (the default for EGSnrc), while `ESTEPE` in DOSRZ was set to 0.0 (the default in EGS4, indicating the use of PRESTA to determine maximum step length). What effect will this difference in `ESTEPE` have on the results?

So the question becomes, how closely do these EGSnrc calculations emulate EGS4/PRESTA?

5.1 Water phantom

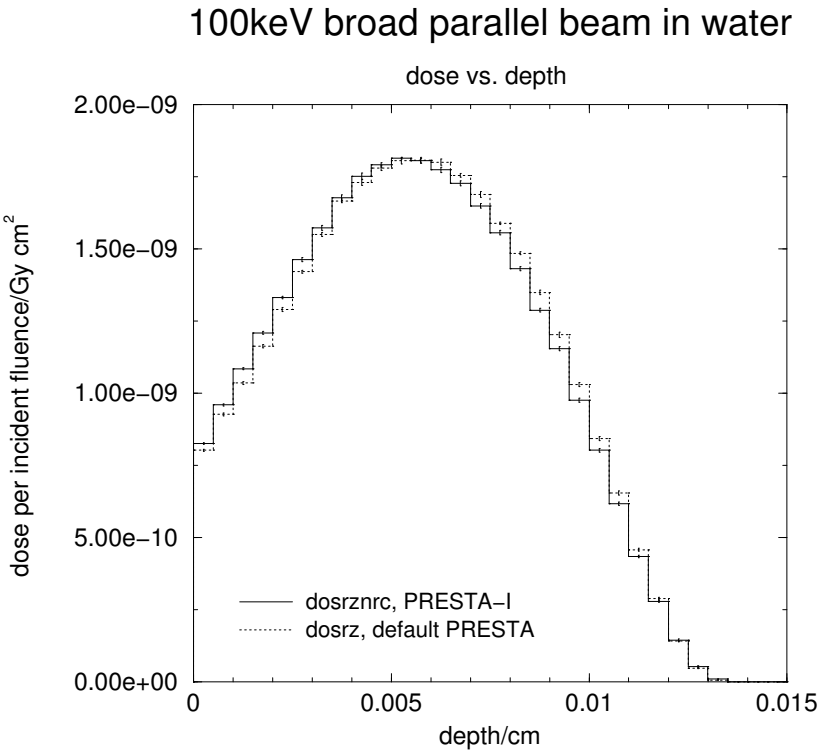

Figure 39: Depth-dose histogram for a 100 keV broad parallel beam in a water phantom, using the PRESTA-I algorithm for transport in the new DOSRZnrc.

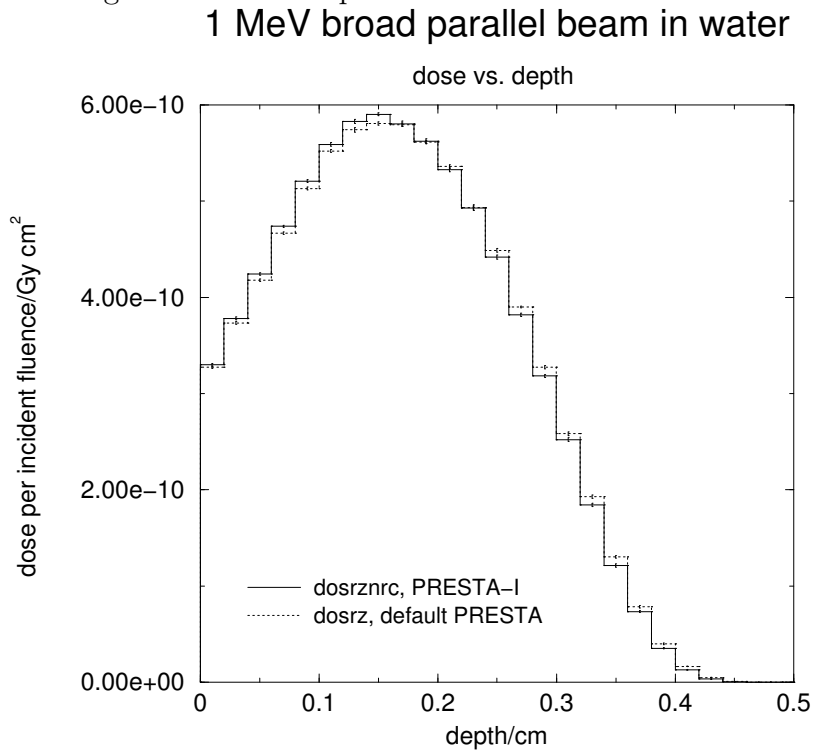

Figure 40: Depth-dose histogram for a 1 MeV broad parallel beam in a water phantom, using the PRESTA-I algorithm for transport in the new DOSRZnrc.

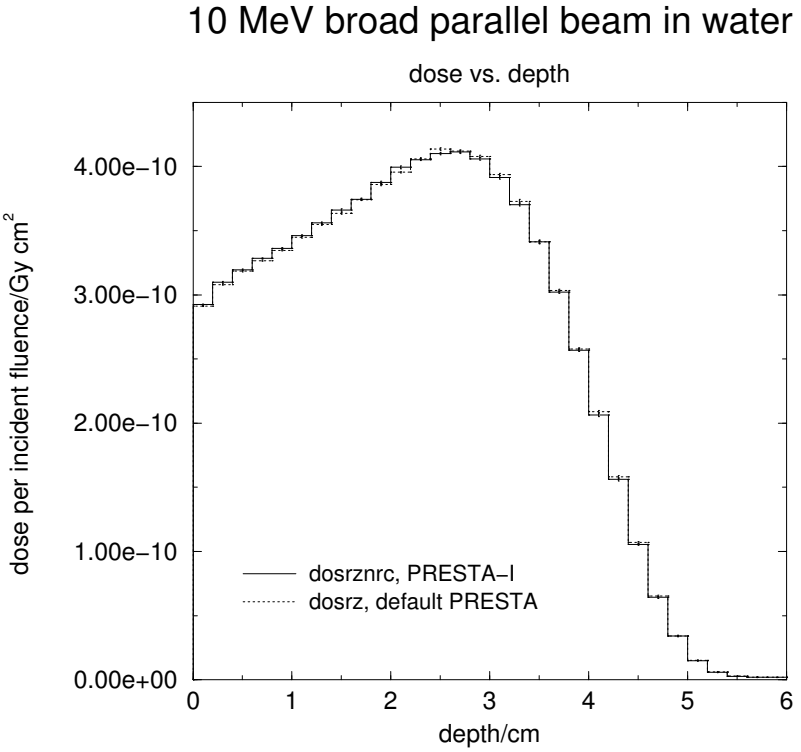

Figure 41: Depth-dose histogram for a 10 MeV broad parallel beam in a water phantom, using the PRESTA-I algorithm for transport in the new DOSRZnrc.

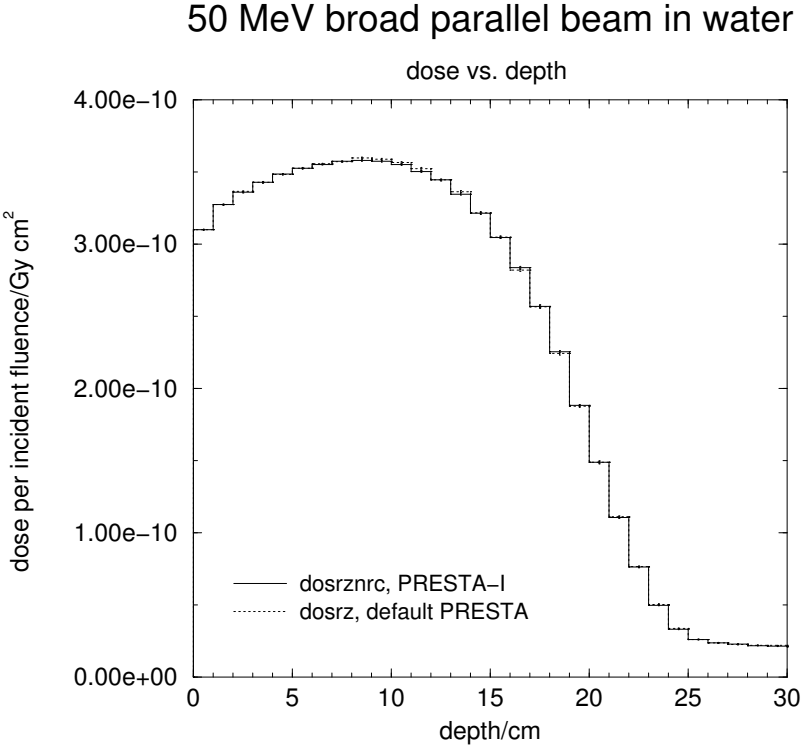

Figure 42: Depth-dose histogram for a 50 MeV broad parallel beam in a water phantom, using the PRESTA-I algorithm for transport in the new DOSRZnrc.

5.2 Lead phantom

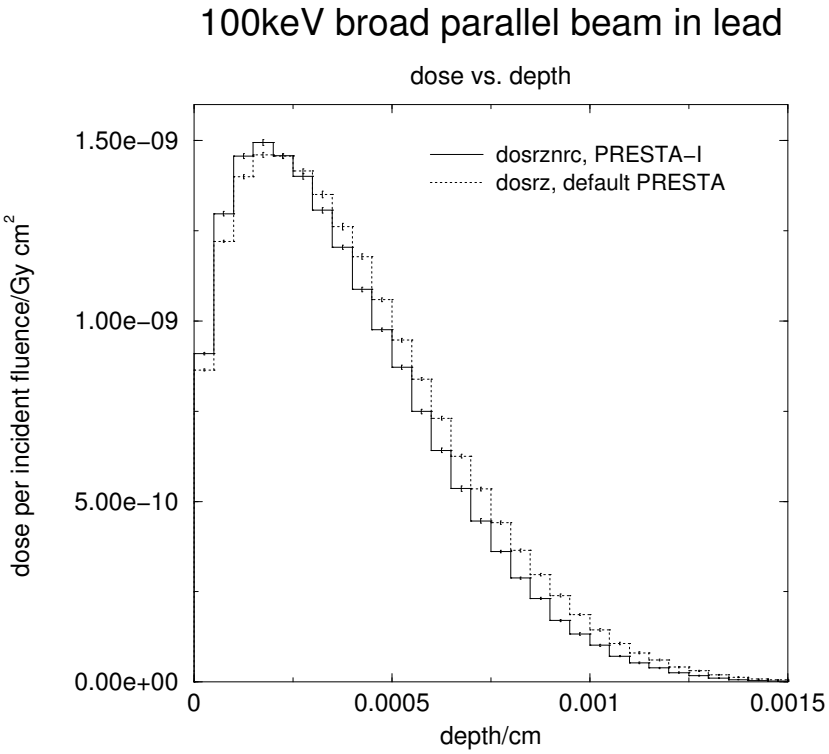

Figure 43: Depth-dose histogram for a 100 keV broad parallel beam in a lead phantom, using the PRESTA-I algorithm for transport in the new DOSRZnrc.

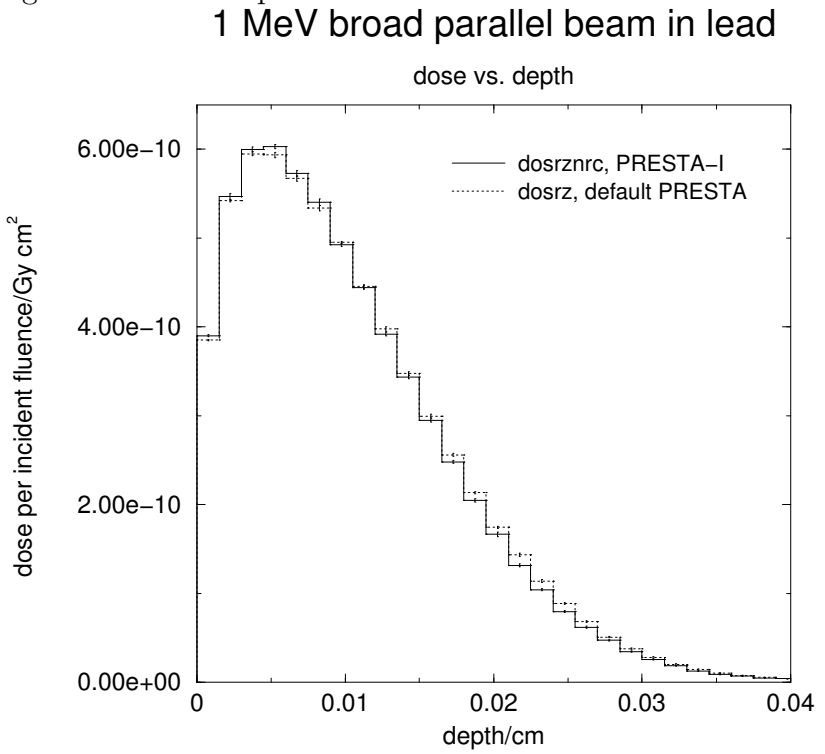

Figure 44: Depth-dose histogram for a 1 MeV broad parallel beam in a lead phantom, using the PRESTA-I algorithm for transport in the new DOSRZnrc.

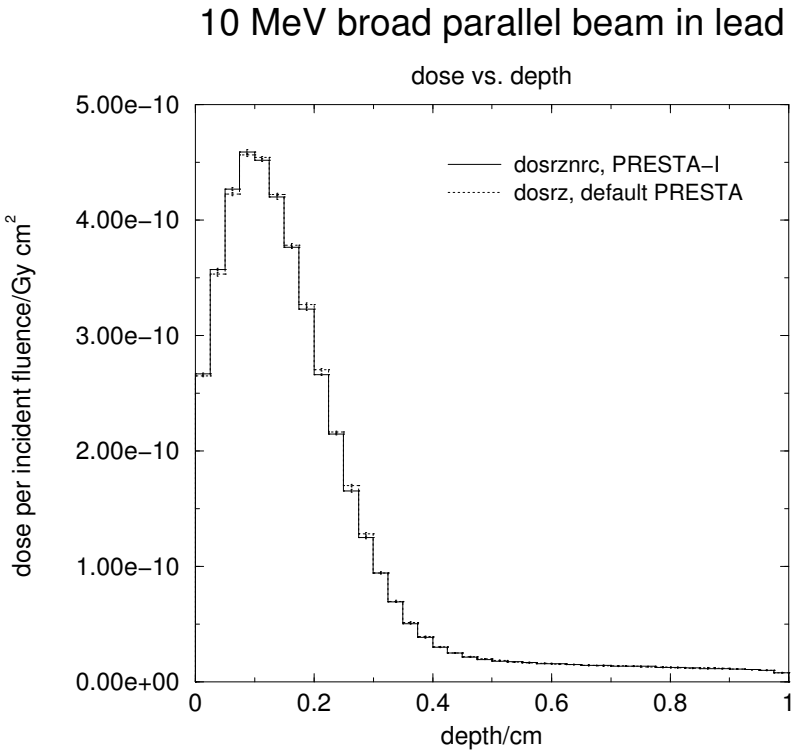

Figure 45: Depth-dose histogram for a 10 MeV broad parallel beam in a lead phantom, using the PRESTA-I algorithm for transport in the new DOSRZnrc.

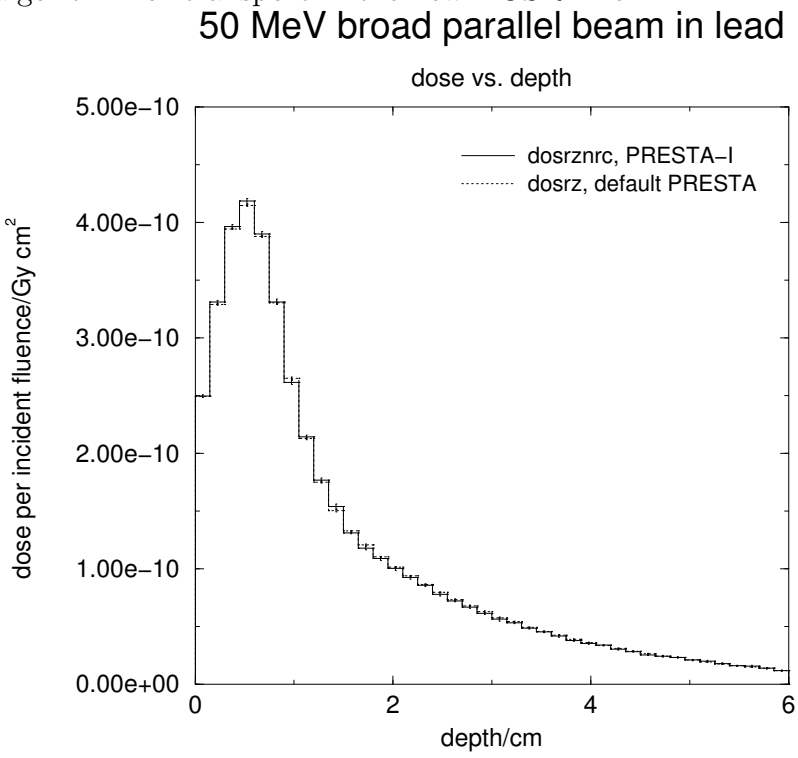

Figure 46: Depth-dose histogram for a 50 MeV broad parallel beam in a lead phantom, using the PRESTA-I algorithm for transport in the new DOSRZnrc.

6 R_{50} calculations in water and lead

Monte Carlo calculations done with EGS4/PRESTA of R_{50} in a water phantom have become the standard method for assigning the energy to electron beams used in radiotherapy[**?**, **?**]. It is therefore of considerable interest to investigate the differences in the values calculated by EGSnrc and EGS4/PRESTA.

R_{50} calculations were performed using both DOSRZ and DOSRZnrc (spin option on and off) in water and lead. Both broad beams and point sources (SSD=100cm) were used. Table **??** below shows some of the simulation parameters.

Table 1: Simulation parameters for the R_{50} calculations in water and lead using both broad beams ("bpb") and point sources ("pt"). All point sources had SSD=100 cm and field radius=5.6 cm (4-10 MeV) or 11.3 cm (15-50MeV) on the front face of the phantom. In all cases, phantoms were divided into 100 depth zones of equal thickness. In all cases, `ECUT` was 0.6 MeV and `PCUT` was 0.01 MeV.

energy (MeV)	no. histories		phantom thickness h2o/lead (cm)		dose zone radii (cm)	
	bpb	pt	bpb	pt	bpb	pt
4	$1x10^6$	$5x10^6$	3/0.3	3/0.3	N/A	2.0
5	$1x10^6$	$5x10^6$	3/0.3	3/0.3	N/A	2.0
8	$1x10^6$	$5x10^6$	5/0.5	5/0.5	N/A	2.0
10	$1x10^6$	$5x10^6$	7/0.7	7/0.7	N/A	2.0
15	$1x10^6$	$5x10^6$	10/1	10/1	N/A	2.0
20	$1x10^6$	$5x10^6$	15/1.5	15/1.5	N/A	2.0
30	$1x10^6$	$5x10^6$	20/2	20/2	N/A	2.0
40	$1x10^6$	$5x10^6$	30/3	30/3	N/A	2.0
50	$1x10^6$	$5x10^6$	30/3	30/3	N/A	2.0

R_{50} was estimated from the depth-dose curves using the program `rpr50`[**?**]. It should be noted that, unmodified, the program's fits to the depth-dose curves were unsatisfactory, and the number of points included in the fit had to be substantially reduced for reasonable estimates of R_{50}. In most cases, the segment of the depth-dose curve included in the fit was reduced by decreasing the parameter `DIVISOR` in the code `rpr501.mortran` (a sub-code of the `rpr50` system) from 5 to 1.3. However, for some depth-dose curves, `DIVISOR` had to be set to another number (usually close to 1.3) or else the range of points to be included in the fit had to be set explicitly within `rpr501.mortran`. In all cases, a simple linear estimate of R_{50} was used as a gauge of the `rpr50` fit and the uncertainty on R_{50} was taken as the uncertainty on this linear estimate. To calculate the uncertainty, we started from the linear estimate of R_{50}:

$$R_{50} = \frac{(D_{50} - D_1)}{(D_2 - D_1)}(R_2 - R_1) + R_1 \tag{1}$$

where D_{50} is the dose at R_{50} (ie 50% of the max. dose) and (R_{50}, D_{50}) is between the adjacent data points (R_1,D_1), (R_2,D_2) on the depth dose curve (with $D_1 > D_{50}$ and $D_2 <$

D_{50}). Assuming no uncertainty on R_{50},R_1,R_2 and D_{50}, then simple error propagation gives:

$$\Delta R_{50} = \sqrt{(\frac{\Delta D_1}{D_{50} - D_1})^2 + \frac{(\Delta D_1)^2 + (\Delta D_2)^2}{(D_2 - D_1)^2}} * (R_{50} - R_1) \quad (2)$$

Table **??** shows the estimated values of R_{50} for beams incident on water. Table **??** shows the estimated values of R_{50} in lead.

Table 2: R_{50} estimates in water with broad beam and point (SSD=100 cm) sources using both DOSRZ and DOSRZnrc (spin on except for the case of a broad beam, where spin off was also implemented).

energy	broad beam			pt source	
(MeV)	DOSRZ	DOSRZnrc		DOSRZ	DOSRZnrc
		spin on	spin off		
4	1.5165(6)	1.5520(6)	1.513(1)	1.517(1)	1.555(1)
5	1.942(1)	1.986(1)	1.939(1)	1.947(2)	1.987(2)
8	3.244(2)	3.299(2)	3.236(1)	3.243(2)	3.304(2)
10	4.110(2)	4.178(1)	4.103(2)	4.112(3)	4.192(7)
15	6.267(2)	6.363(3)	6.266(2)	6.28(1)	6.351(7)
20	8.391(4)	8.492(3)	8.382(3)	8.38(1)	8.47(1)
30	12.446(5)	12.572(6)	12.447(7)	12.21(2)	12.34(1)
40	16.219(8)	16.35(1)	16.228(9)	15.62(3)	15.68(3)
50	19.721(7)	19.862(9)	19.736(8)	18.53(4)	18.57(4)

Table 3: R_{50} estimates in lead with broad beam and point (SSD=100 cm) sources using both DOSRZ and DOSRZnrc.

energy	broad beam			pt source	
(MeV)	DOSRZ	DOSRZnrc		DOSRZ	DOSRZnrc
		spin on	spin off		spin on
4	0.0813(2)	0.0748(1)	0.0808(2)	0.0816(2)	0.0750(2)
5	0.1056(2)	0.0972(3)		0.1058(4)	0.0975(2)
8	0.1808(2)	0.1686(2)		0.1804(5)	0.1686(3)
10	0.2312(3)	0.2170(3)		0.2316(5)	0.2172(4)
15	0.3570(6)	0.3387(4)		0.3560(7)	0.3374(8)
20	0.4761(5)	0.456(1)	0.4755(5)	0.478(2)	0.453(2)
30	0.707(1)	0.6805(9)		0.704(3)	0.681(2)
40	0.923(1)	0.896(1)		0.921(3)	0.894(3)
50	1.139(2)	1.112(4)	1.138(2)	1.126(8)	1.099(9)

Once estimates of R_{50} were obtained, the data was plotted in the form of E_o (or incident energy)/R_{50} vs R_{50}. In this form, differences in R_{50} are much easier to see, and it allowed easier comparison with results calculated by Bielajew and Rogers using an older version of DOSRZ[**?**]. Figure **??** below show the E_o/R_{50} vs R_{50} results in water and lead.

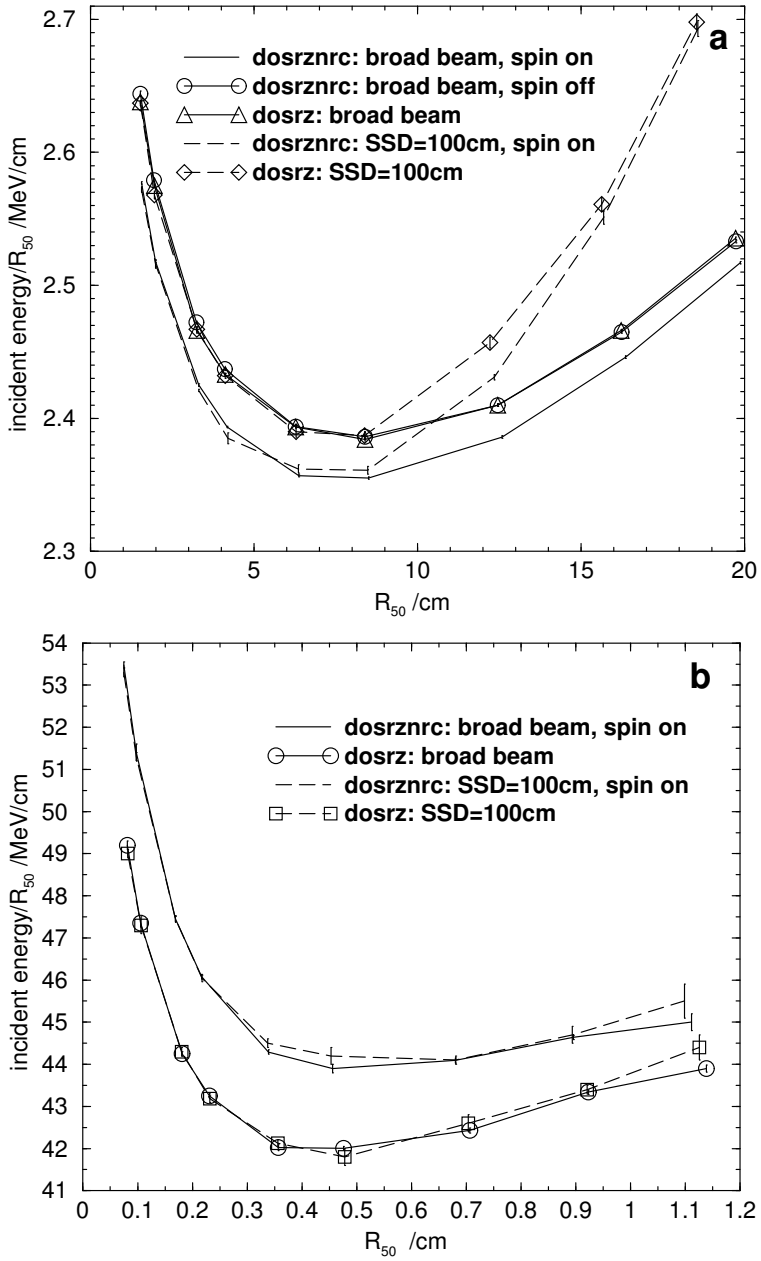

Figure 47: Plot of E_o/R_{50} vs R_{50} for broad beams and point sources (SSD=100 cm) in (a) water and (b) lead using DOSRZnrc and DOSRZ. For case of a broad beam in water, DOSRZnrc was run with spin effects off and spin effects on. Fractional uncertainties in E_o/R_{50} are the same as fractional uncertainties in the estimate of R_{50} (See Table **??** above).

Figure **??** below shows normalized depth dose curves for the 5 MeV and 20 MeV point sources (SSD=100 cm) in water. The E_o in the DOSRZ calculations was increased to 5.1026 MeV and 20.2179 MeV respectively to match the R_{50} estimated using DOSRZ with that estimated using DOSRZnrc. In each graph, the DOSRZnrc data has been normalized to its own maximum dose, while the DOSRZ data has been normalized both to its own maximum and to the DOSRZnrc maximum. This is to illustrate that, while the R_{50}'s may agree after E_o has been adjusted, the depth dose curves are not absolutely the same.

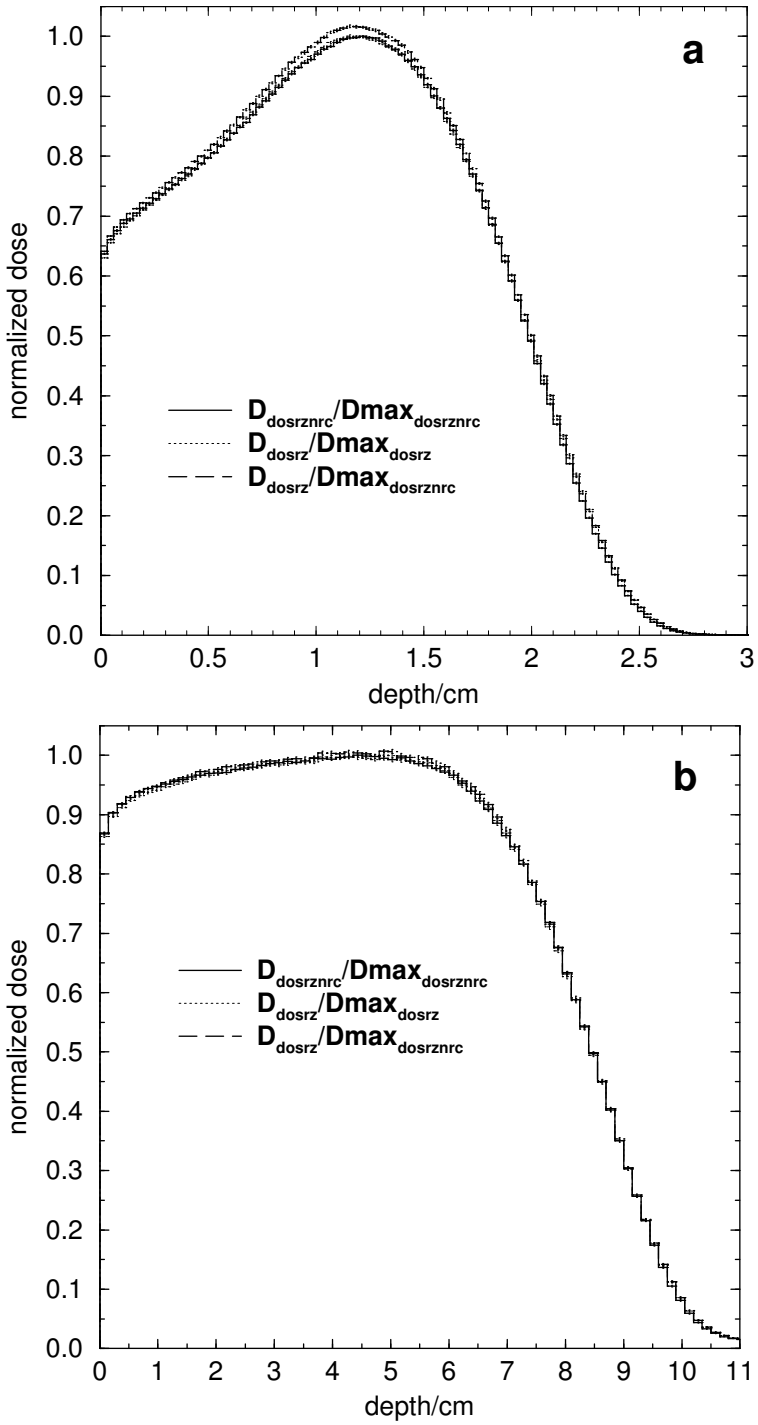

Figure 48: Normalized depth dose curves for DOSRZnrc (spin on) and DOSRZ for (a) a 5 MeV point source (SSD=100 cm) and (b) a 20 MeV point source. In (a) E_o in DOSRZ was increased to 5.1026 MeV to match R_{50} with that estimated using DOSRZnrc. In (b) E_o in DOSRZ was increased to 20.2179 MeV to obtain R_{50} agreement. The DOSRZ curves have been normalized both to their own maxima ($Dmax_{dosrz}$) and to the DOSRZnrc maxima ($Dmax_{dosrznrc}$).

7 Angular Distribution of Fluence

FLURZ and FLURZnrc were used to compare the angular distribution of photon and electron fluence when an electron beam of radius 0.05 cm is incident on lead and beryllium targets. A schematic of the cylindrical geometry used to do this is shown in Figure **??** below. The target thickness, t, was variable and approximately equal to the CSDA range of electrons in lead or beryllium at the beam energy up to a maximum target thickness of 14.34 cm in beryllium and 1.24 cm in lead. The radial zones were designed to give equal angular bins on a logarithmic scale up to a maximum angle of 89 degrees. Photon and electron energy fluence was scored in the 0.1 cm thick radial zones at the top and bottom of the cylindrical geometry.

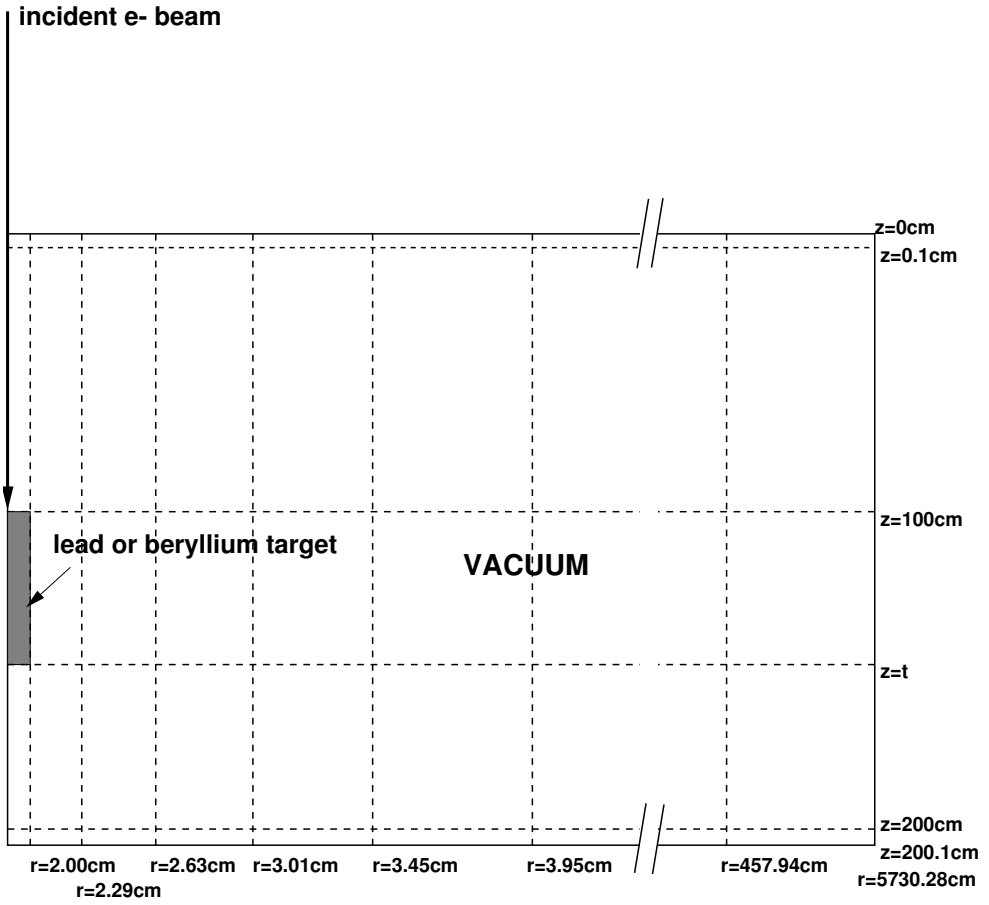

Figure 49: Cylindrical geometry used in FLURZnrc and FLURZ to determine angular distribution of photon and electron energy fluence. The geometry has radial symmetry about the incident electron beam. The target thickness, t, was variable and equal to the CSDA range of electrons in the target material up to a maximum thickness of 1.24 cm for lead and 14.34 cm for beryllium. The target radius was set approximately equal to the target thickness (its radius had to correspond to one of the radial region boundaries) with a minimum radius of 2.00 cm. Energy fluence was scored in the 0.1cm thick radial zones at the top and bottom of the geometry. In the case of lower beam energies, radial bins near the centre of the geometry were combined together to improve statistics. In the case of the higher beam energies, extra radial bins were added at the centre at angular intervals of 2^o to improve resolution at small angles.

7.1 Lead target

Simulation parameters for determining angular energy fluence of photons and electrons from lead targets are shown in Table **??** below.

Table 4: Simulation parameters used to determine the angular distribution of photon and electron energy fluence from lead targets using FLURZnrc and FLURZ. In all cases, `PCUT` was 0.01 MeV.

energy	target thickness (cm)	target radius (cm)	no. histories		splitting no.		`ECUT` (MeV)
			FLURZnrc	FLURZ	FLURZnrc	FLURZ	
100 keV	0.00274	1.9999	1x10^6	100x10^6	30	0	0.521
500 keV	0.029612	1.9999	1x10^6	1x10^6	30	30	0.521
1 MeV	0.0691	1.9999	1x10^6	1x10^6	30	30	0.521
5 MeV	0.32362	1.9999	1x10^6	1x10^6	30	30	0.700
10 MeV	0.54036	1.9999	1x10^6	100,000	30	30	0.700
50 MeV	1.23612	1.9999	10,000	100,000	20	30	0.700
100 MeV	1.23612	1.9999	35,000	100,000	20	30	1.511
500 MeV	1.23612	1.9999	25,000	100,000	10	30	1.511
1 GeV	1.23612	1.9999	15,000	100,000	10	30	1.511
5 GeV	1.23612	1.9999	25,000	100,000	5	30	1.511
10 GeV	1.23612	1.9999	25,000	100,000	5	30	1.511

For FLURZnrc, the other Monte Carlo transport parameters are as follows:

```
Global SMAX= 0.0
ESTEPE= 1.0
XImax= 0.5
Boundary crossing algorithm= EXACT
Skin depth for BCA= 3
Electron-step algorithm= PRESTA-II
Spin effects= on
Brems angular sampling= KM
Brems cross sections= BH
Bound Compton scattering= off
Pair angular sampling= Simple
Photoelectron angular sampling= off
Rayleigh scattering= off
Atomic relaxations= off

CHARGED PARTICLE RUSSIAN ROULETTE= Off
```

For FLURZ, the following transport parameters were used:

```
ANGULAR BREM DISTRIBUTION= On

ESTEPE=  0.0000
SMAX=  0.0000
RAYLEIGH SCATTERING= off
ELECTRON RANGE REJECTION= off
X-RAY FLUORESCENCE= off
NESTEP= 0
NSMAX= 0
```

7.1.1 Spin Effects

Figure **??** below shows the ratio of the photon energy fluence with "Spin effects=Off" to that with "Spin effects=On" (ie the standard case here) vs angle for a 10 MeV beam on lead.

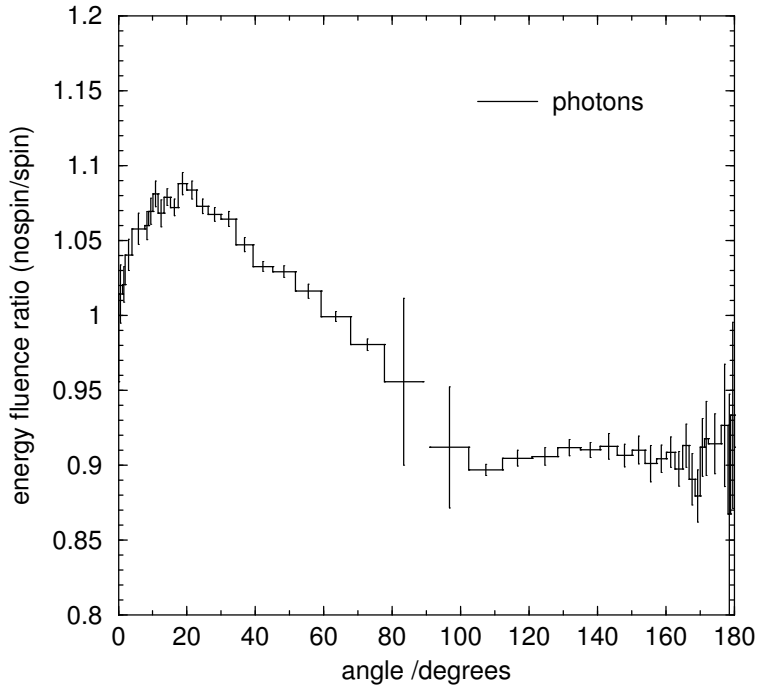

Figure 50: Ratio of photon energy fluence with Spin off to that with Spin on as a function of angle for a 10 MeV beam incident on lead. This is obviously the cause of the differences between EGSnrc and EGS4/PRESTA in this case.

7.1.2 Bremsstrahlung Angular Sampling

Figure **??** below shows the ratio of the photon energy fluence with "Brems angular sampling= Simple" (ie use only the leading term in the Koch-Motz distribution to determine the emission

angle of bremsstrahlung photons) to that with "Brems angular sampling= KM" (the default) as a function of angle for a 10 MeV beam on lead. The small differences at forward angles are enough to justify the default being "KM".

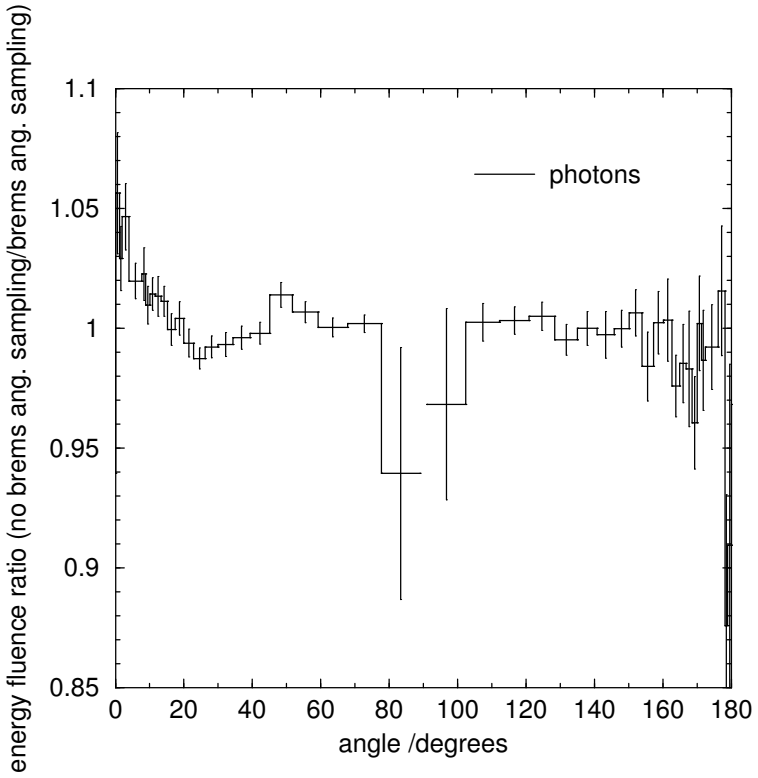

Figure 51: Ratio of photon energy fluence using only the leading term of the K-M distribution to determine angle of bremsstrahlung photons to that using the full K-M distribution as a function of angle for a 10 MeV beam incident on lead.

7.1.3 QA of Brem Splitting and Russian Roulette

As a basic test to see whether the bremsstrahlung splitting and charged particle Russian Roulette features of FLURZnrc cause any systematic differences in fluence, the 10 MeV beam on lead case was also simulated without bremsstrahlung splitting, and with 30x bremsstrahlung splitting plus charged particle Russian Roulette. Figure **??** below shows the ratio of photon fluence with 30x bremsstrahlung splitting (the standard case in this QA) to that with no splitting as a function of angle. Figure **??** shows the ratio of the photon fluence with 30x bremsstrahlung splitting plus charged particle Russian Roulette vs that with just 30x bremsstrahlung splitting as a function of angle. There are no statistically significant differences, as expected.

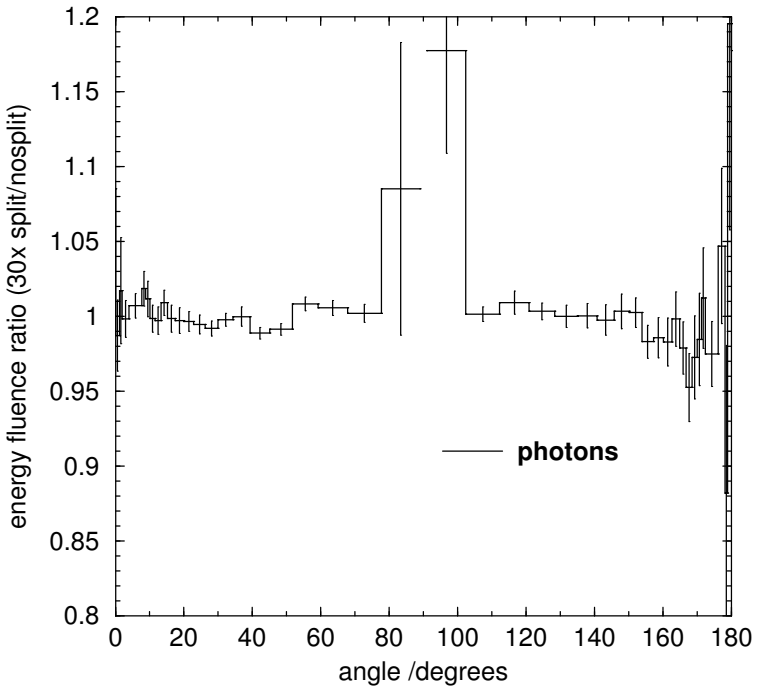

Figure 52: Ratio of photon energy fluence with 30x bremsstrahlung splitting (the standard case here) to that without bremsstrahlung splitting as a function of angle for a 10 MeV beam incident on lead.

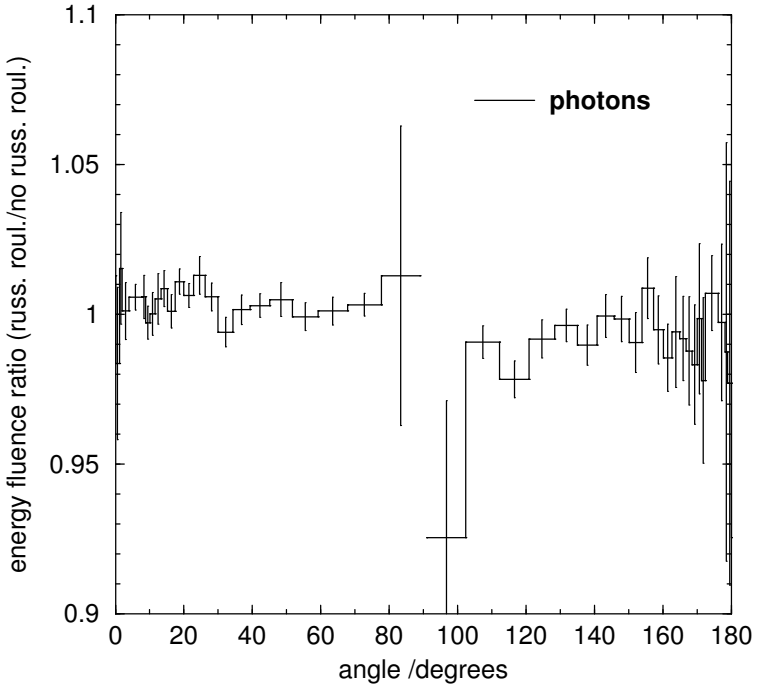

Figure 53: Ratio of photon energy fluence with 30x bremsstrahlung splitting and charged particle Russian Roulette to that with just 30x bremsstrahlung splitting (the standard case) as a function of angle for a 10 MeV beam incident on lead.

7.2 Overall QA Results for Various Beam Energies

Plots of energy fluence vs angle for 100 keV, 10 MeV, 100 MeV and 10 GeV sources are shown in Figures **??**-**??**.

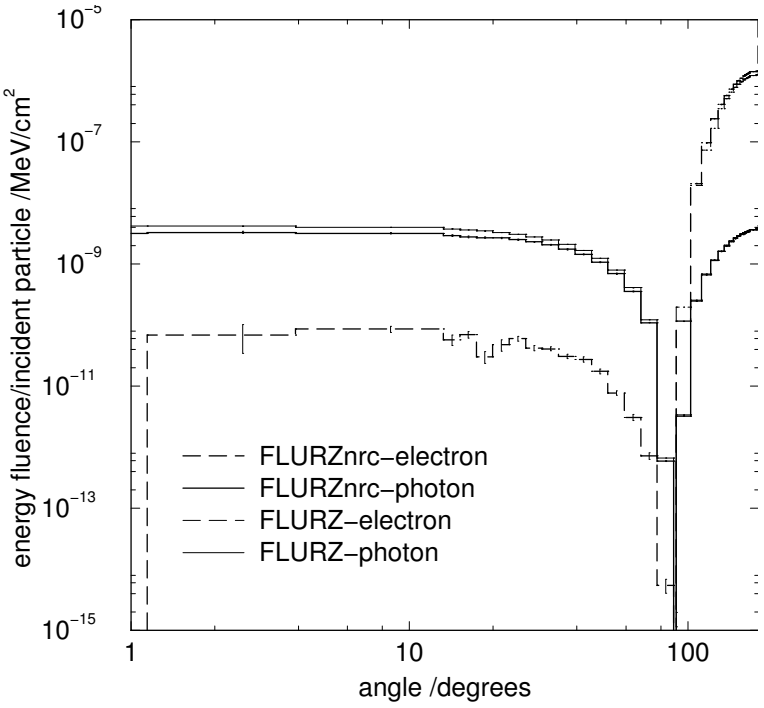

Figure 54: Energy fluence vs angle for a 100 keV beam on lead.

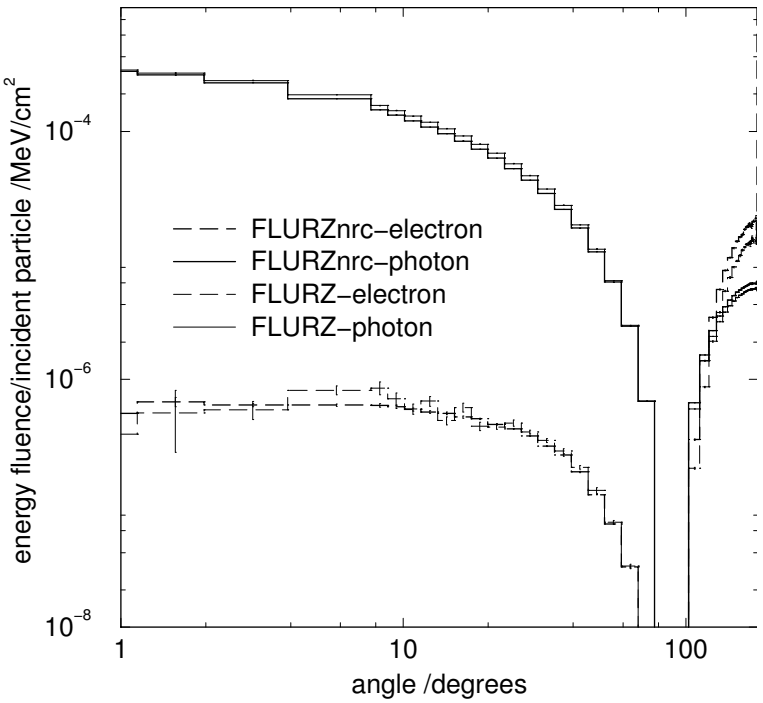

Figure 55: Energy fluence vs angle for a 10 MeV beam on lead.

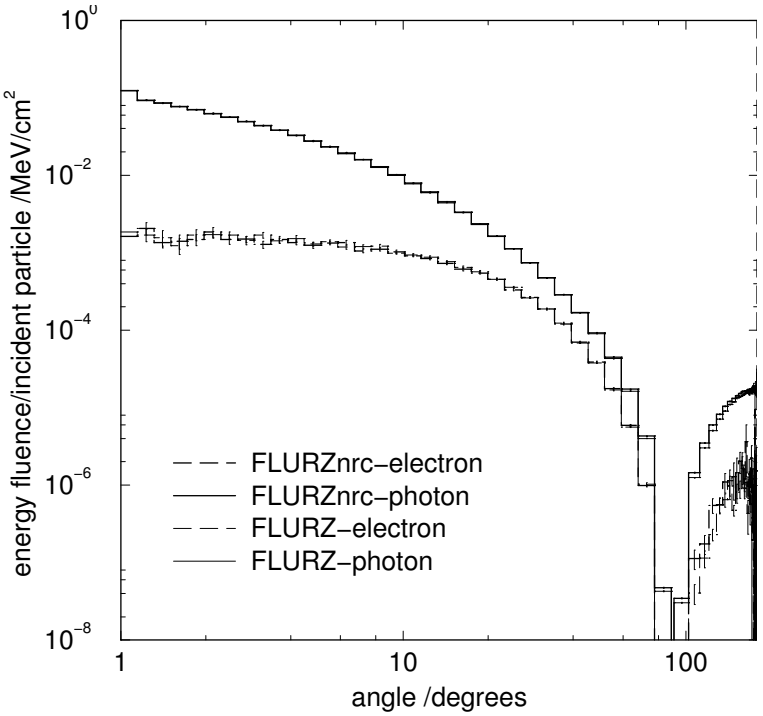

Figure 56: Energy fluence vs angle for a 100 MeV beam on lead.

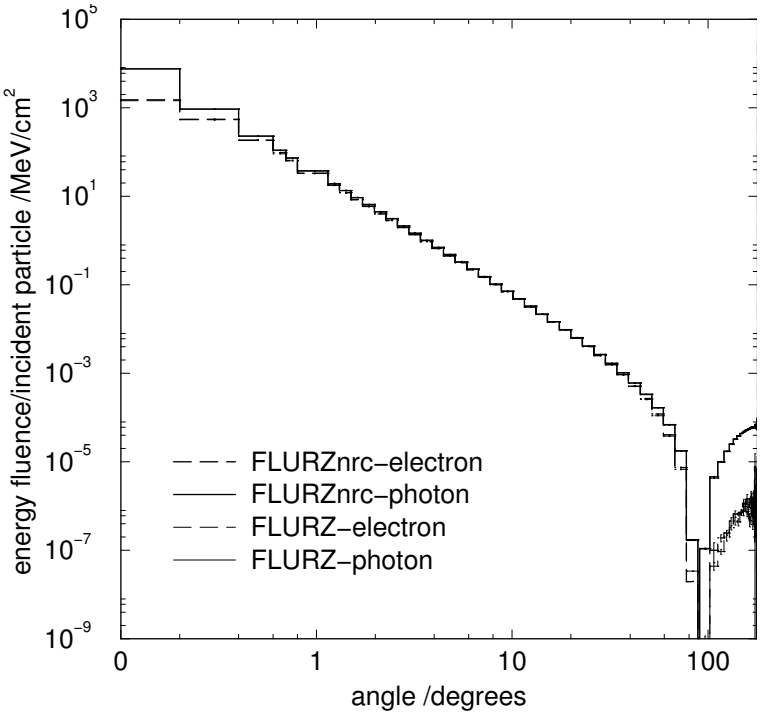

Figure 57: Energy fluence vs angle for a 10 GeV beam on lead.

Figures **??**-**??** below plot the ratio of the energy fluence obtained using FLURZnrc to that obtained using FLURZ as a function of angle. These plots have been scaled to display the photon energy fluence ratio which means that, in many cases, the electron energy fluence ratio is off the scale. Also, in some plots, the error bars on the electron energy fluence ratios were omitted to avoid confusion.

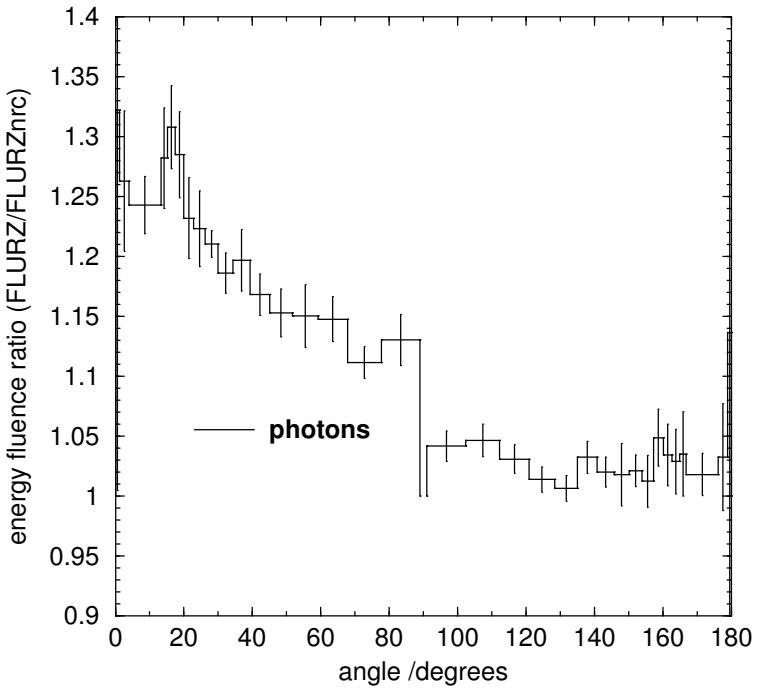

Figure 58: Energy fluence ratio (FLURZnrc/FLURZ) for a 100 keV beam on lead.

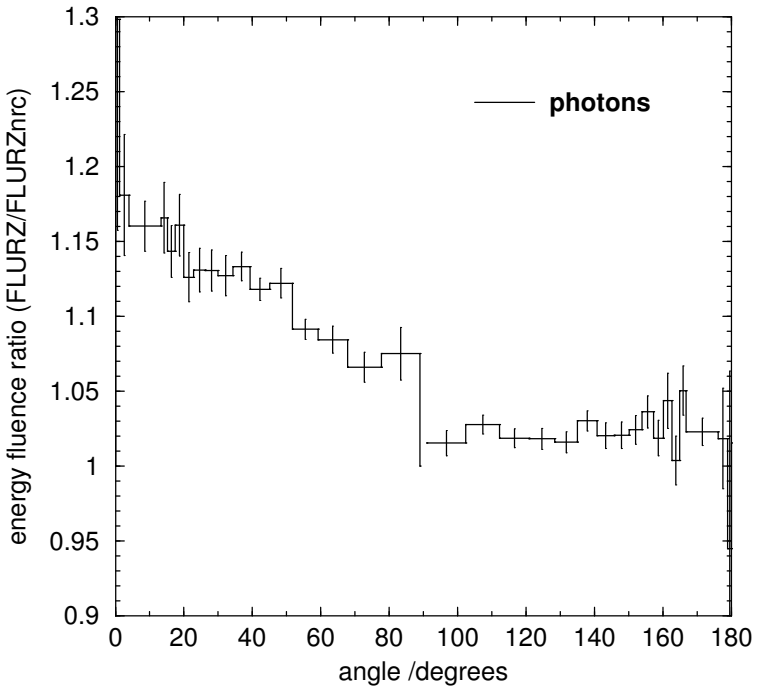

Figure 59: Energy fluence ratio (FLURZnrc/FLURZ) for a 500 keV beam on lead.

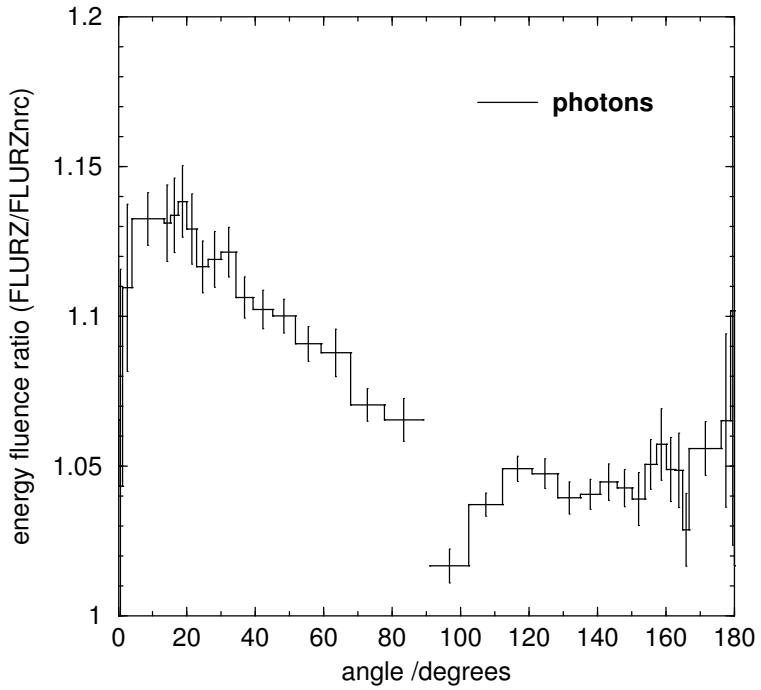

Figure 60: Energy fluence ratio (FLURZnrc/FLURZ) for a 1 MeV beam on lead.

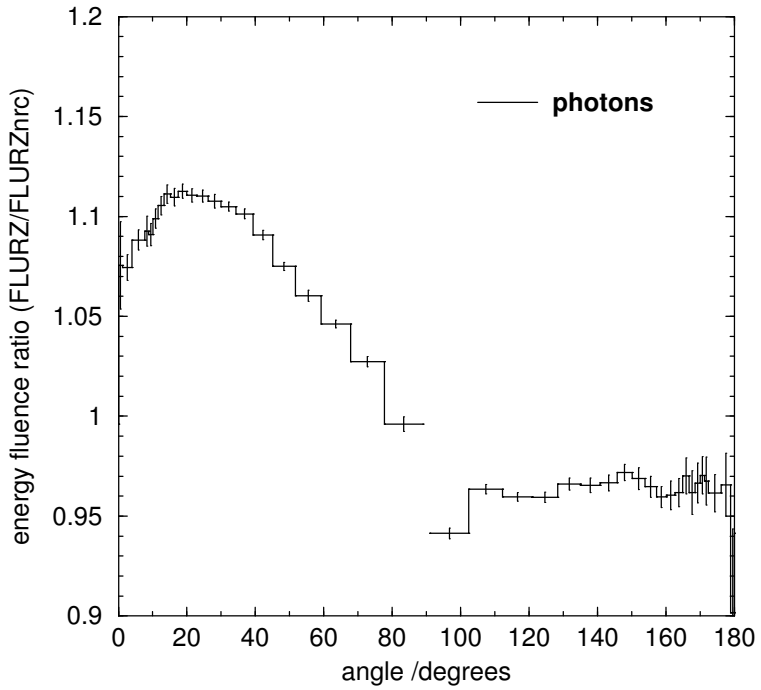

Figure 61: Energy fluence ratio (FLURZnrc/FLURZ) for a 5 MeV beam on lead.

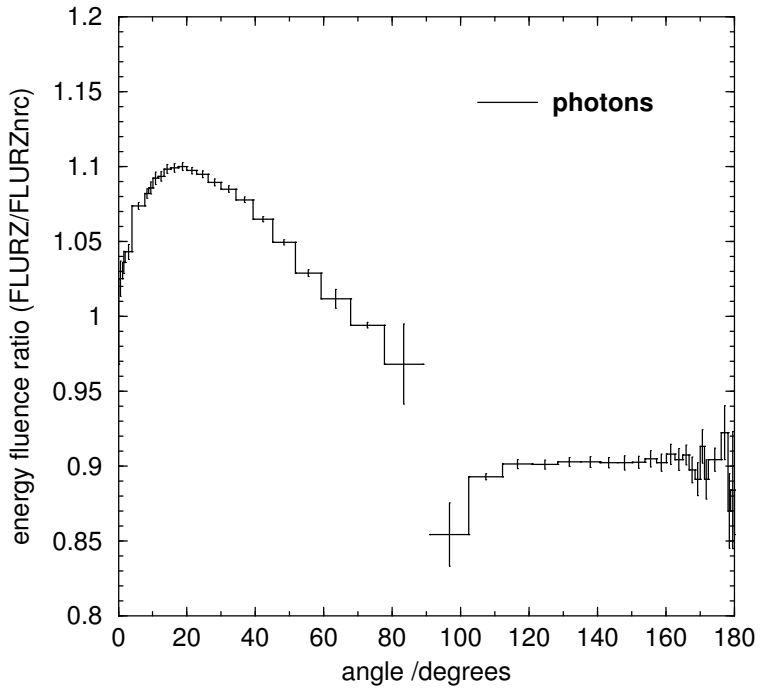

Figure 62: Energy fluence ratio (FLURZnrc/FLURZ) for a 10 MeV beam on lead.

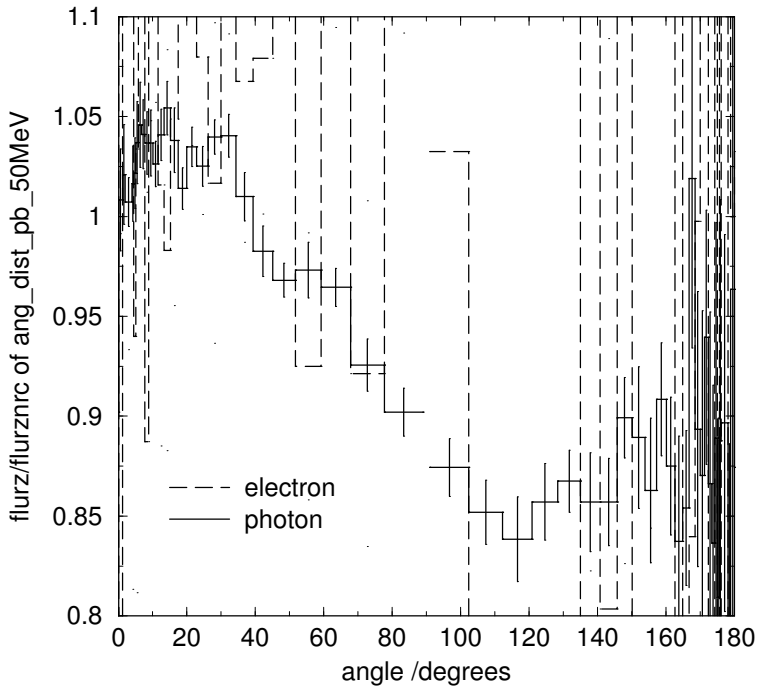

Figure 63: Energy fluence ratio (FLURZnrc/FLURZ) for a 50 MeV beam on lead.

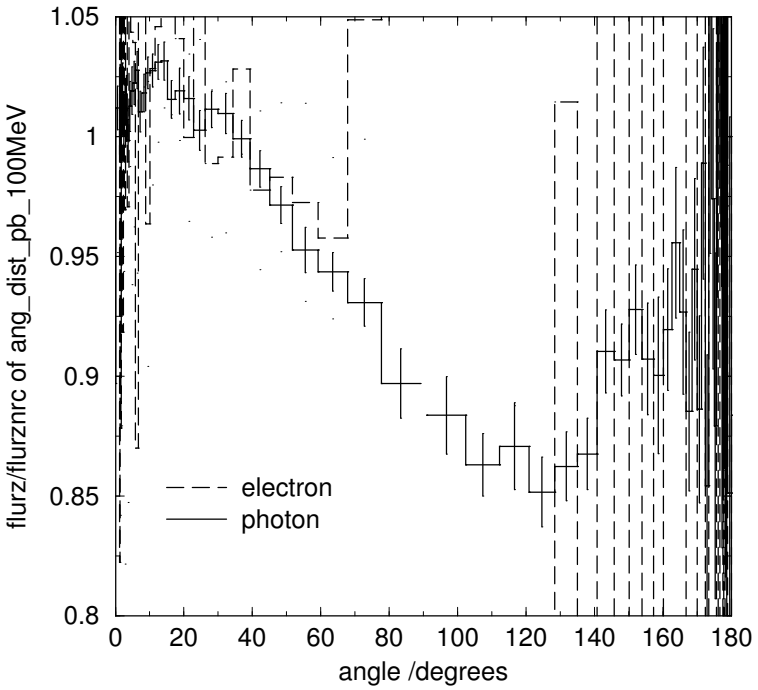

Figure 64: Energy fluence ratio (FLURZnrc/FLURZ) for a 100 MeV beam on lead.

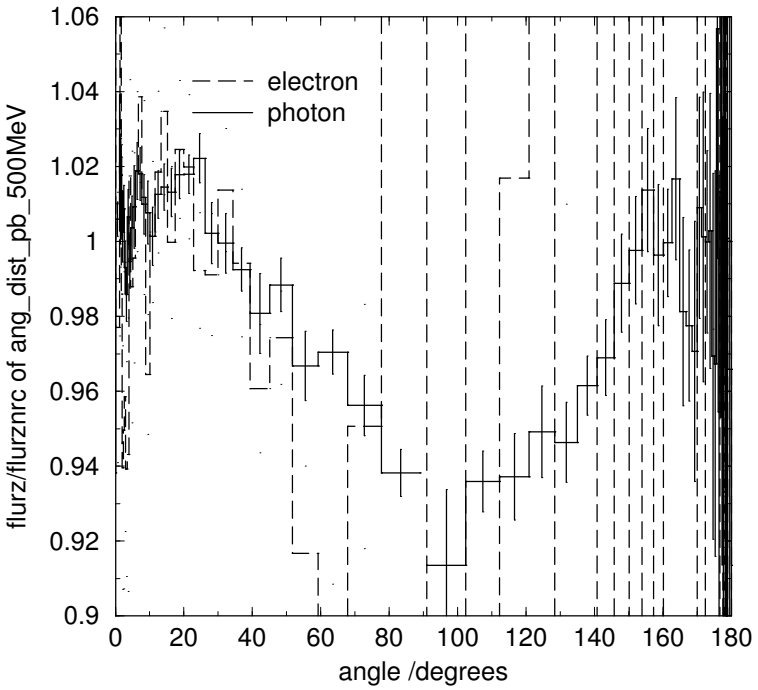

Figure 65: Energy fluence ratio (FLURZnrc/FLURZ) for a 500 MeV beam on lead.

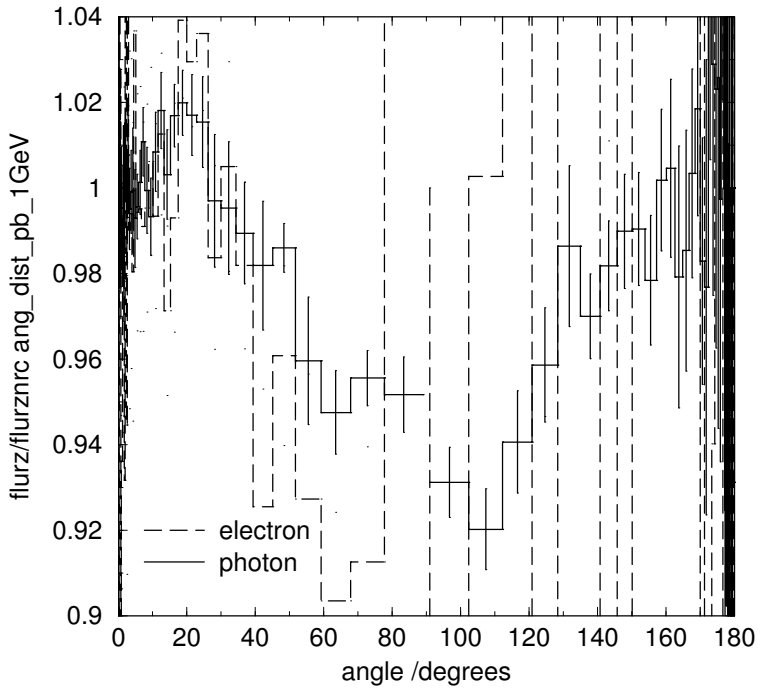

Figure 66: Energy fluence ratio (FLURZnrc/FLURZ) for a 1 GeV beam on lead.

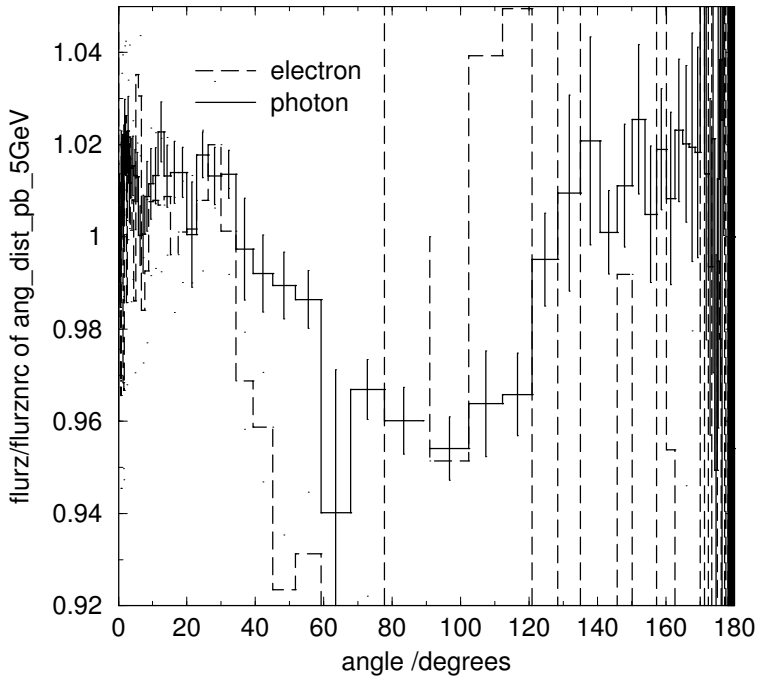

Figure 67: Energy fluence ratio (FLURZnrc/FLURZ) for a 5 GeV beam on lead.

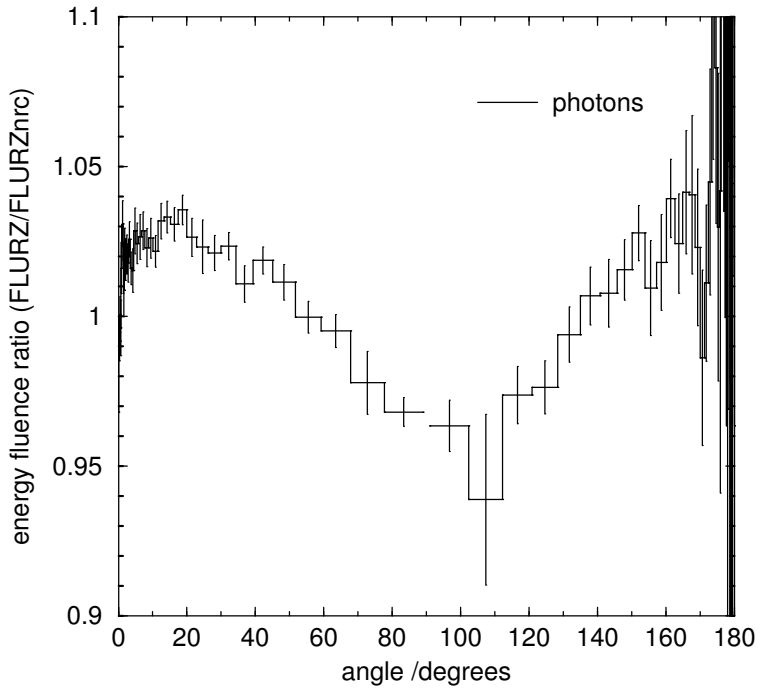

Figure 68: Energy fluence ratio (FLURZnrc/FLURZ) for a 10 GeV beam on lead.

7.3 Beryllium target

Simulation parameters for determining angular energy fluence of photons and electrons from beryllium targets are shown in Table **??** below.

Table 5: Simulation parameters used to determine the angular distribution of photon and electron energy fluence from beryllium targets using FLURZnrc and FLURZ. In all cases, `PCUT` was 0.01 MeV.

energy	target thickness (cm)	target radius (cm)	no. histories		splitting no.		`ECUT` (MeV)
			FLURZnrc	FLURZ	FLURZnrc	FLURZ	
100 keV	0.00946	1.9999	$10x10^6$	$200x10^6$	30	30	0.521
500 keV	0.1184	1.9999	$1x10^6$	$10x10^6$	30	30	0.521
1 MeV	0.29546	1.9999	$1x10^6$	$1x10^6$	30	30	0.521
5 MeV	1.73702	1.9999	$1x10^6$	$1x10^6$	30	30	0.700
10 MeV	3.41126	3.44677	$1x10^6$	$1x10^6$	30	30	0.700
50 MeV	14.33982	13.50782	500,000	$1x10^6$	30	30	0.700
100 MeV	14.33982	13.50782	500,000	$1x10^6$	30	30	1.511
500 MeV	14.33982	13.50782	250,000	$1x10^6$	30	30	1.511
1 GeV	14.33982	13.50782	200,000	$1x10^6$	30	30	1.511
5 GeV	14.33982	13.50782	100,000	$1x10^6$	30	30	1.511
10 GeV	14.33982	13.50782	100,000	$1x10^6$	30	30	1.511

Plots of energy fluence vs angle for 100 keV, 10 MeV, 100 MeV and 10 GeV sources are shown in Figures **??**-**??**.

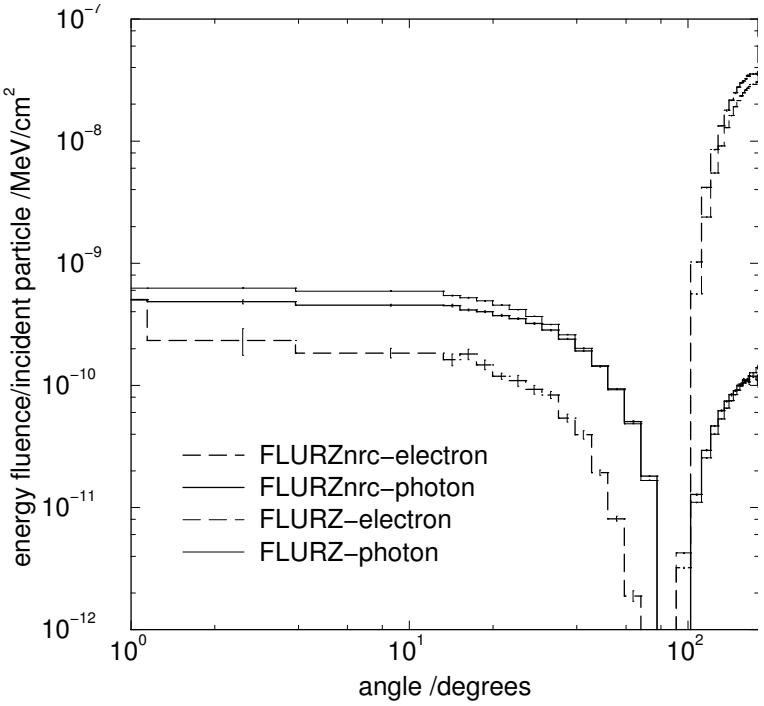

Figure 69: Energy fluence vs angle for a 100 keV beam on beryllium.

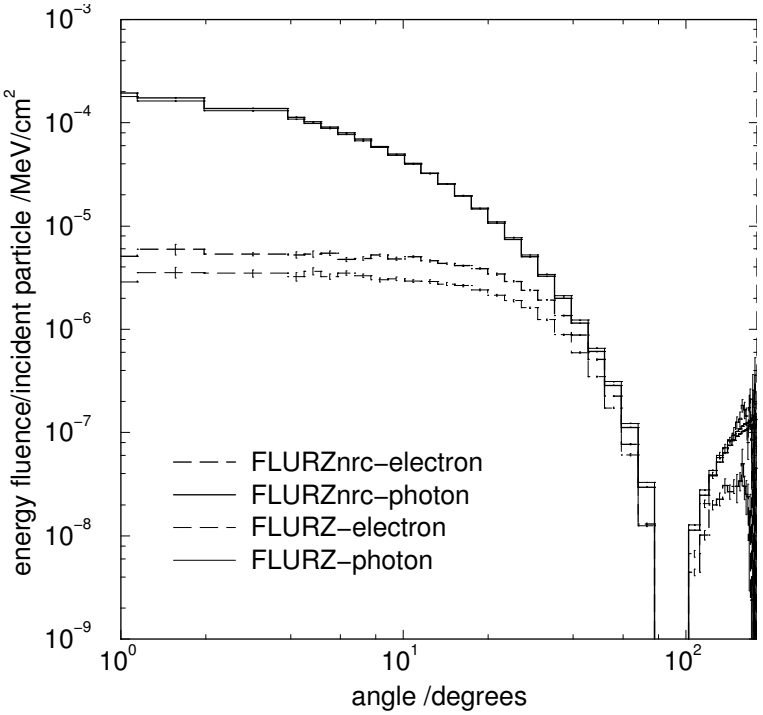

Figure 70: Energy fluence vs angle for a 10 MeV beam on beryllium.

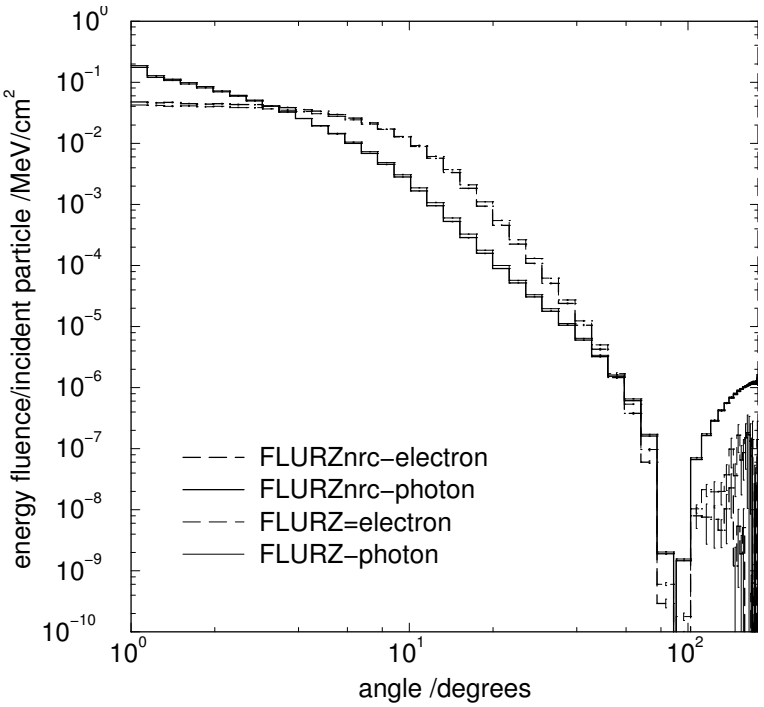

Figure 71: Energy fluence vs angle for a 100 MeV beam on beryllium.

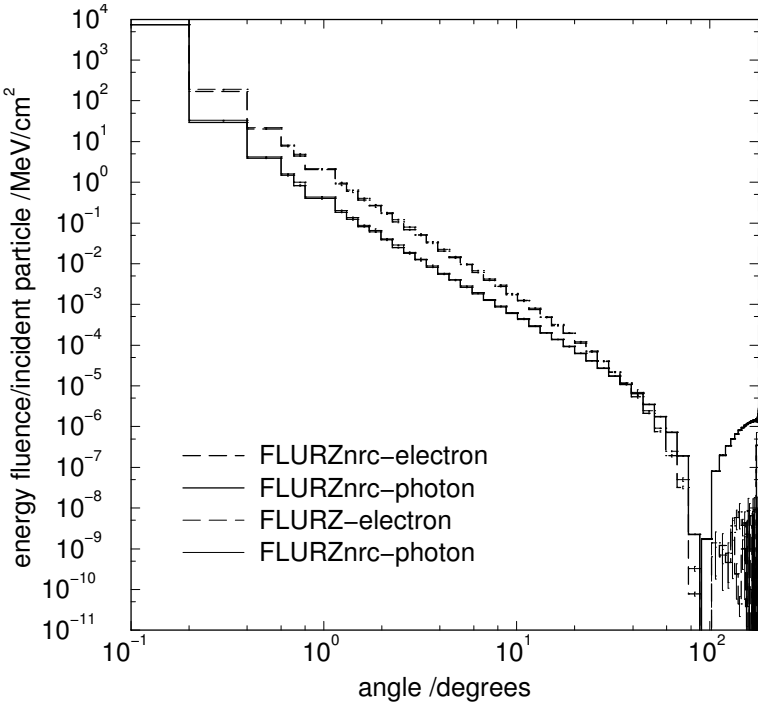

Figure 72: Energy fluence vs angle for a 10 GeV beam on beryllium.

Figures ??-?? below plot the ratio of the energy fluence obtained using FLURZnrc to that obtained using FLURZ as a function of angle.

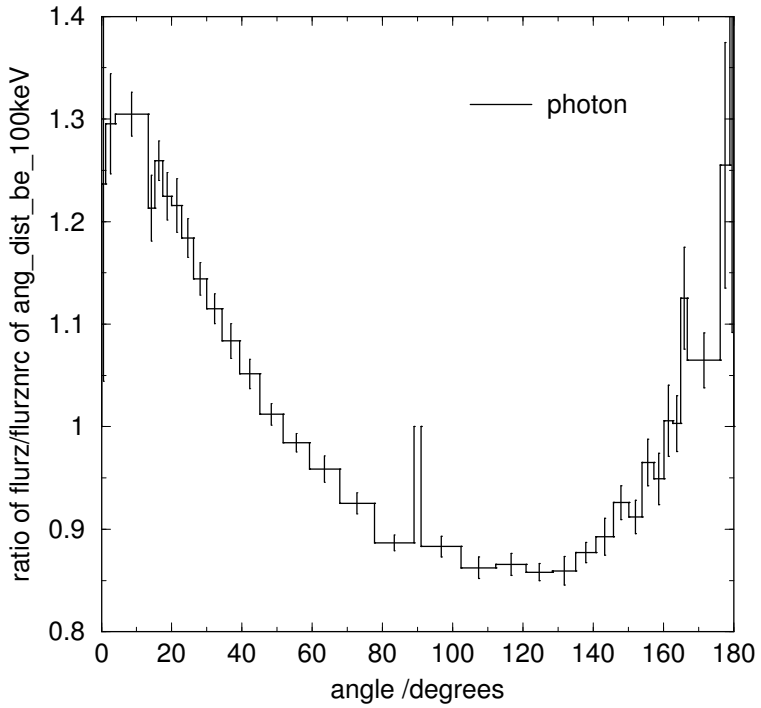

Figure 73: Energy fluence ratio (FLURZnrc/FLURZ) for a 100 keV beam on beryllium.

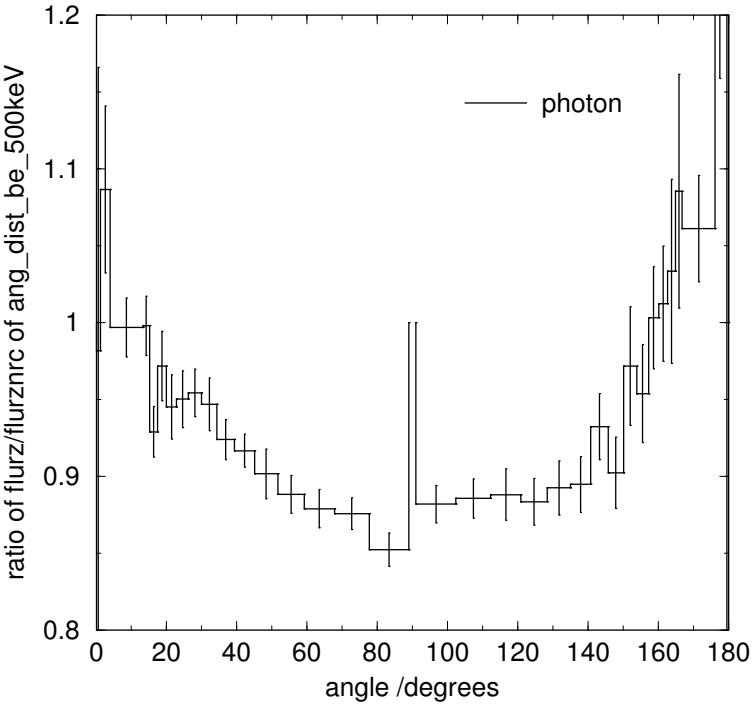

Figure 74: Energy fluence ratio (FLURZnrc/FLURZ) for a 500 keV beam on beryllium.

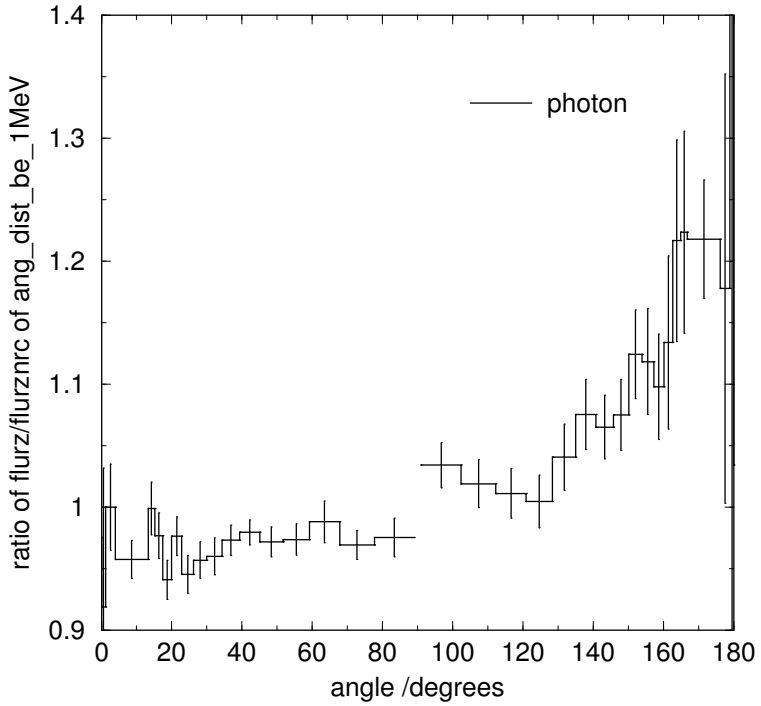

Figure 75: Energy fluence ratio (FLURZnrc/FLURZ) for a 1 MeV beam on beryllium.

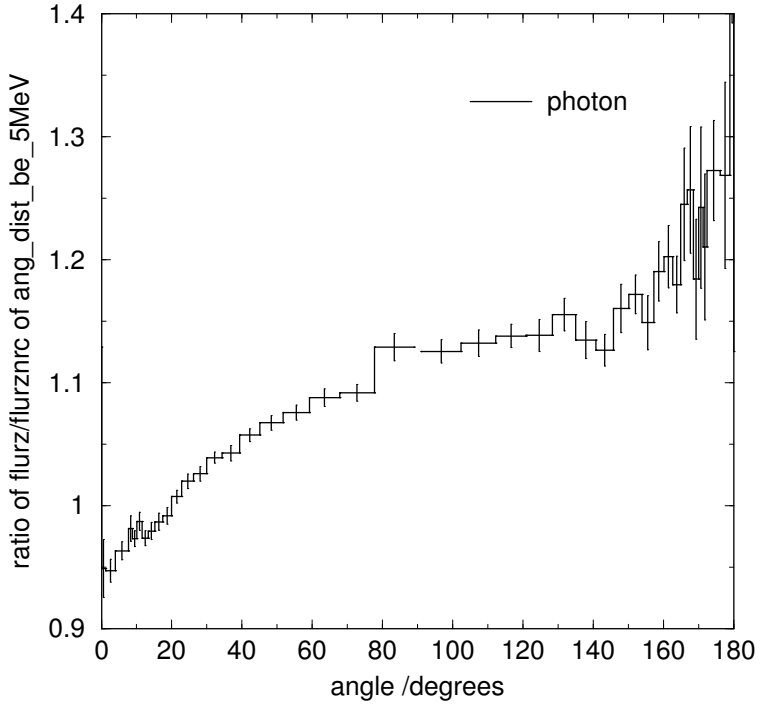

Figure 76: Energy fluence ratio (FLURZnrc/FLURZ) for a 5 MeV beam on beryllium.

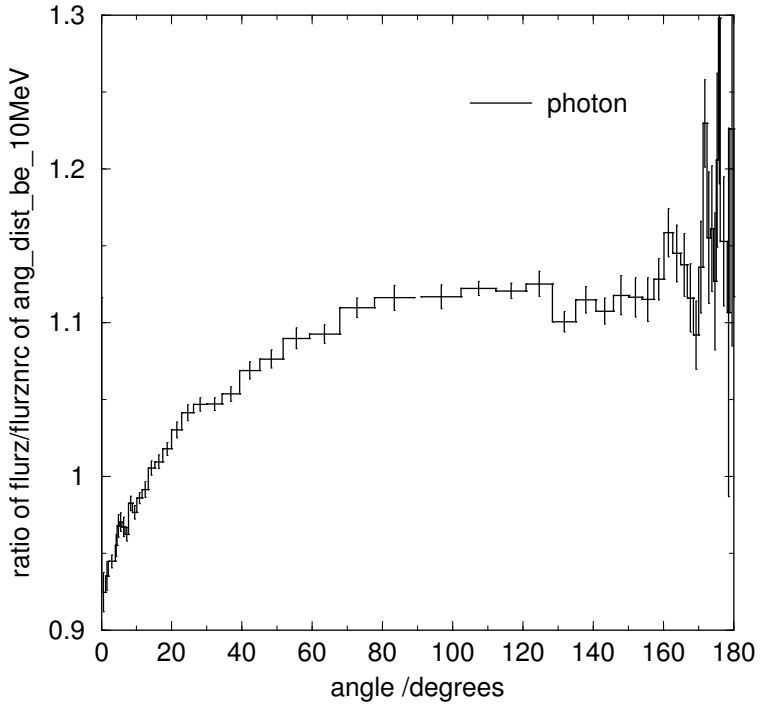

Figure 77: Energy fluence ratio (FLURZnrc/FLURZ) for a 10 MeV beam on beryllium.

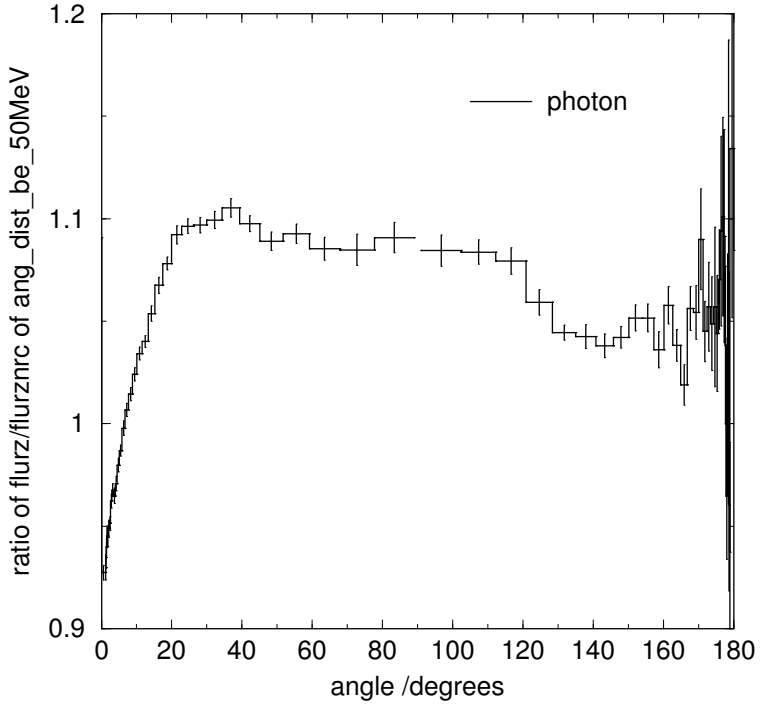

Figure 78: Energy fluence ratio (FLURZnrc/FLURZ) for a 50 MeV beam on beryllium.

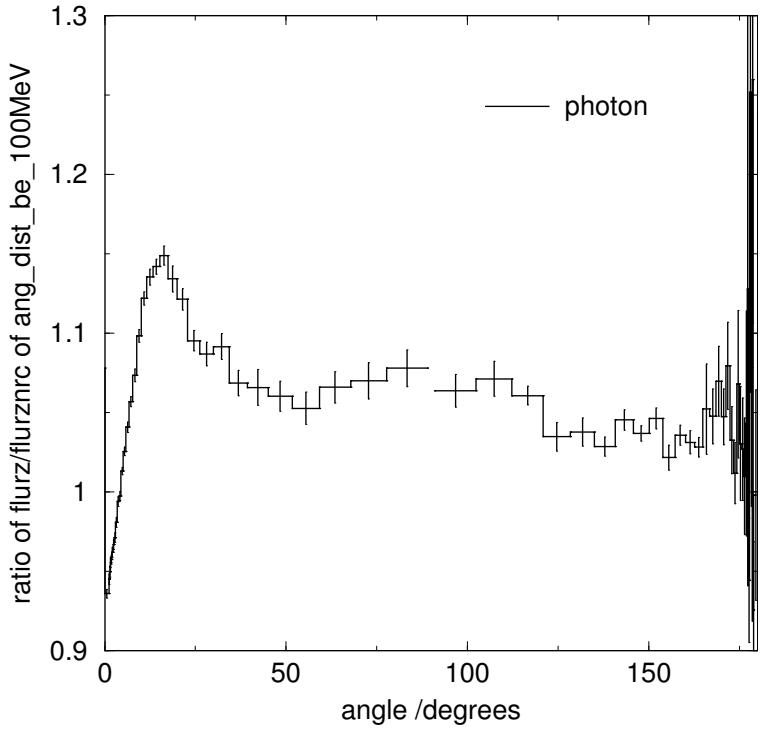

Figure 79: Energy fluence ratio (FLURZnrc/FLURZ) for a 100 MeV beam on beryllium.

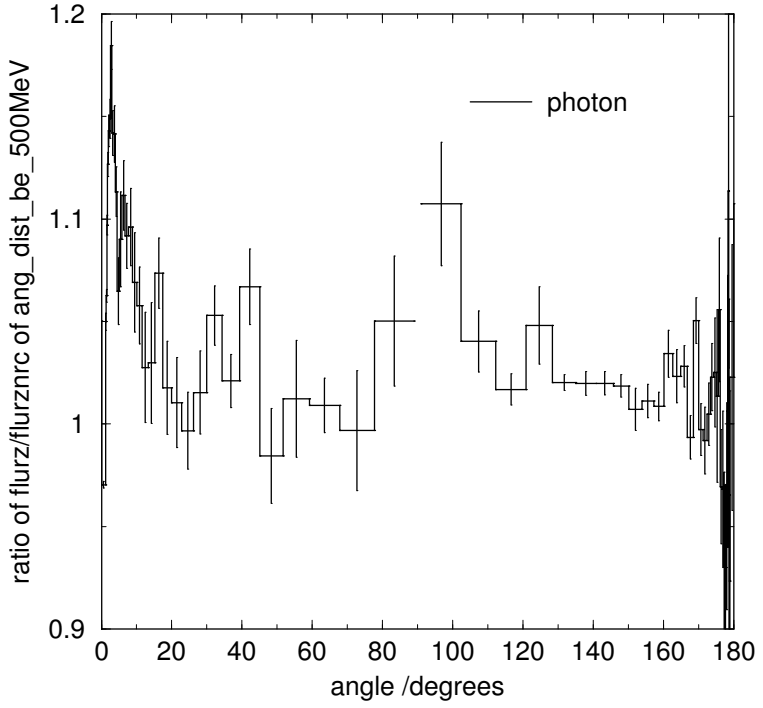

Figure 80: Energy fluence ratio (FLURZnrc/FLURZ) for a 500 MeV beam on beryllium.

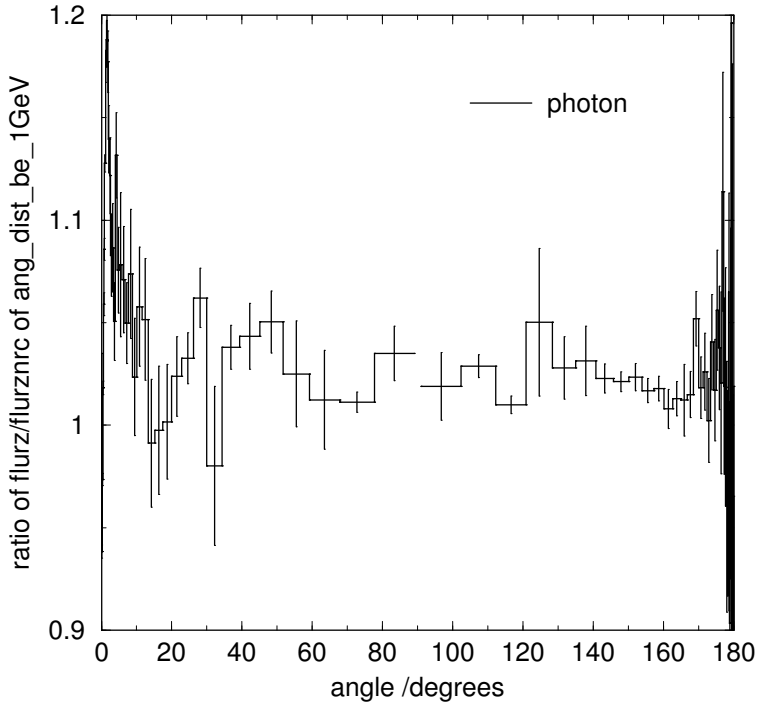

Figure 81: Energy fluence ratio (FLURZnrc/FLURZ) for a 1 GeV beam on beryllium.

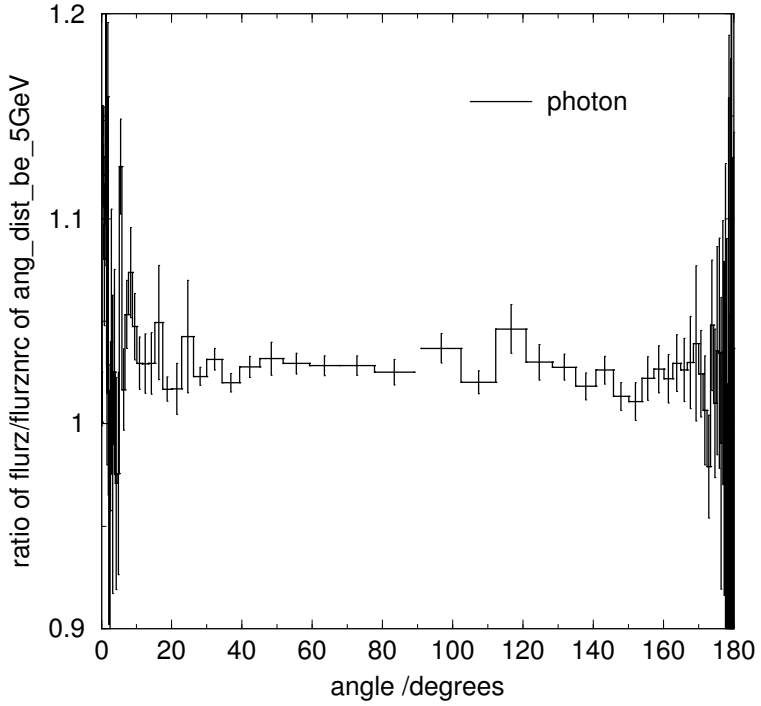

Figure 82: Energy fluence ratio (FLURZnrc/FLURZ) for a 5 GeV beam on beryllium.

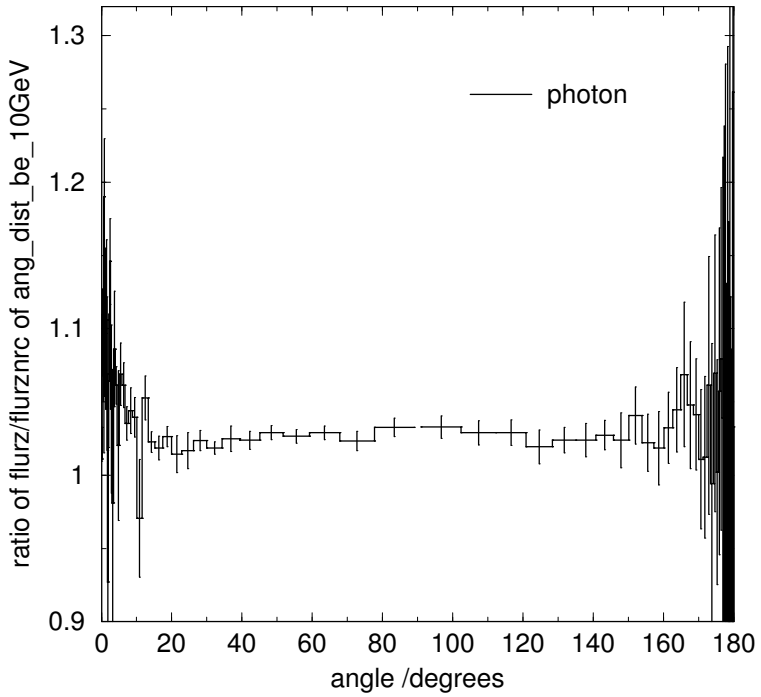

Figure 83: Energy fluence ratio (FLURZnrc/FLURZ) for a 10 GeV beam on beryllium.

8 Energy Spectra at Various Angles

Using FLURZ/FLURZnrc with the same simulation parameters as those used to determine the angular distribution of fluence, we examined photon/electron energy spectra at 3 different angles, 0^o, 42^o and 138^o. In some cases, we increased the number of histories to improve statistics. In addition, at the lower energies, we combined the 2 or 3 innermost radial bins (up to a maximum angle of $< 5^o$) to improve statistics in the 0^o spectra.

8.1 Results for Lead Targets

8.1.1 QA of Brem Splitting and Russian Roulette

In order to ensure that the bremsstrahlung splitting option is not introducing artifacts in photon spectra, we compared cases with 1x splitting (10x10^6 histories, no Russ. Roul.), 100x splitting (1x10^6 histories, with Russ. Roul.) and 1000x splitting (100,000 histories, with Russ. Roul.) to the base case with 30x splitting (1x10^6 histories, no Russ. Roul.) for a 10 MeV beam on lead. The ratios of the photon spectra for the 3 angles are shown in Figures **??**-**??** below. Within uncertainty, bremsstrahlung splitting does not alter the photon spectra.

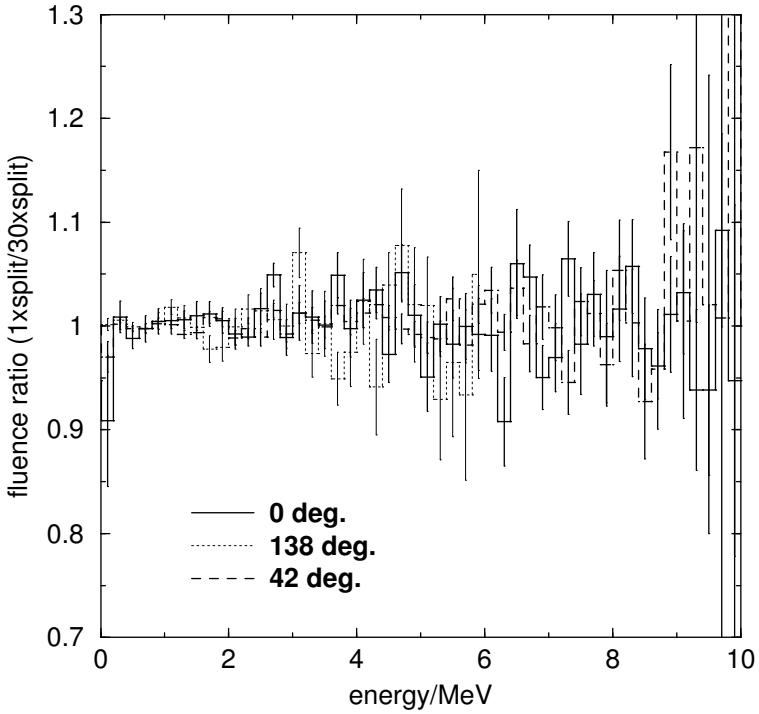

Figure 84: Ratio of photon spectra with 1x bremsstrahlung splitting (ie no splitting) to photon spectra with 30x bremsstrahlung splitting for a 10 MeV beam on lead.

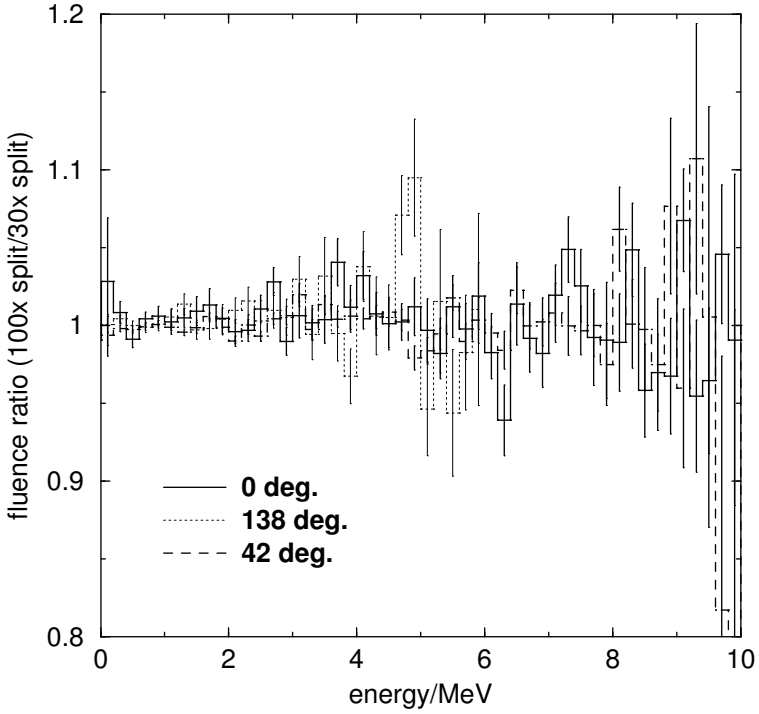

Figure 85: Ratio of photon spectra with 100x bremsstrahlung splitting to those with 30x bremsstrahlung splitting for a 10 MeV beam on lead.

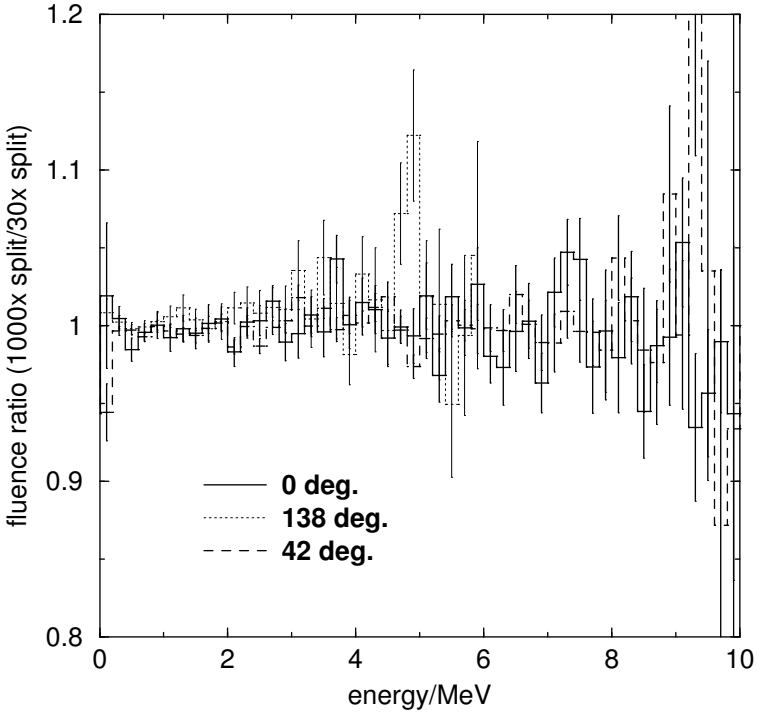

Figure 86: Ratio of photon spectra with 1000x bremsstrahlung splitting to those with 30x bremsstrahlung splitting for a 10 MeV beam on lead.

We also examined the effect of charged particle Russian Roulette in detail by comparing the photon and electron spectra for the 10 MeV beam on lead with 30x bremsstrahlung splitting with Russian Roulette off and Russian Roulette on. Figure **??** below shows the electron spectra at the 3 angles and Figure **??** shows the ratios of the electron spectra with Russian Roulette on to those with Russian Roulette off. The ratios of the photon spectra are shown in Figure **??**. The figures show that Russian Roulette does not introduce any artifacts in either the photon or electron spectra.

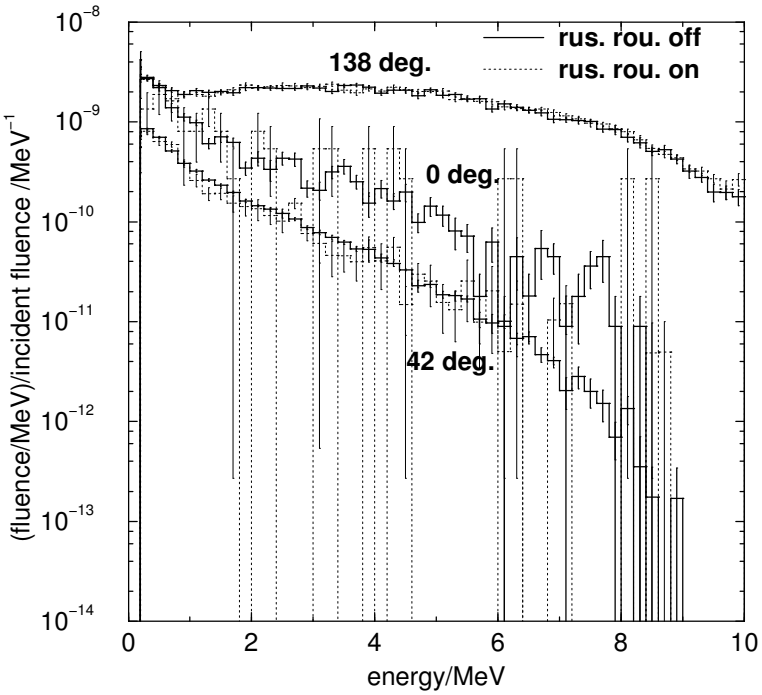

Figure 87: Electron spectra at 0^o, 42^o and 138^o for a 10 MeV beam on lead with 30x bremsstrahlung splitting with and without Russian Roulette.

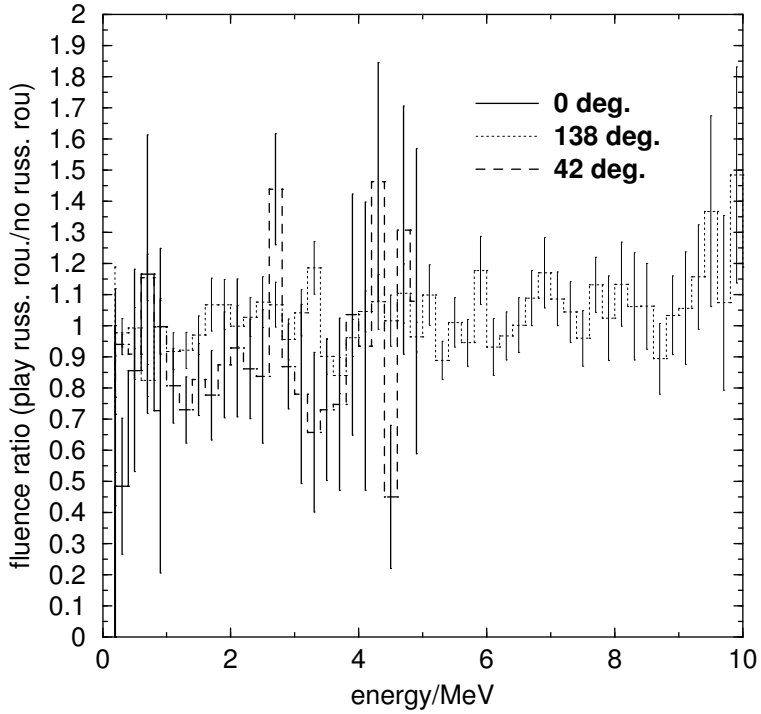

Figure 88: Ratio of electron spectra for a 10 MeV beam on lead with 30x bremsstrahlung splitting with Russian Roulette on to spectra with Russian Roulette off.

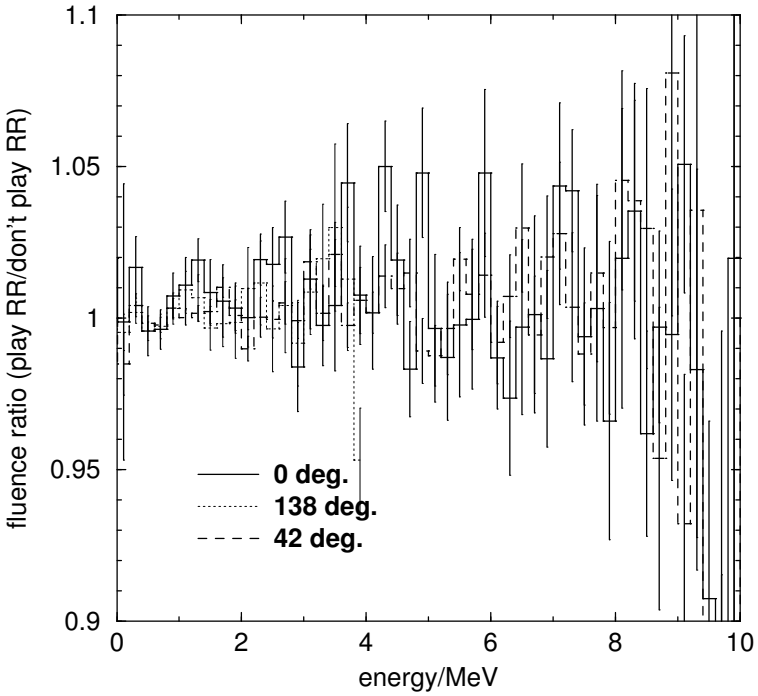

Figure 89: Ratio of photon spectra for a 10 MeV beam on lead with 30x bremsstrahlung splitting with Russian Roulette on to spectra with Russian Roulette off.

8.1.2 Effect of Spin

Figure **??** below shows the ratio of the photon spectra at 0, 42 and 138 degrees calculated with FLURZ to those calculated with FLURZnrc with spin effects off for the 10 MeV beam on lead. Within statistics, the spectra are the same, indicating that, at 10 MeV, differences in photon spectra between FLURZ and FLURZnrc are primarily due to spin effects.

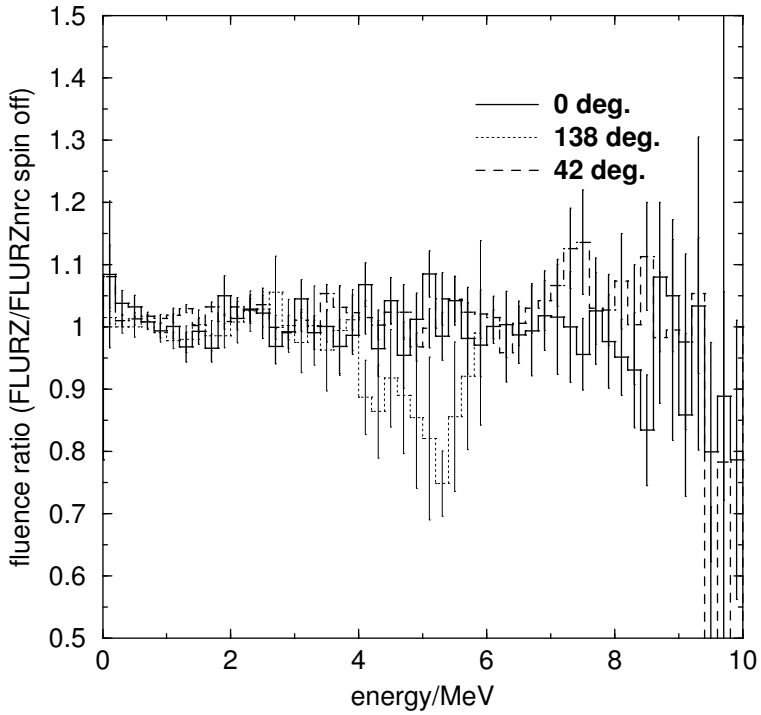

Figure 90: Ratio of photon spectra for a 10 MeV beam on lead calculated with FLURZ to those calculated with FLURZnrc with spin effects off.

8.1.3 Overall Results

The photon spectra at 0, 42 and 138 degrees for all incident beam energies calculated with FLURZ and with FLURZnrc are shown below along with the ratio of FLURZ-calculated spectra to those calculated using FLURZnrc.

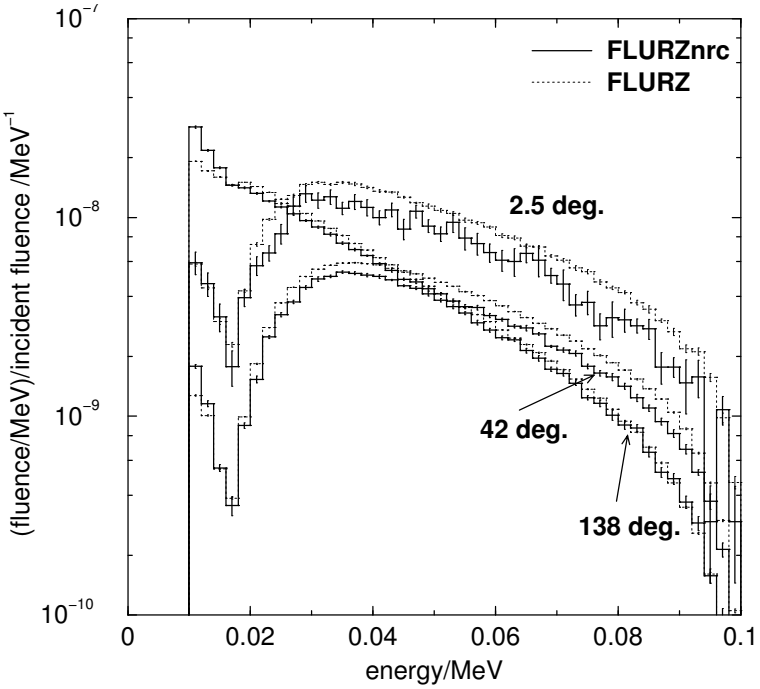

Figure 91: Photon spectra calculated for a 100 keV beam on lead.

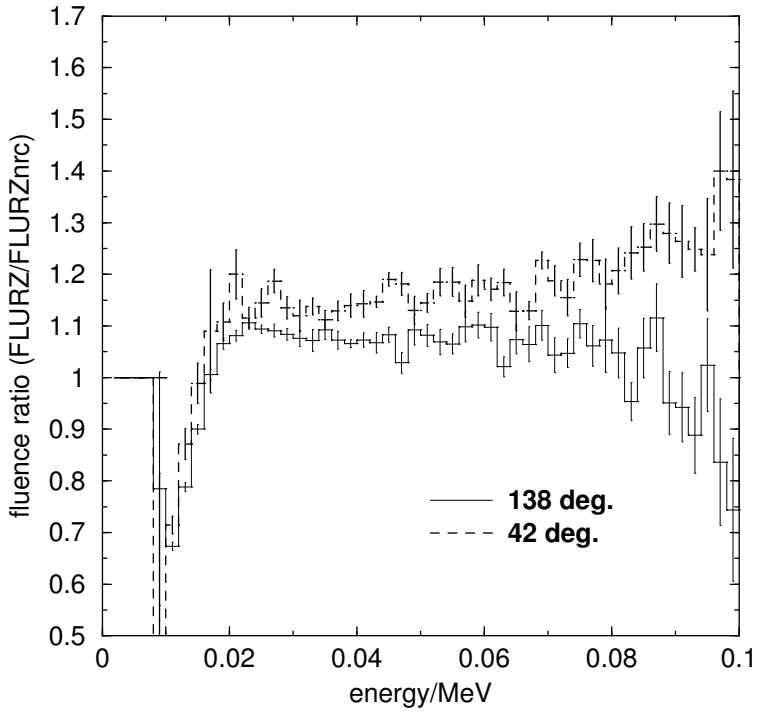

Figure 92: Ratio of FLURZ-calculated photon spectra to FLURZnrc-calculated spectra for 100 keV beam on lead.

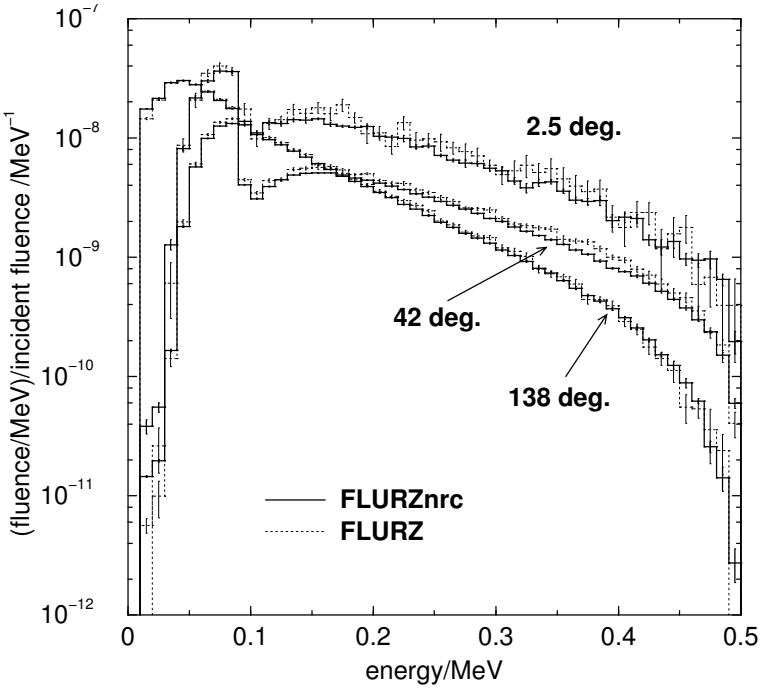

Figure 93: Photon spectra calculated for a 500 keV beam on lead.

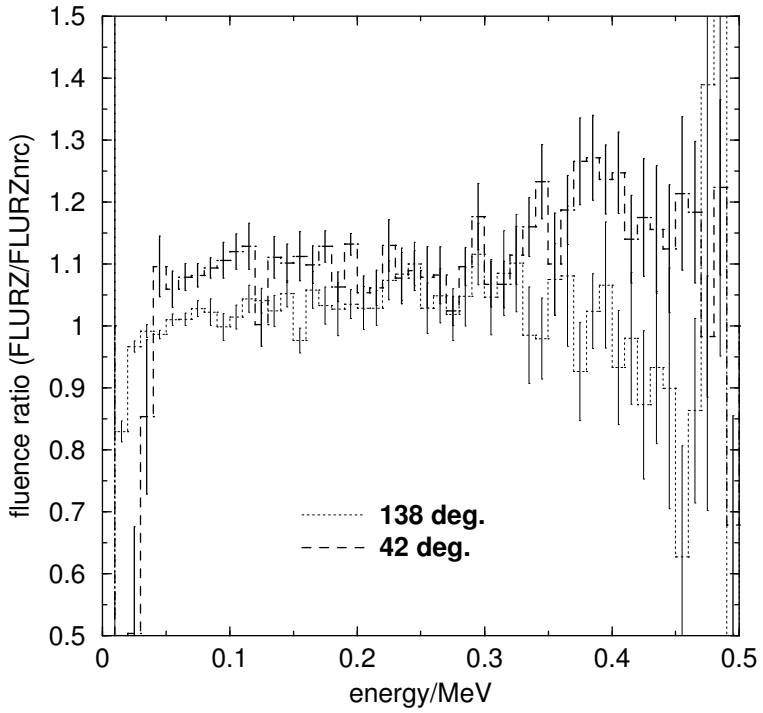

Figure 94: Ratio of FLURZ-calculated photon spectra to FLURZnrc-calculated spectra for 500 keV beam on lead.

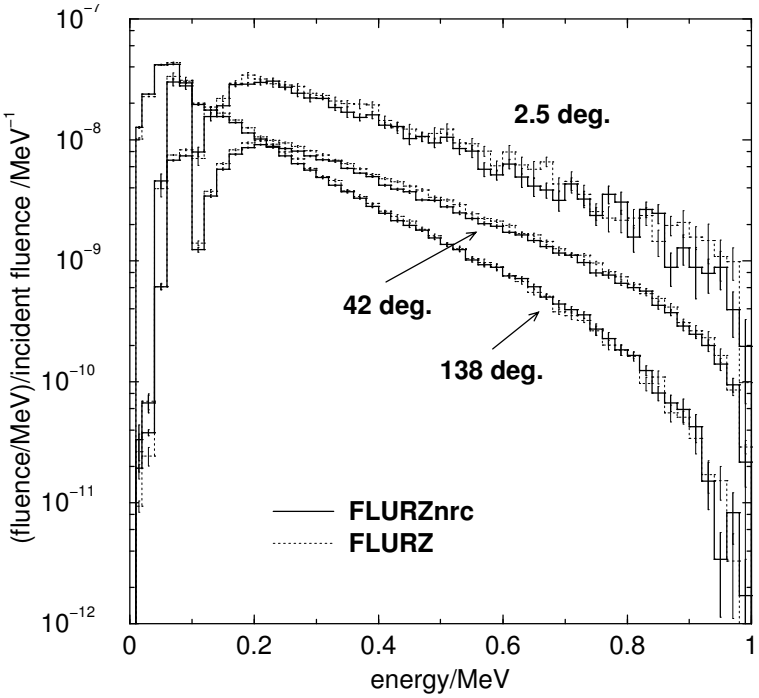

Figure 95: Photon spectra calculated for a 1 MeV beam on lead.

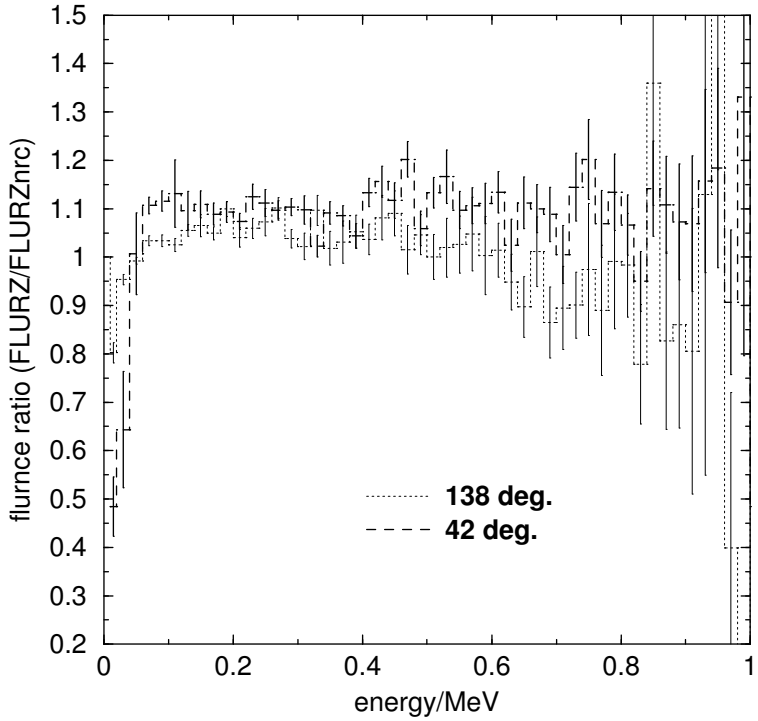

Figure 96: Ratio of FLURZ-calculated photon spectra to FLURZnrc-calculated spectra for 1 MeV beam on lead.

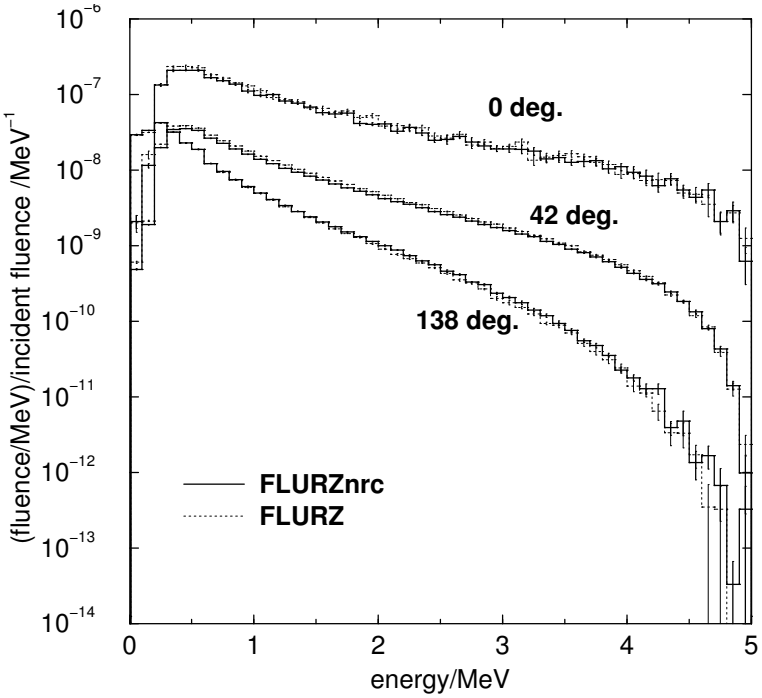

Figure 97: Photon spectra calculated for a 5 MeV beam on lead.

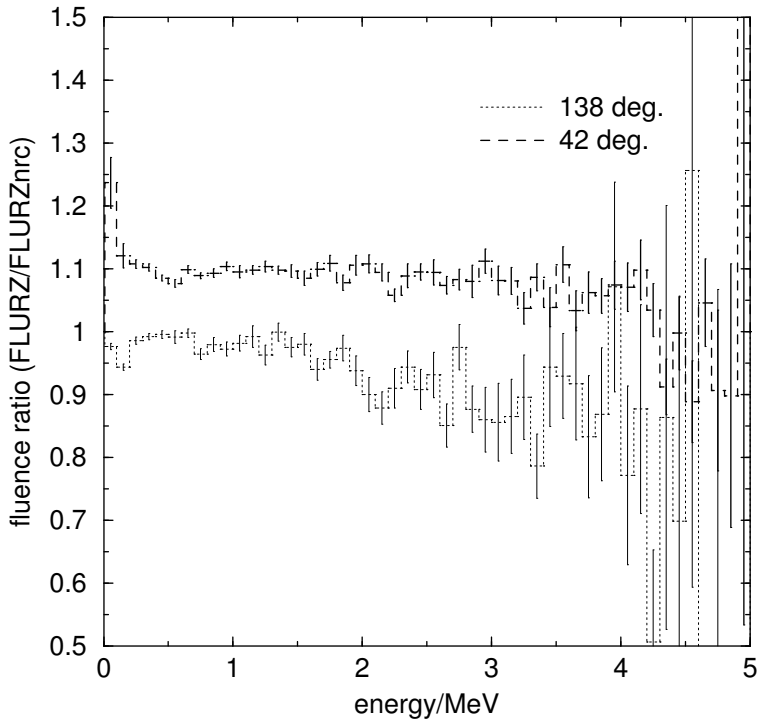

Figure 98: Ratio of FLURZ-calculated photon spectra to FLURZnrc-calculated spectra for 5 MeV beam on lead.

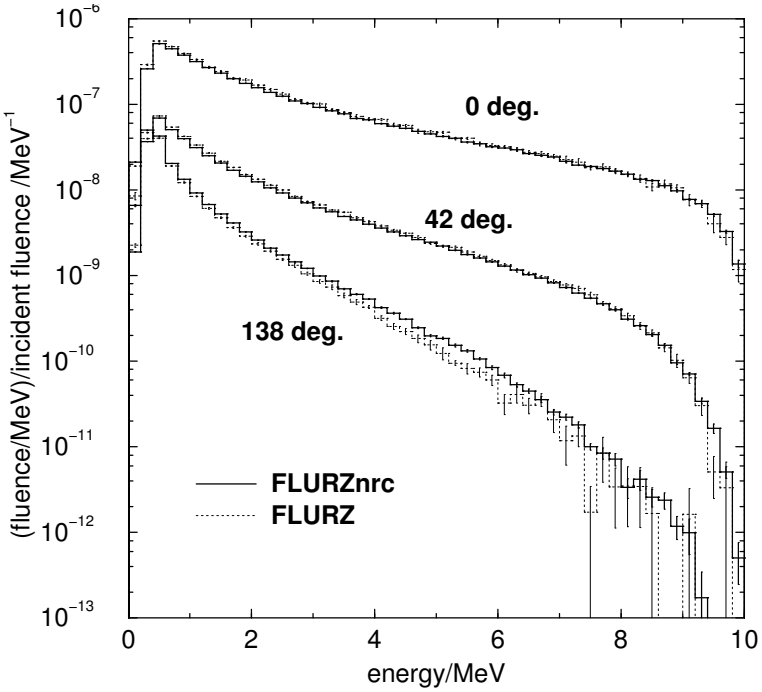

Figure 99: Photon spectra calculated for a 10 MeV beam on lead.

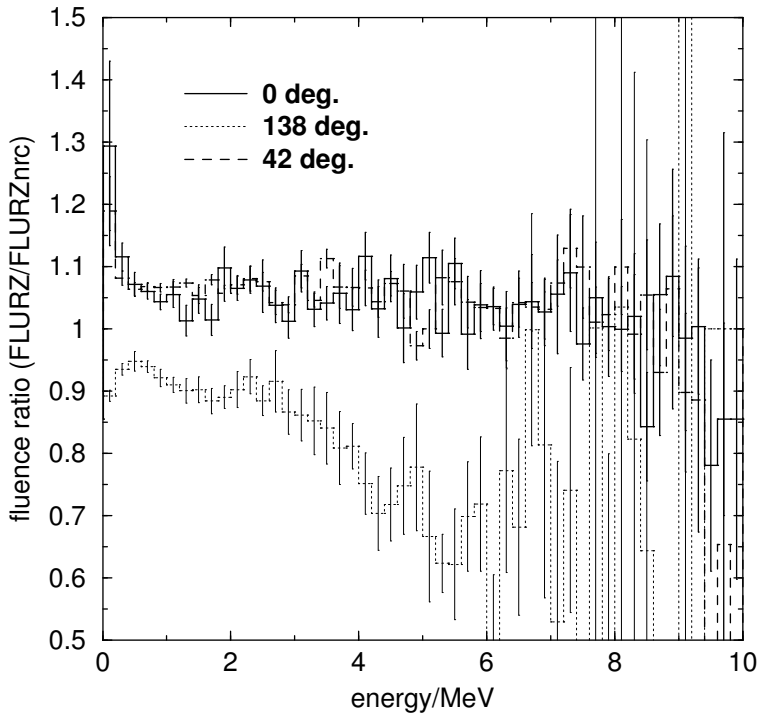

Figure 100: Ratio of FLURZ-calculated photon spectra to FLURZnrc-calculated spectra for 10 MeV beam on lead.

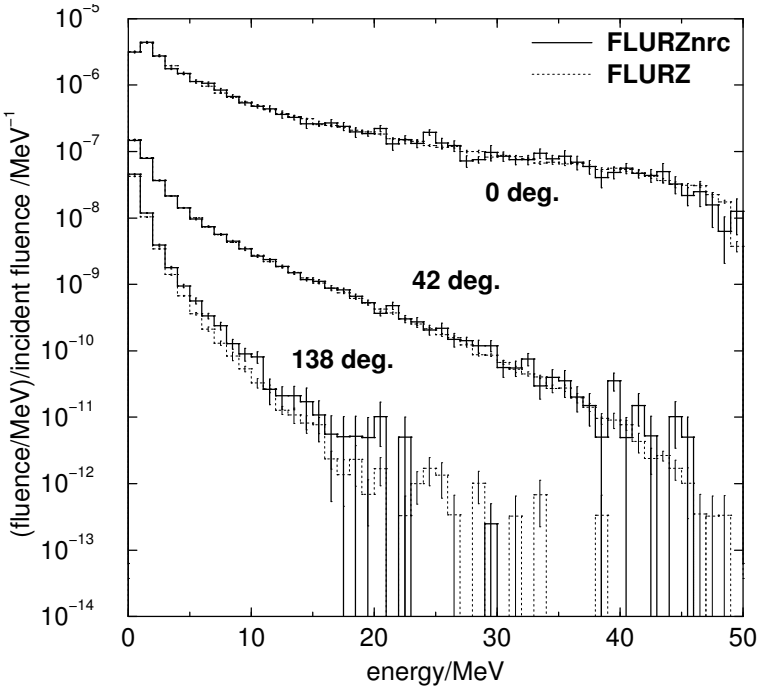

Figure 101: Photon spectra calculated for a 50 MeV beam on lead.

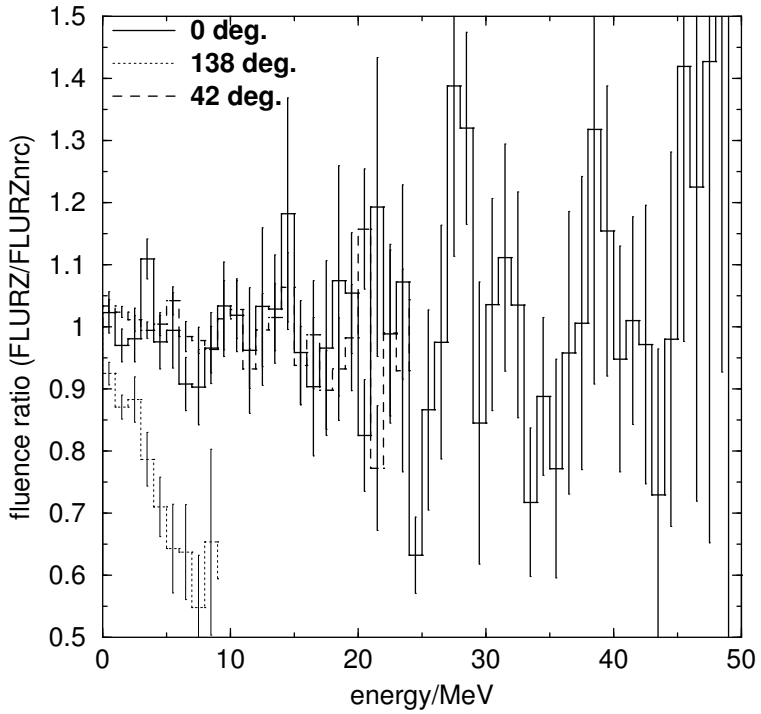

Figure 102: Ratio of FLURZ-calculated photon spectra to FLURZnrc-calculated spectra for 50 MeV beam on lead.

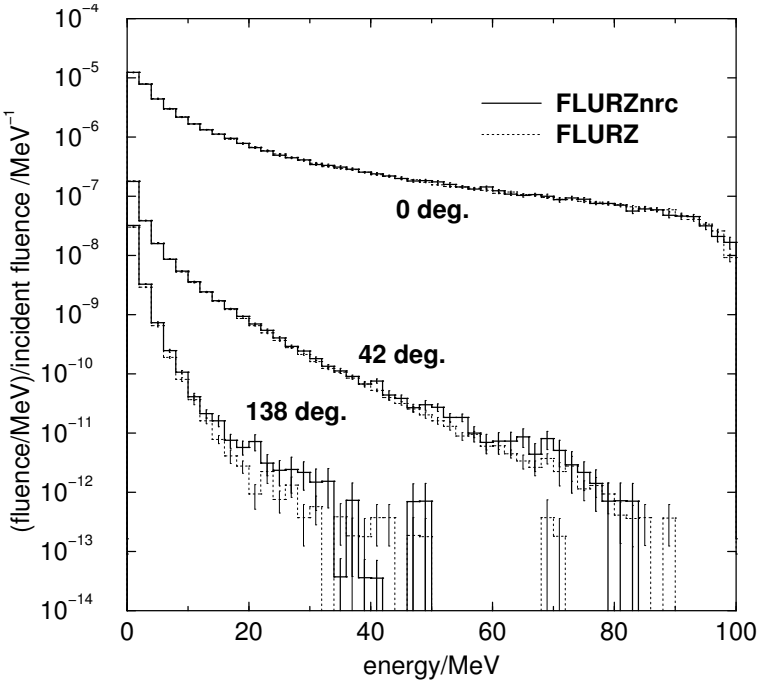

Figure 103: Photon spectra calculated for a 100 MeV beam on lead.

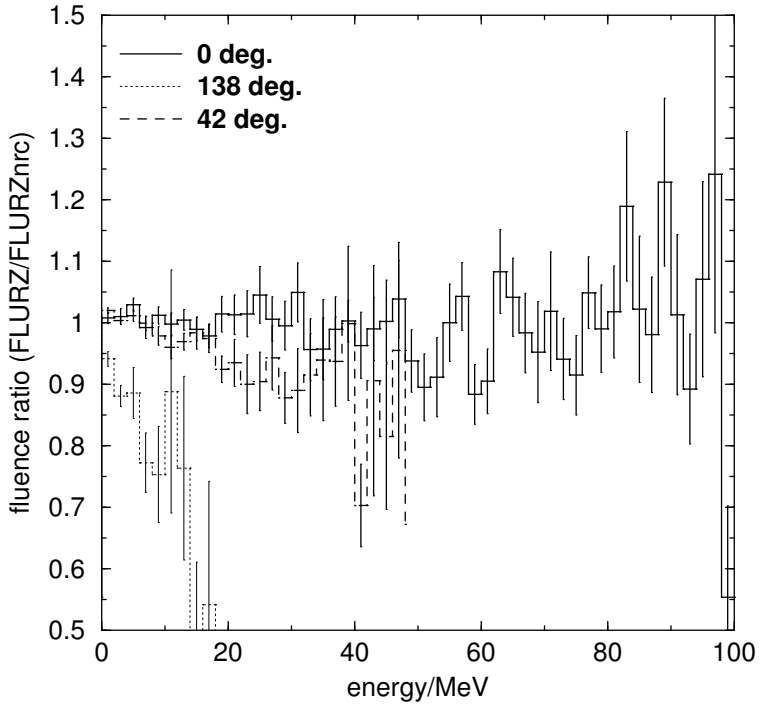

Figure 104: Ratio of FLURZ-calculated photon spectra to FLURZnrc-calculated spectra for 100 MeV beam on lead.

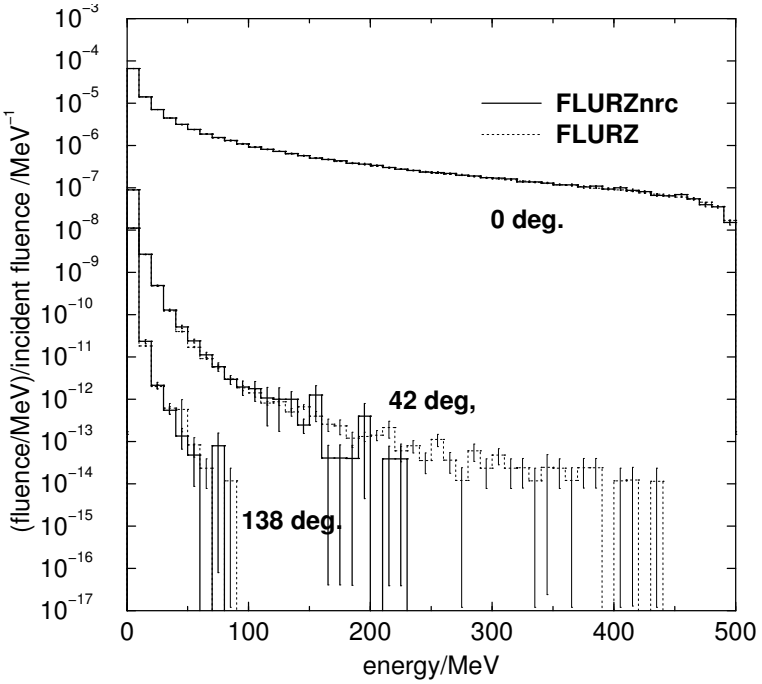

Figure 105: Photon spectra calculated for a 500 MeV beam on lead.

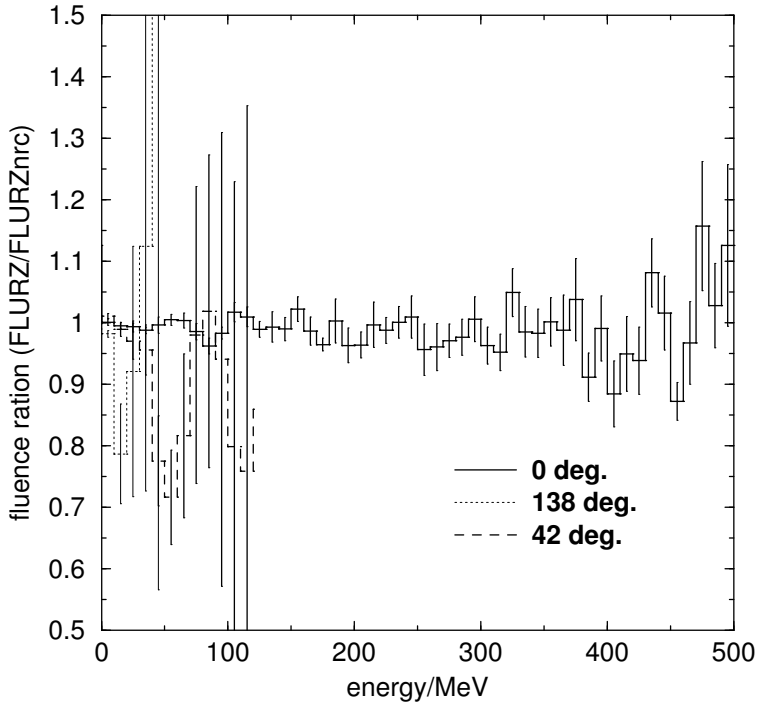

Figure 106: Ratio of FLURZ-calculated photon spectra to FLURZnrc-calculated spectra for 500 MeV beam on lead.

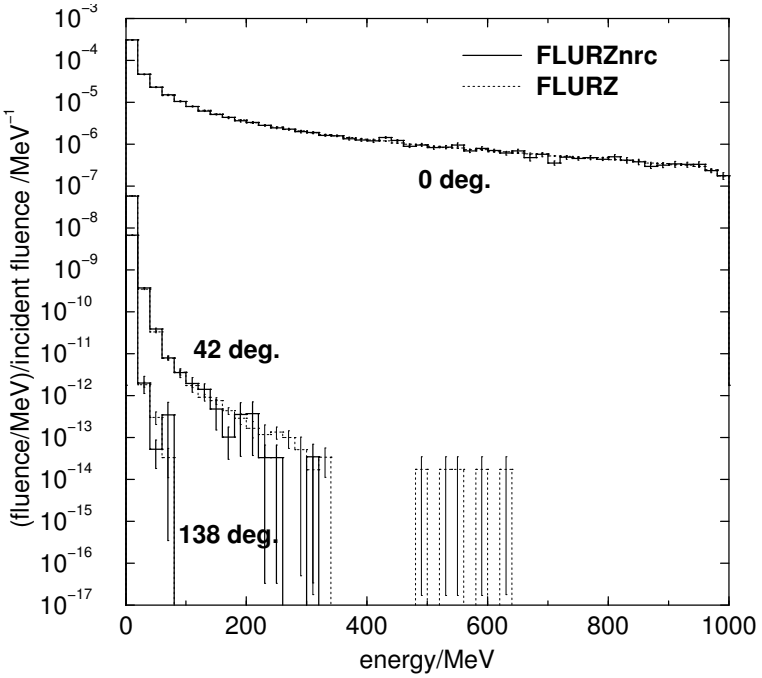

Figure 107: Photon spectra calculated for a 1 GeV beam on lead.

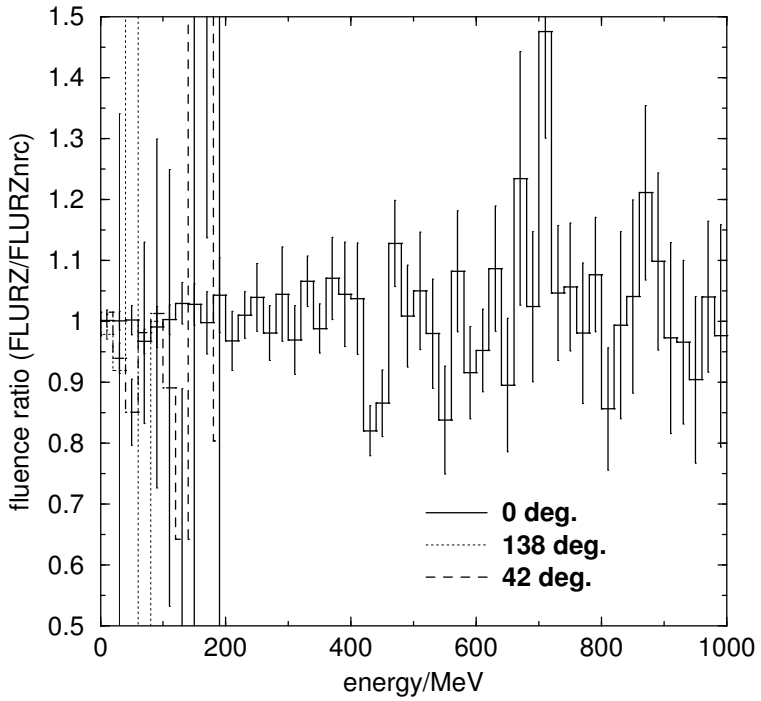

Figure 108: Ratio of FLURZ-calculated photon spectra to FLURZnrc-calculated spectra for 1 GeV beam on lead.

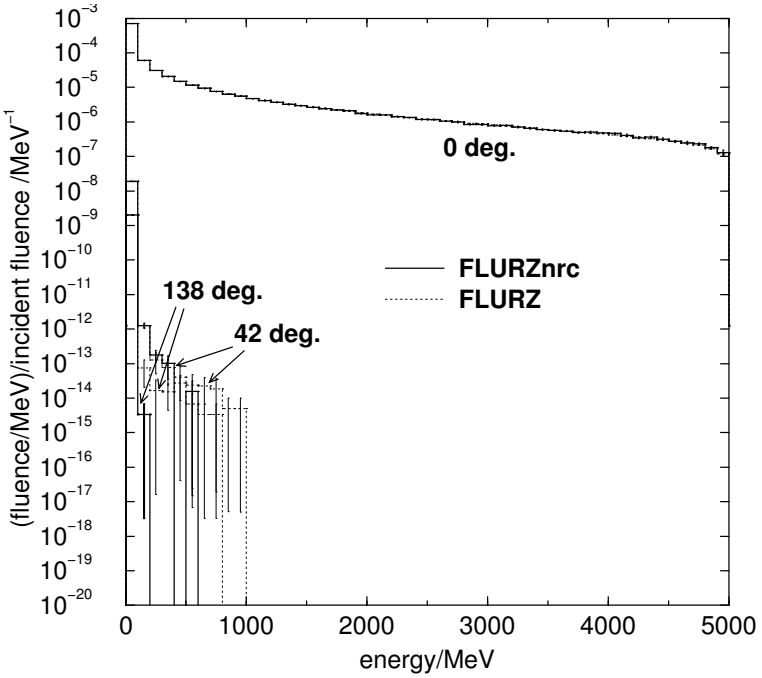

Figure 109: Photon spectra calculated for a 5 GeV beam on lead.

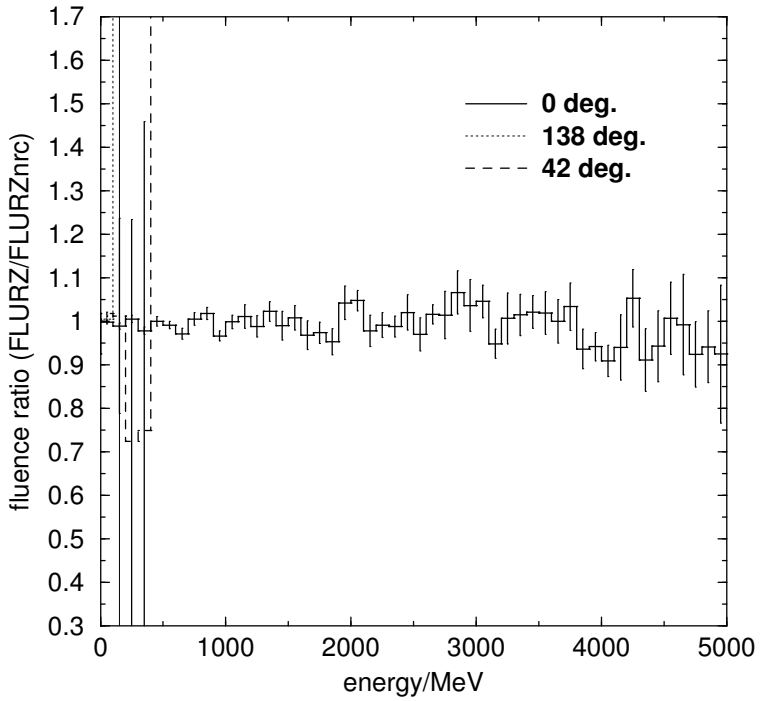

Figure 110: Ratio of FLURZ-calculated photon spectra to FLURZnrc-calculated spectra for 5 GeV beam on lead.

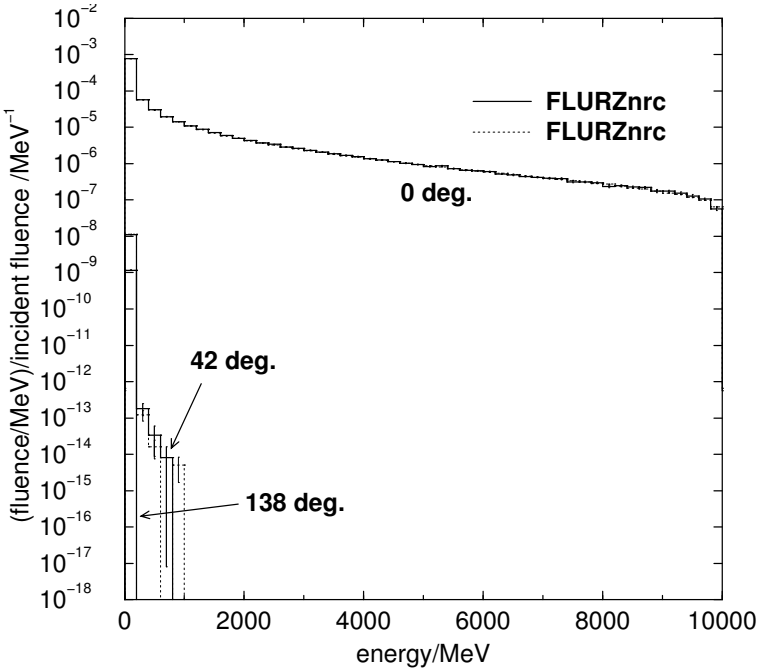

Figure 111: Photon spectra calculated for a 10 GeV beam on lead.

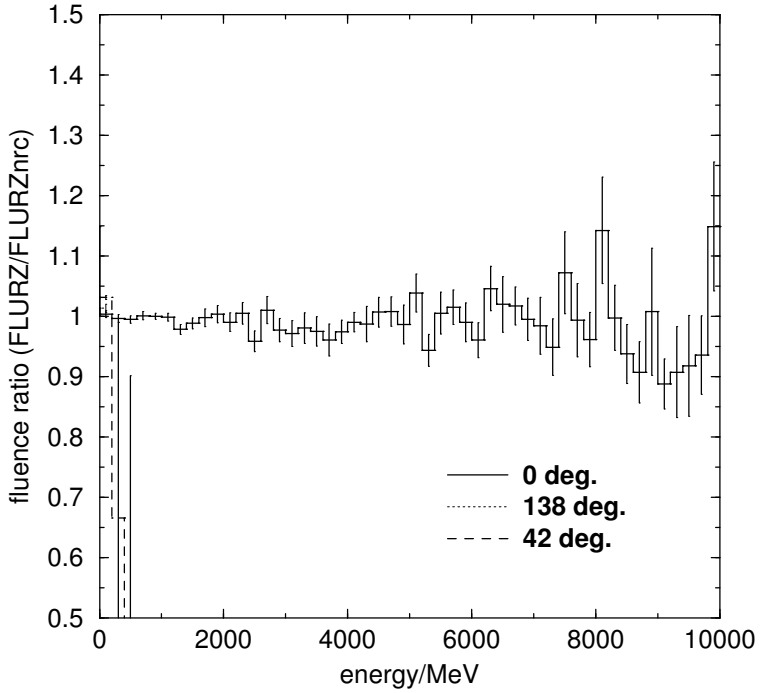

Figure 112: Ratio of FLURZ-calculated photon spectra to FLURZnrc-calculated spectra for 10 GeV beam on lead.

8.2 Results for Beryllium Target

8.2.1 Effect of Spin

Similar to lead, we studied the effect of spin on the photon spectra emanating from a beryillium target at 0, 42 and 138 degrees from the incident beam direction for a 10 MeV incident beam. Figure **??** below shows the ratio of the FLURZ-calculated photon spectra to those calculated with FLURZnrc with spin effects off. The fact that the spectra do not differ significantly is an indication that spin effects account for most significant differences between the FLURZ and FLURZnrc photon spectra.

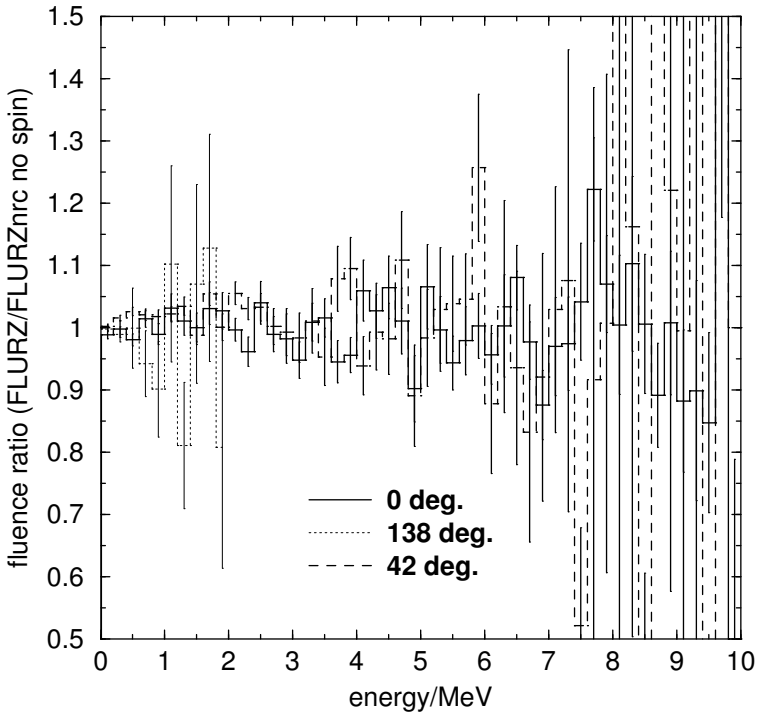

Figure 113: Ratio of FLURZ-calculated photon spectra to FLURZnrc-calculated spectra with no spin effects for 10 MeV beam on beryllium.

8.2.2 Overall Results

The figures below show the photon spectra emanating from a beryllium target at 0, 42 and 138 degrees from the incident beam direction for all energies as calculated using FLURZ and FLURZnrc. Also shown are the ratios of the FLURZ-calculated spectra to those calculated using FLURZnrc.

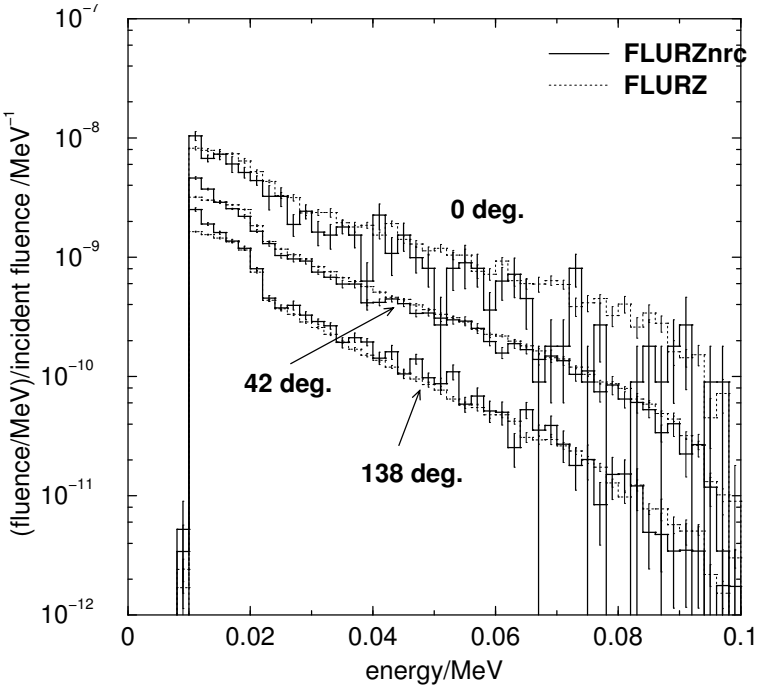

Figure 114: Photon spectra calculated for a 100 keV beam on beryllium.

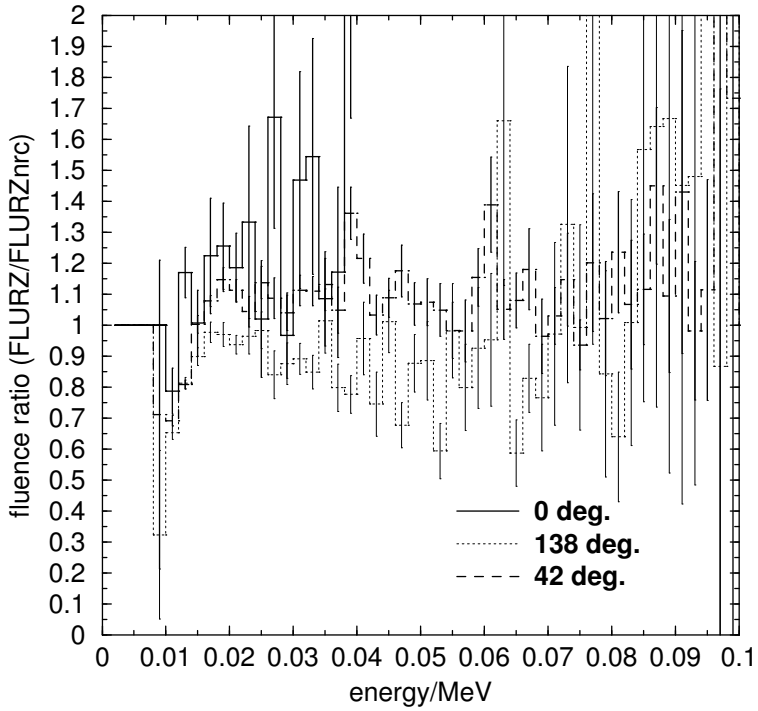

Figure 115: Ratio of FLURZ-calculated photon spectra to FLURZnrc-calculated spectra for 100 keV beam on beryllium.

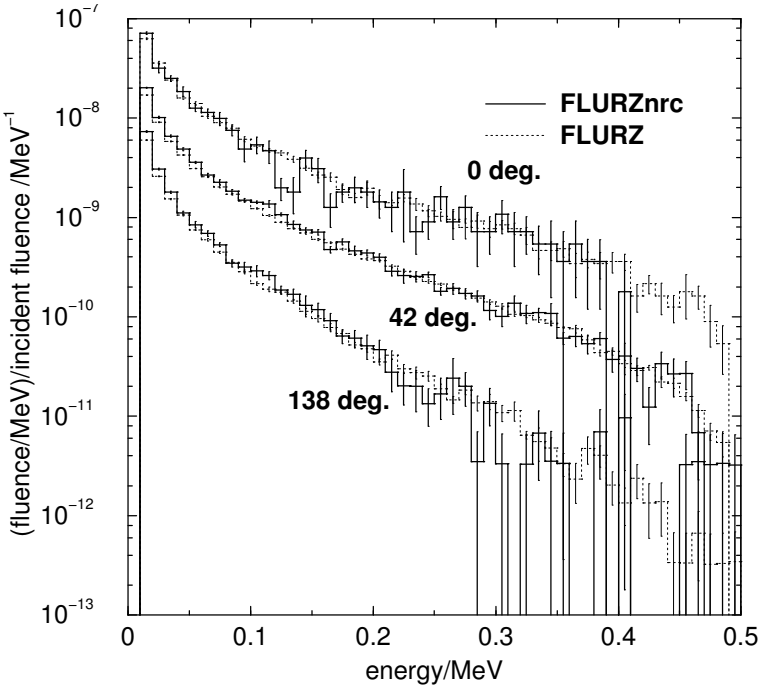

Figure 116: Photon spectra calculated for a 500 keV beam on beryllium.

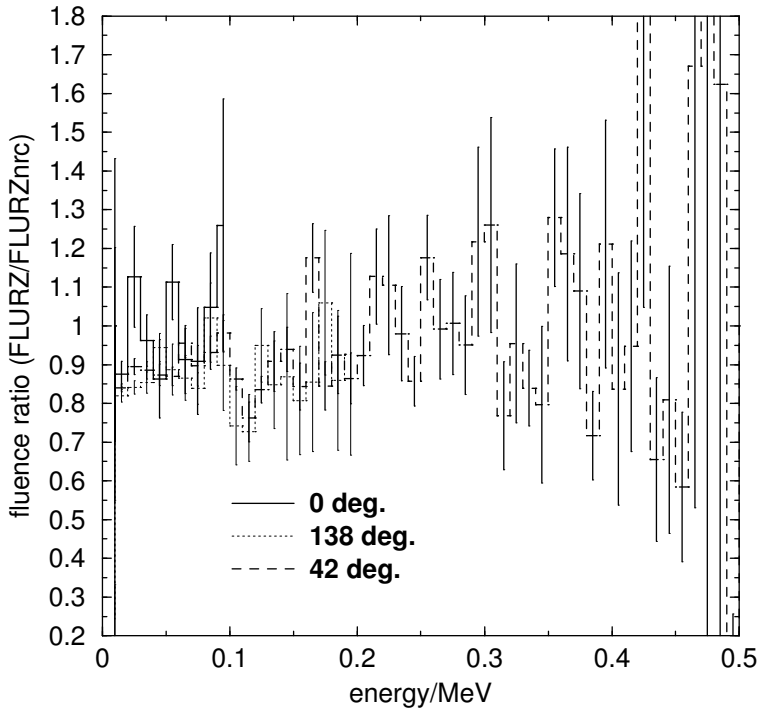

Figure 117: Ratio of FLURZ-calculated photon spectra to FLURZnrc-calculated spectra for 500 keV beam on beryllium.

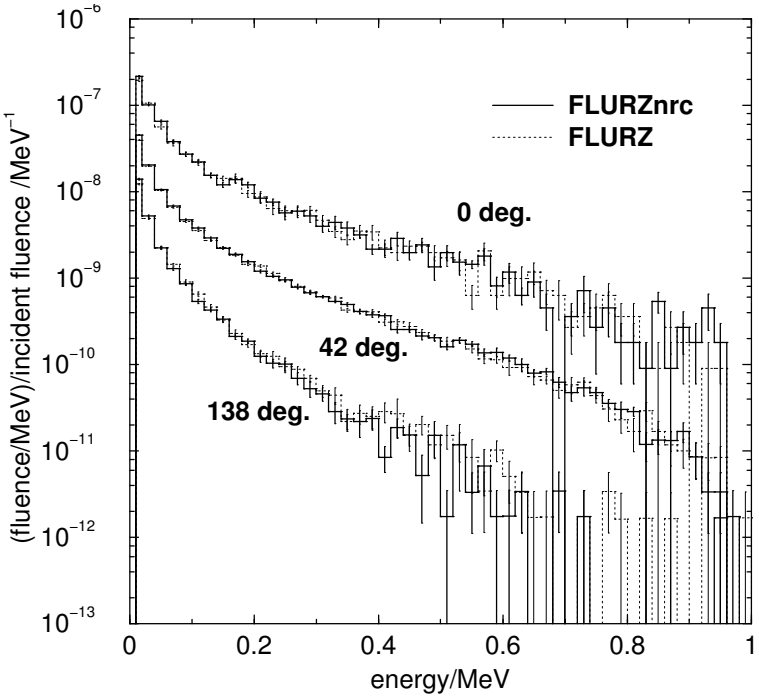

Figure 118: Photon spectra calculated for a 1 MeV beam on beryllium.

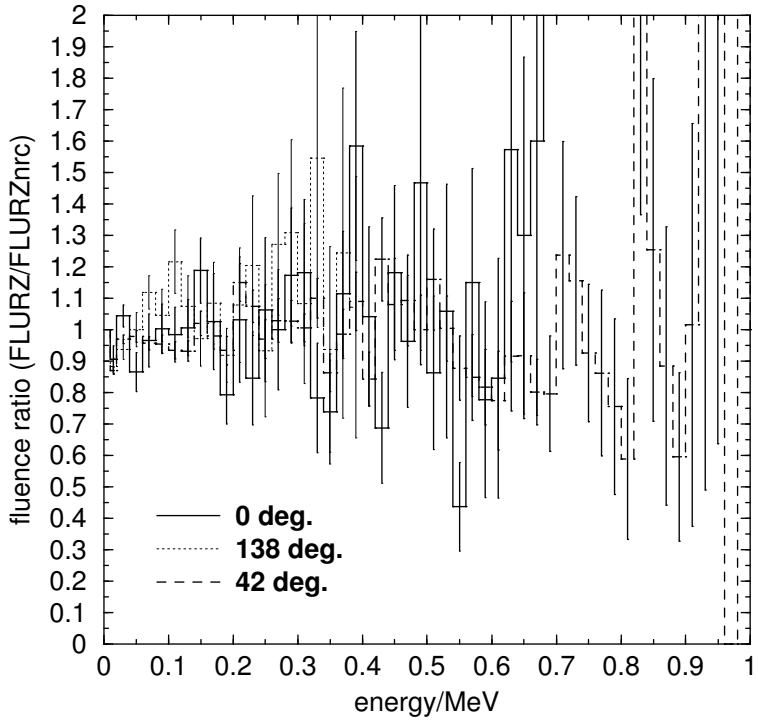

Figure 119: Ratio of FLURZ-calculated photon spectra to FLURZnrc-calculated spectra for 1 MeV beam on beryllium.

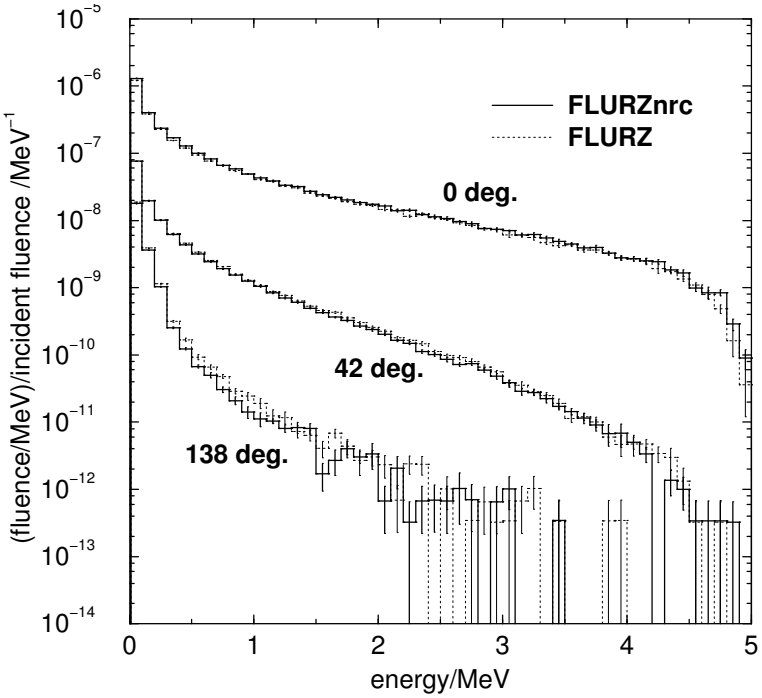

Figure 120: Photon spectra calculated for a 5 MeV beam on beryllium.

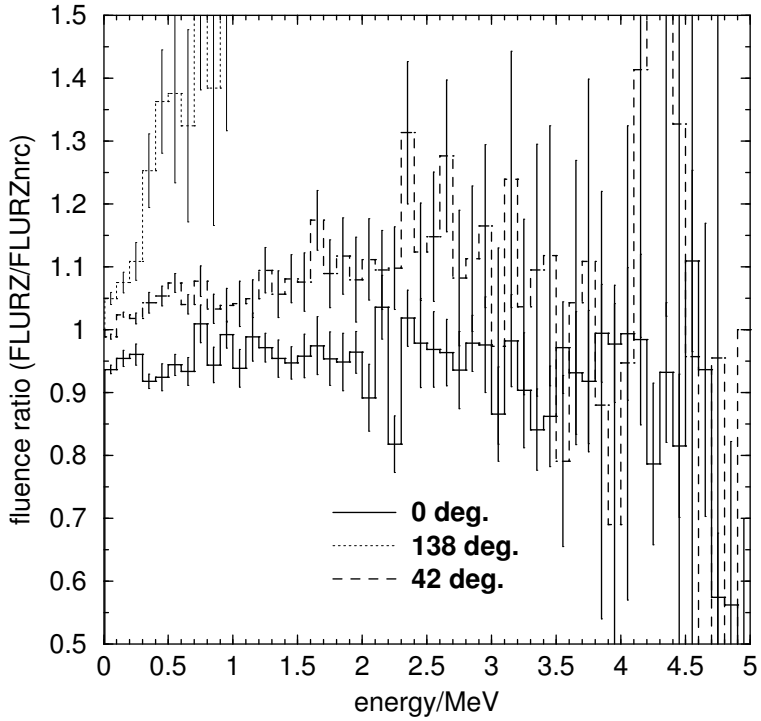

Figure 121: Ratio of FLURZ-calculated photon spectra to FLURZnrc-calculated spectra for 5 MeV beam on beryllium.

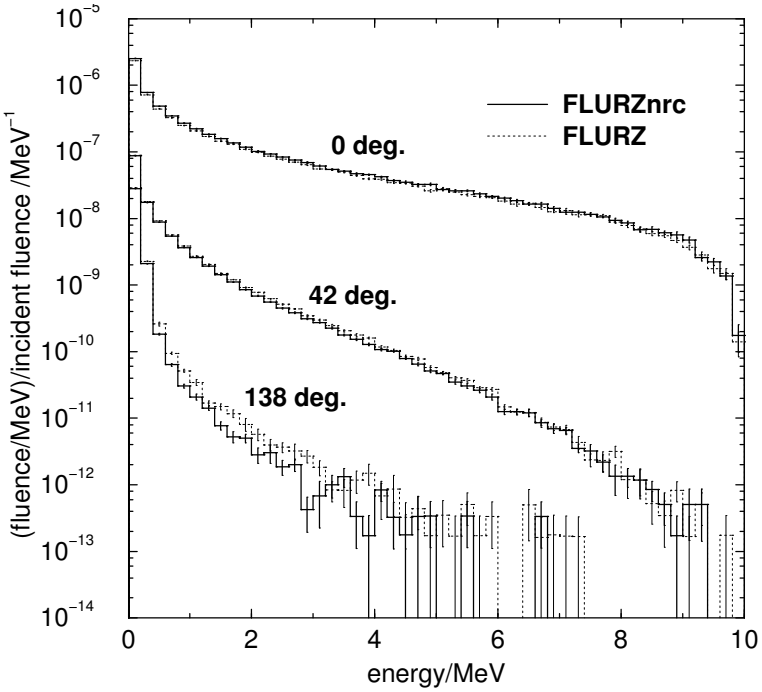

Figure 122: Photon spectra calculated for a 10 MeV beam on beryllium.

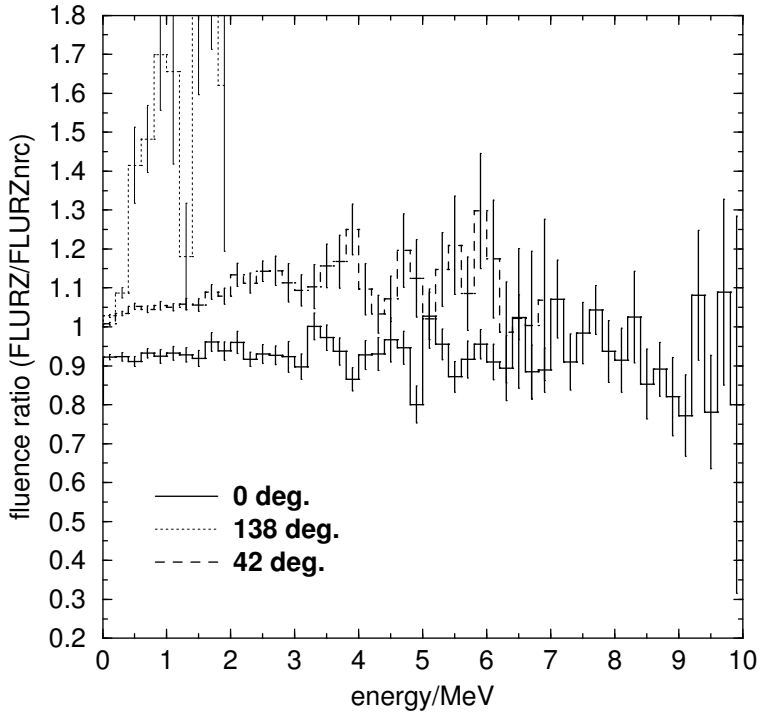

Figure 123: Ratio of FLURZ-calculated photon spectra to FLURZnrc-calculated spectra for 10 MeV beam on beryllium.

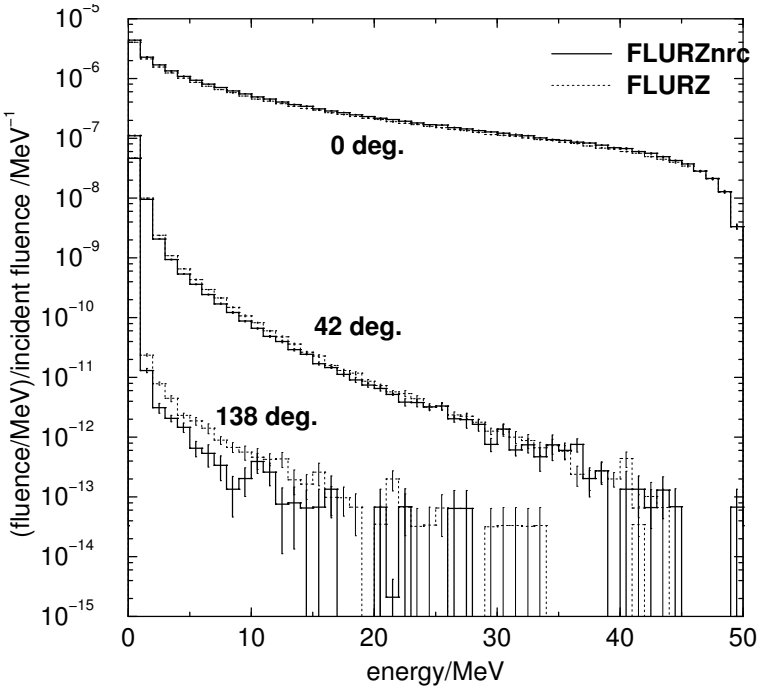

Figure 124: Photon spectra calculated for a 50 MeV beam on beryllium.

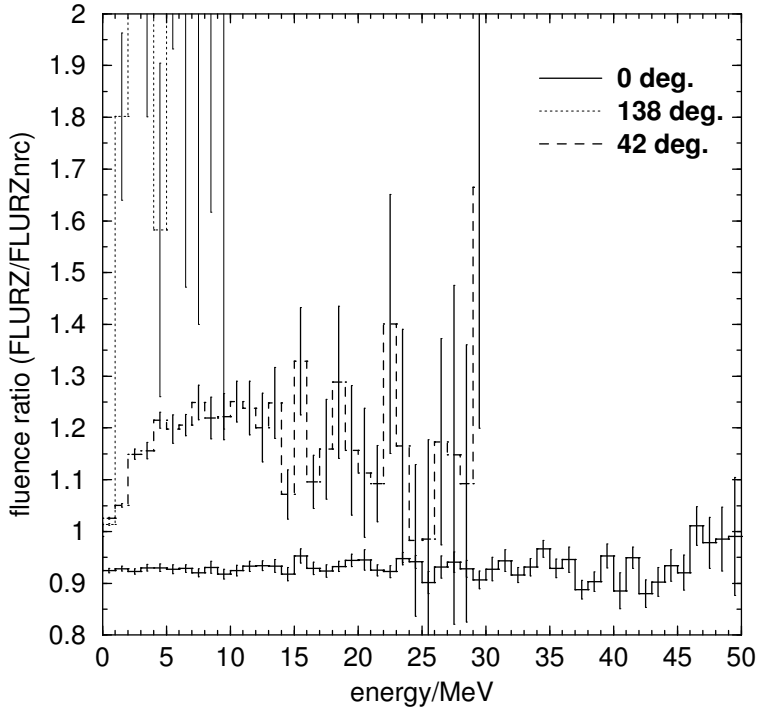

Figure 125: Ratio of FLURZ-calculated photon spectra to FLURZnrc-calculated spectra for 50 MeV beam on beryllium.

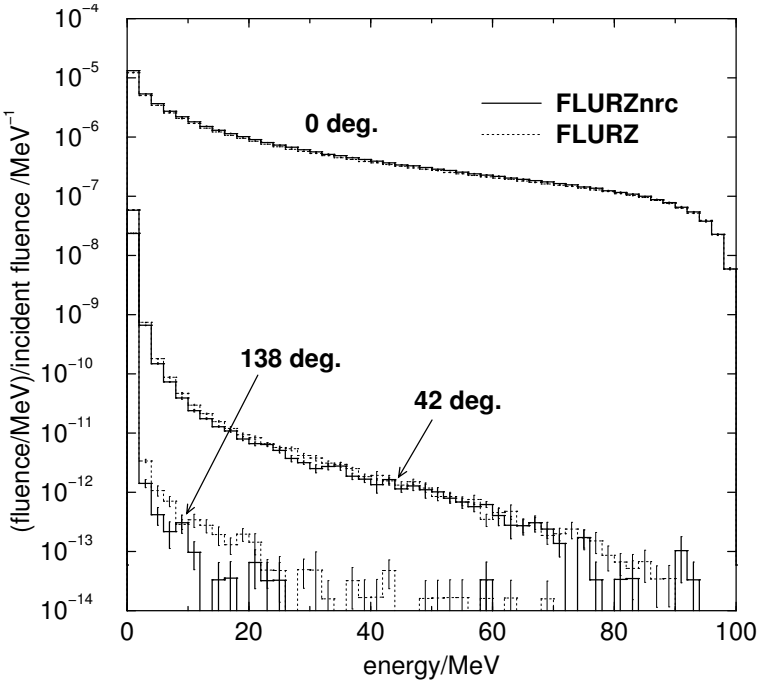

Figure 126: Photon spectra calculated for a 100 MeV beam on beryllium.

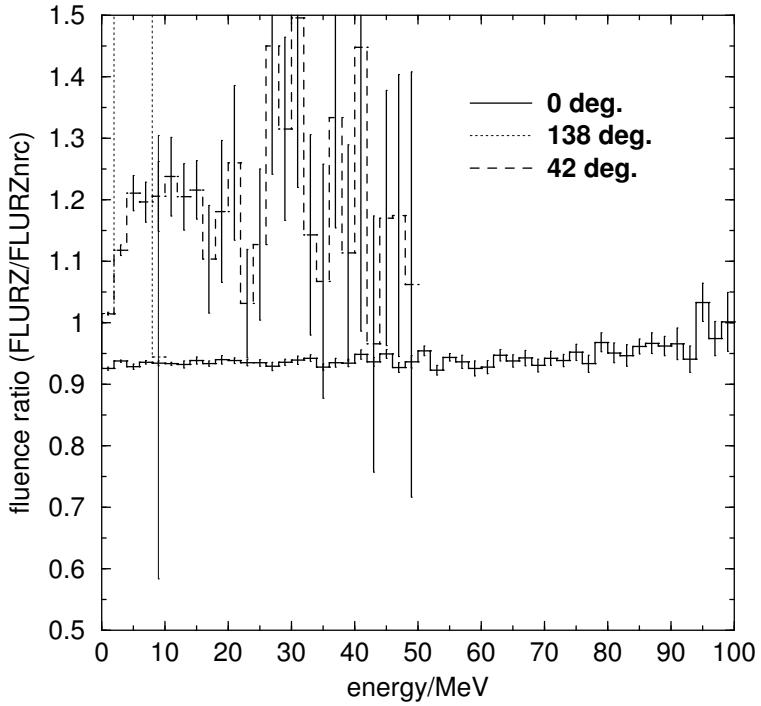

Figure 127: Ratio of FLURZ-calculated photon spectra to FLURZnrc-calculated spectra for 100 MeV beam on beryllium.

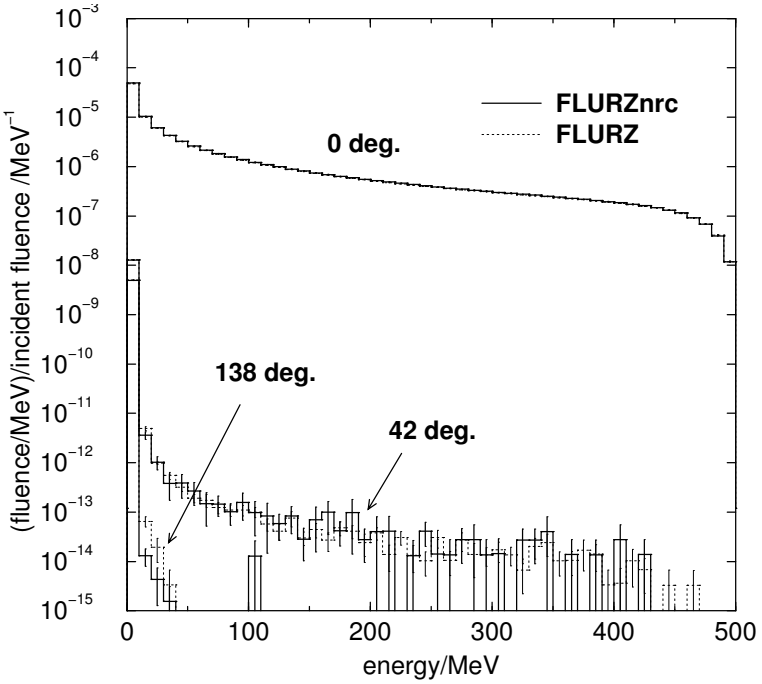

Figure 128: Photon spectra calculated for a 500 MeV beam on beryllium.

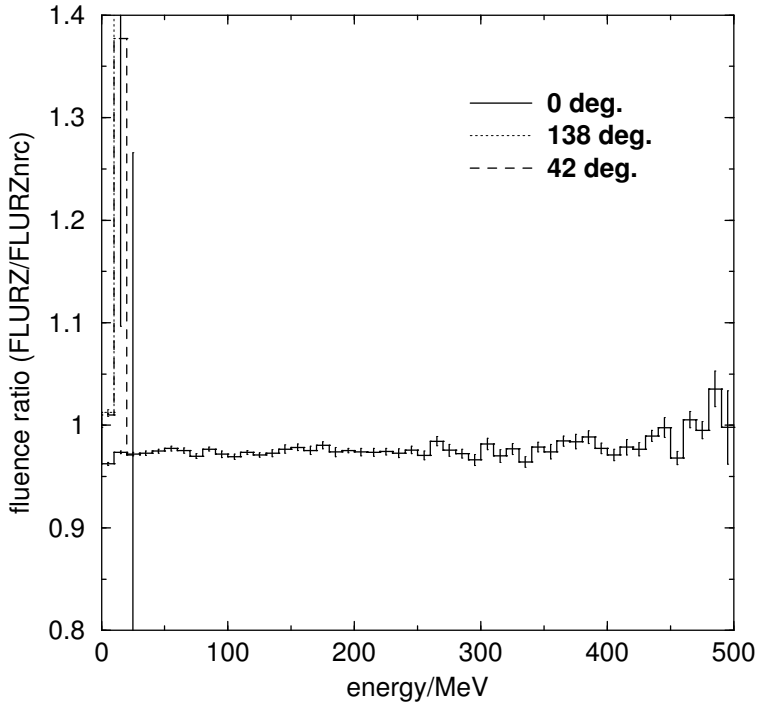

Figure 129: Ratio of FLURZ-calculated photon spectra to FLURZnrc-calculated spectra for 500 MeV beam on beryllium.

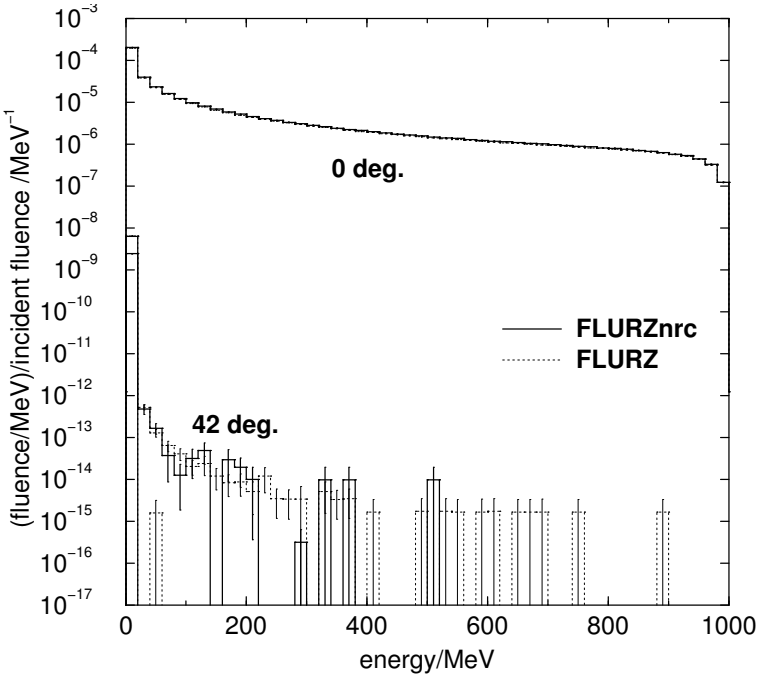

Figure 130: Photon spectra calculated for a 1 GeV beam on beryllium.

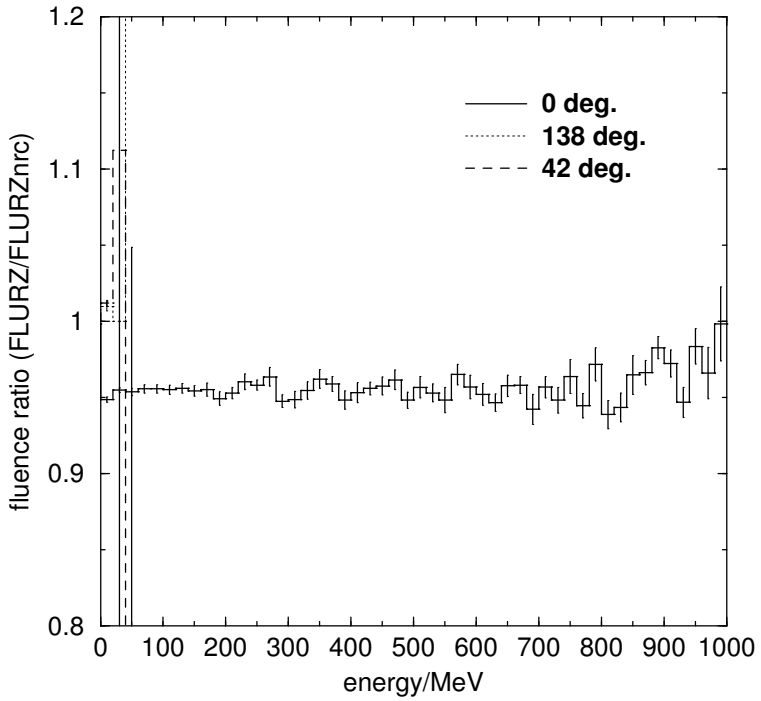

Figure 131: Ratio of FLURZ-calculated photon spectra to FLURZnrc-calculated spectra for 1 GeV beam on beryllium.

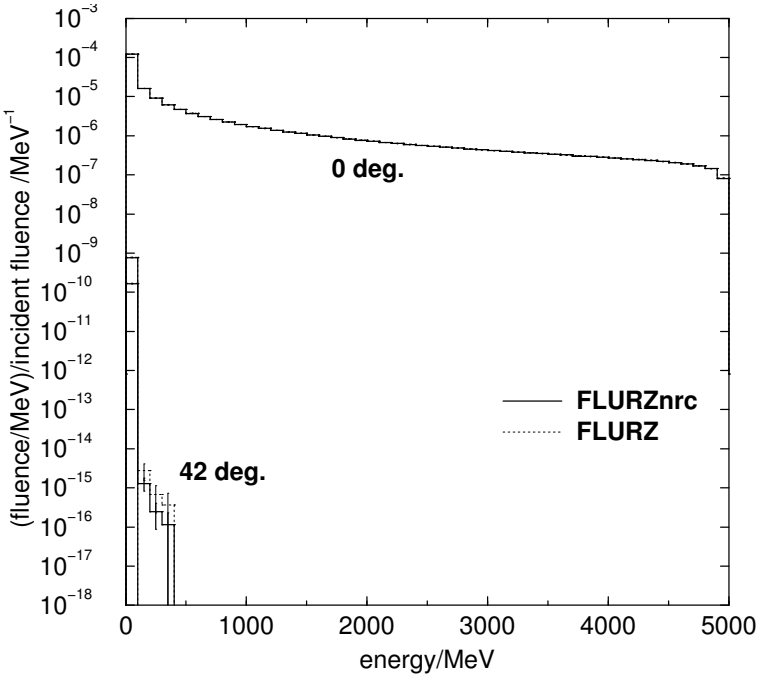

Figure 132: Photon spectra calculated for a 5 GeV beam on beryllium.

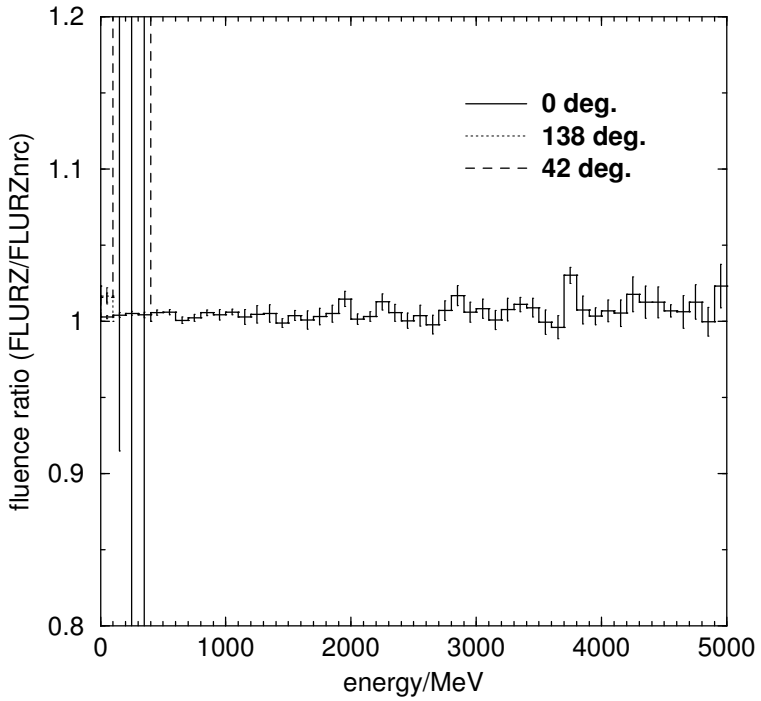

Figure 133: Ratio of FLURZ-calculated photon spectra to FLURZnrc-calculated spectra for 5 GeV beam on beryllium.

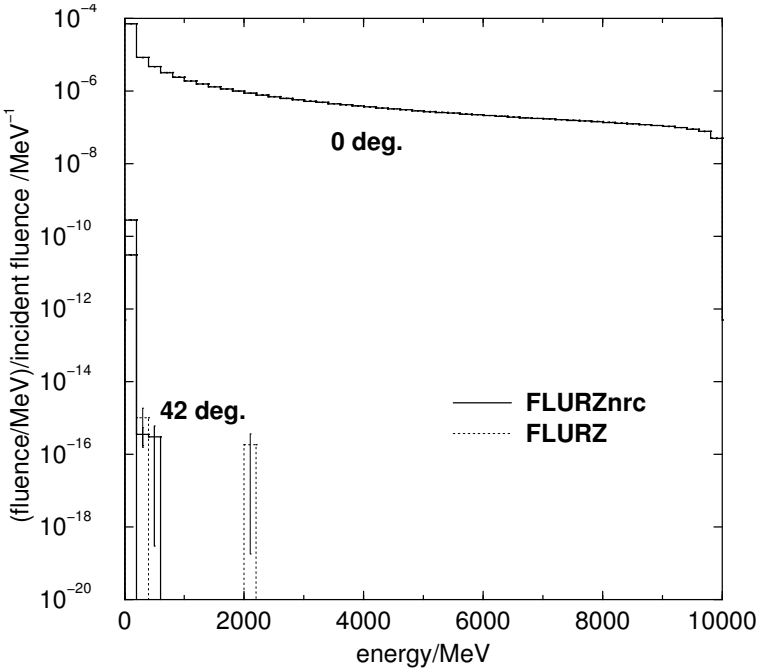

Figure 134: Photon spectra calculated for a 10 GeV beam on beryllium.

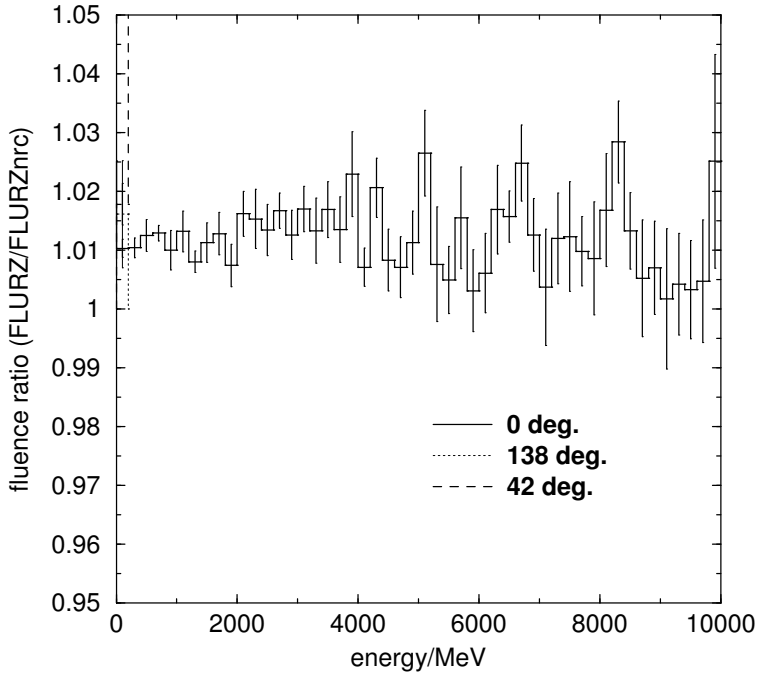

Figure 135: Ratio of FLURZ-calculated photon spectra to FLURZnrc-calculated spectra for 10 GeV beam on beryllium.

9 Stopping Power Ratios

Using SPRRZ and SPRRZnrc, we calculated stopping power ratio of water to air ($SPR_{air}^{H_2O}$) as a function of depth for broad parallel electron beams of energy 4, 5, 8, 10, 15, 20, 30, 40 and 50 MeV. Figures **??-??** below show the ratio of $SPR_{air}^{H_2O}$ calculated using SPRRZ to $SPR_{air}^{H_2O}$ calculated using SPRRZnrc as a function of depth for all beam energies.

In addition we calculated the $SPR_{air}^{graphite}$ for a ^{60}Co beam (parallel beam, radius 0.5 cm) incident on a graphite cylinder with radius 0.5 cm and depth 0.3 cm. Results for SPRRZ and SPRRZnrc are summarized in Table **??** below.

Table 6: $SPR_{air}^{graphite}$ calculated using SPRRZ and SPRRZnrc for a parallel ^{60}Co beam of radius 0.5 cm incident on a graphite cylinder of radius 0.5 cm and thickness 0.3 cm. The "active" volume for which $SPR_{air}^{graphite}$ is shown is a sub-cylinder of radius 0.25 cm and depth 0.15 cm with its front surface flush with the front of the larger cylinder in which it is contained.

$SPR_{air}^{graphite}$	
SPRRZnrc	SPRRZ
0.9989(1)	0.9993(1)

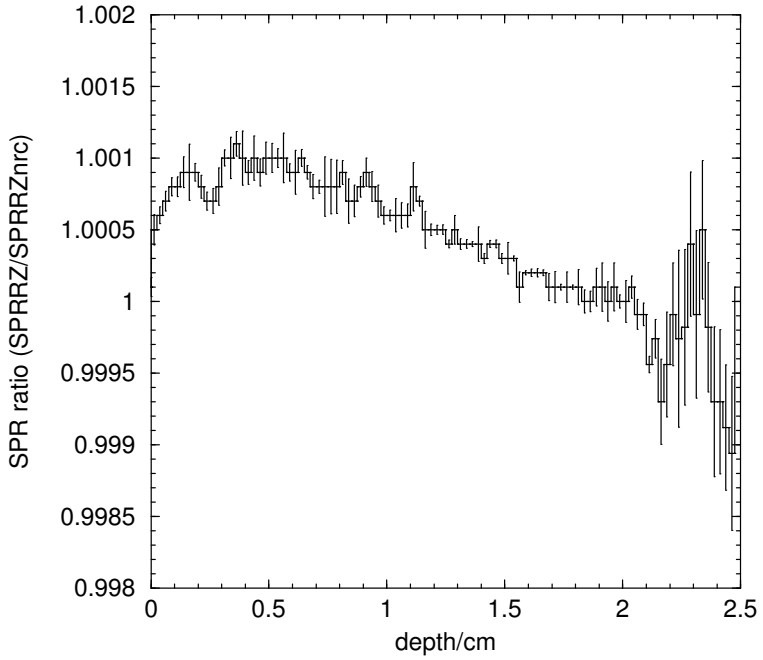

Figure 136: Ratio of $SPR_{air}^{H_2O}$ calculated with SPRRZ to $SPR_{air}^{H_2O}$ calculated with SPRRZnrc vs depth for a 4 MeV broad parallel beam.

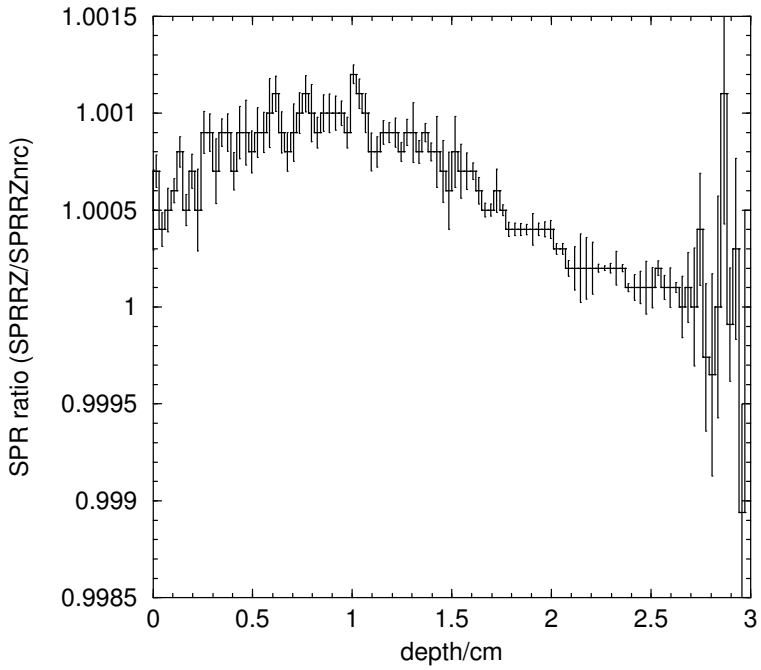

Figure 137: Ratio of $SPR_{air}^{H_2O}$ calculated with SPRRZ to $SPR_{air}^{H_2O}$ calculated with SPRRZnrc vs depth for a 5 MeV broad parallel beam.

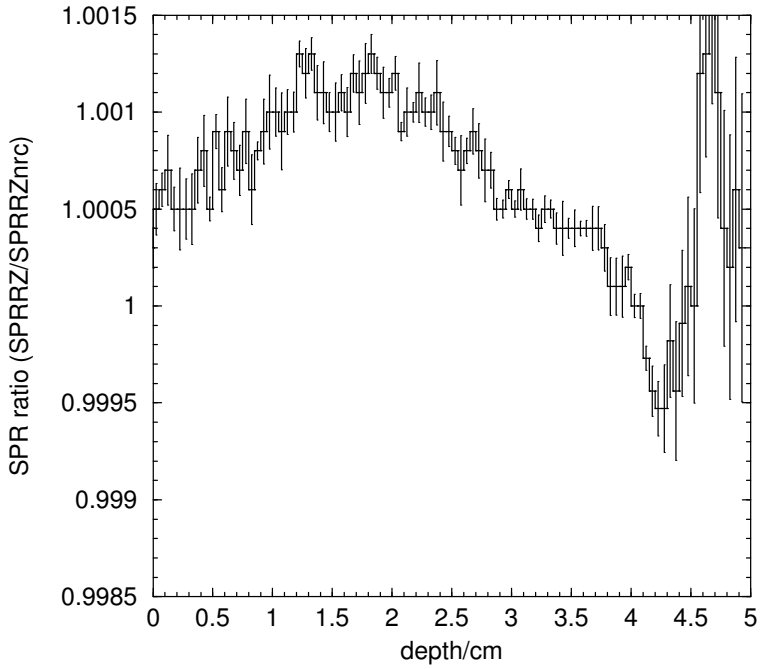

Figure 138: Ratio of $SPR_{air}^{H_2O}$ calculated with SPRRZ to $SPR_{air}^{H_2O}$ calculated with SPRRZnrc vs depth for a 8 MeV broad parallel beam.

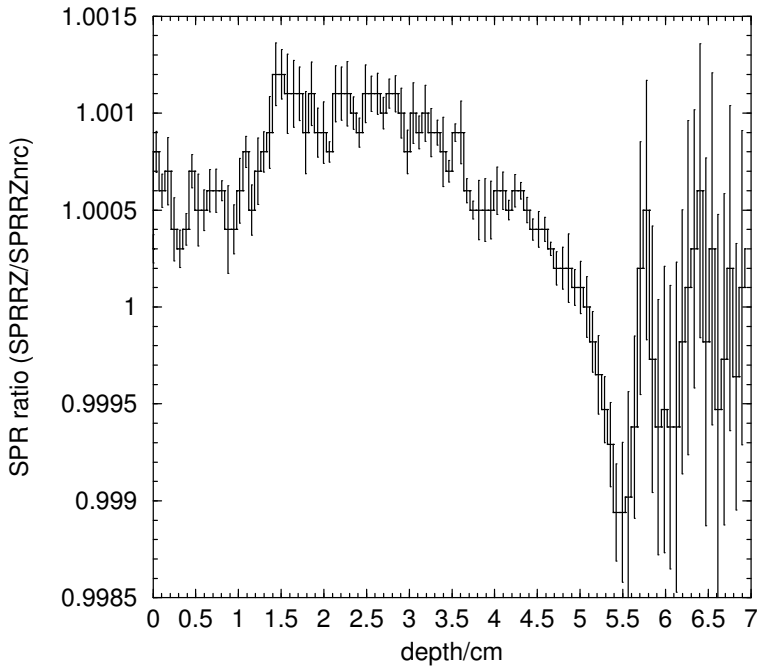

Figure 139: Ratio of $\mathrm{SPR}_{air}^{H_2O}$ calculated with SPRRZ to $\mathrm{SPR}_{air}^{H_2O}$ calculated with SPRRZnrc vs depth for a 10 MeV broad parallel beam.

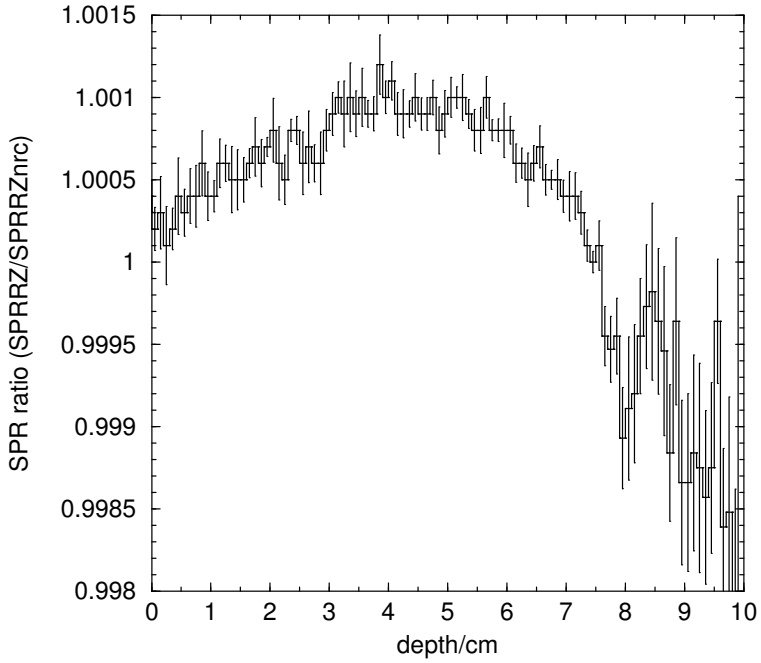

Figure 140: Ratio of $\mathrm{SPR}_{air}^{H_2O}$ calculated with SPRRZ to $\mathrm{SPR}_{air}^{H_2O}$ calculated with SPRRZnrc vs depth for a 15 MeV broad parallel beam.

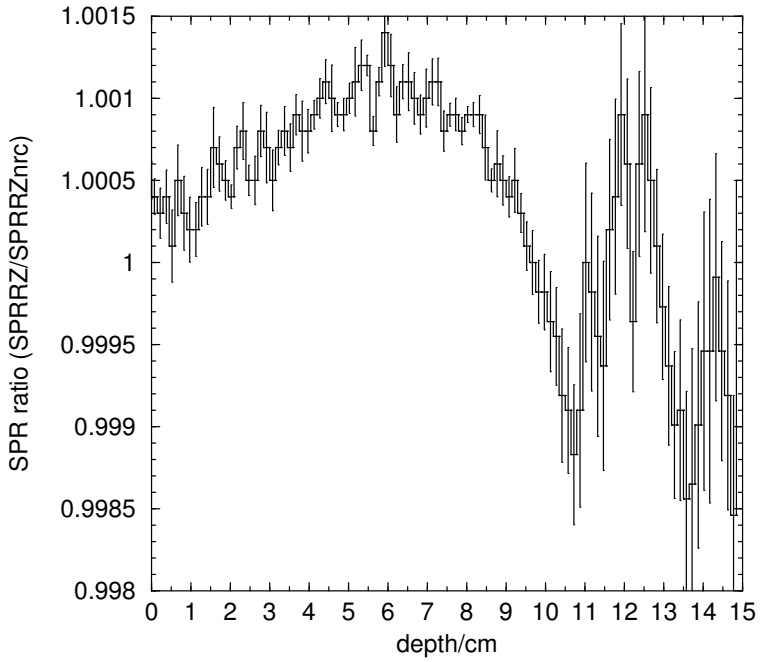

Figure 141: Ratio of $\mathrm{SPR}_{air}^{H_2O}$ calculated with SPRRZ to $\mathrm{SPR}_{air}^{H_2O}$ calculated with SPRRZnrc vs depth for a 20 MeV broad parallel beam.

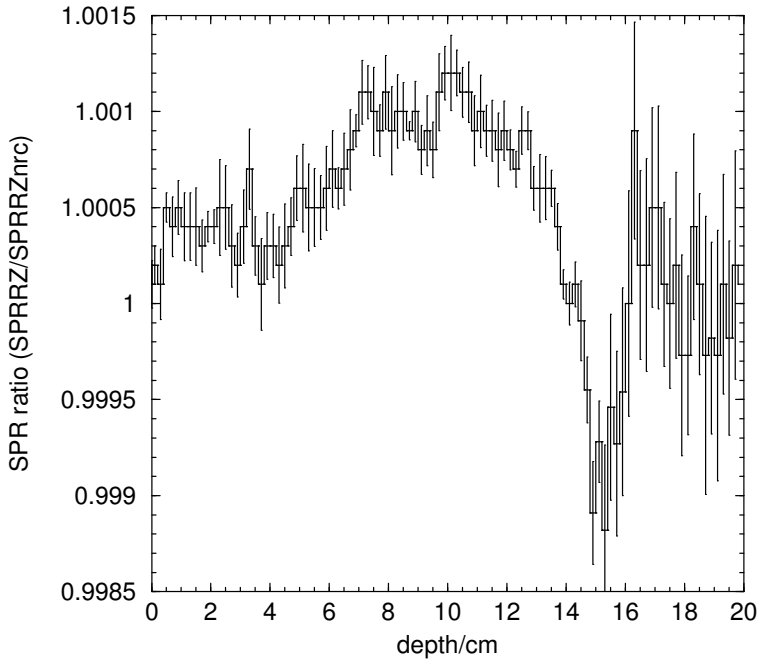

Figure 142: Ratio of $\mathrm{SPR}_{air}^{H_2O}$ calculated with SPRRZ to $\mathrm{SPR}_{air}^{H_2O}$ calculated with SPRRZnrc vs depth for a 30 MeV broad parallel beam.

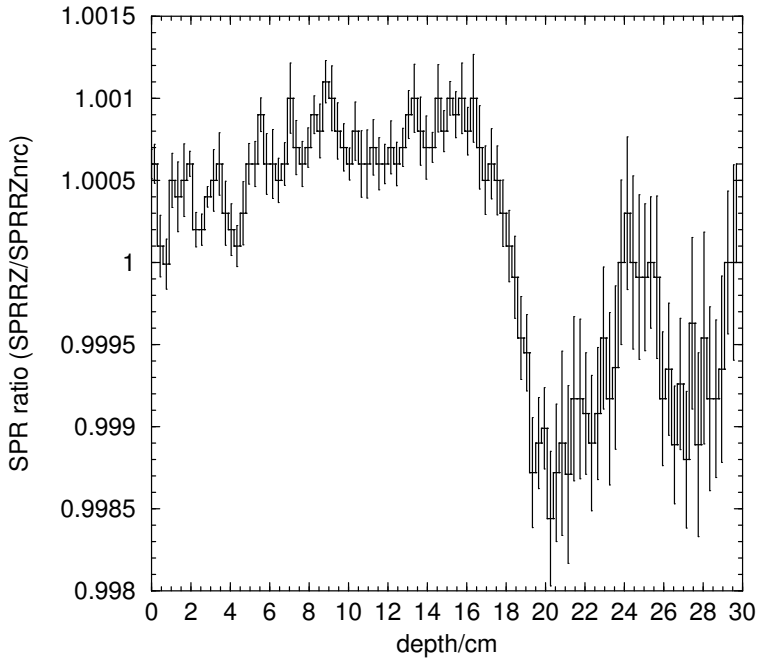

Figure 143: Ratio of $\mathrm{SPR}_{air}^{H_2O}$ calculated with SPRRZ to $\mathrm{SPR}_{air}^{H_2O}$ calculated with SPRRZnrc vs depth for a 40 MeV broad parallel beam.

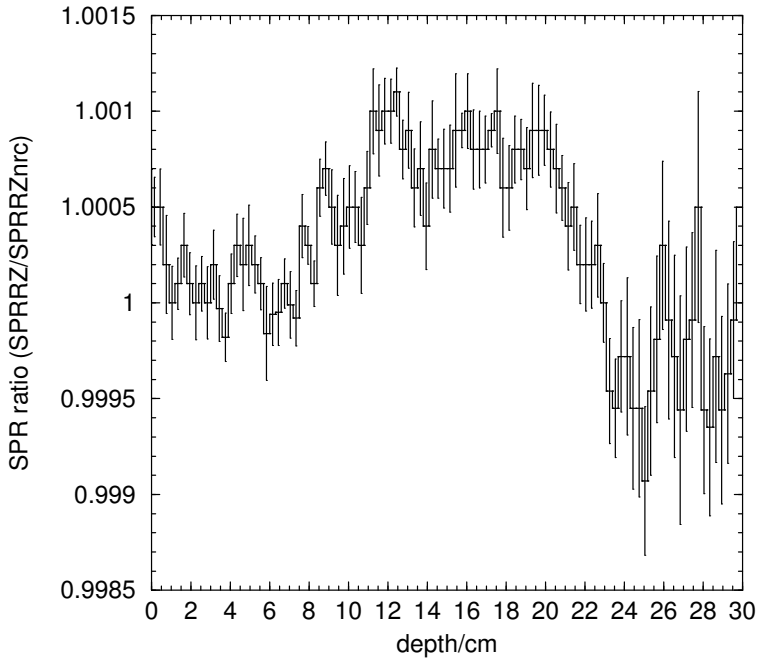

Figure 144: Ratio of $\mathrm{SPR}_{air}^{H_2O}$ calculated with SPRRZ to $\mathrm{SPR}_{air}^{H_2O}$ calculated with SPRRZnrc vs depth for a 50 MeV broad parallel beam.

10 QA of Variance Reduction Options

We tested the variance reduction options (range rejection, bremsstrahlung splitting, charged particle Russian Roulette and photon forcing) in various combinations using the DOSRZnrc code and compared the results to those with all variance reduction options off.

The geometry used in the testing is shown in Figure **??** below.

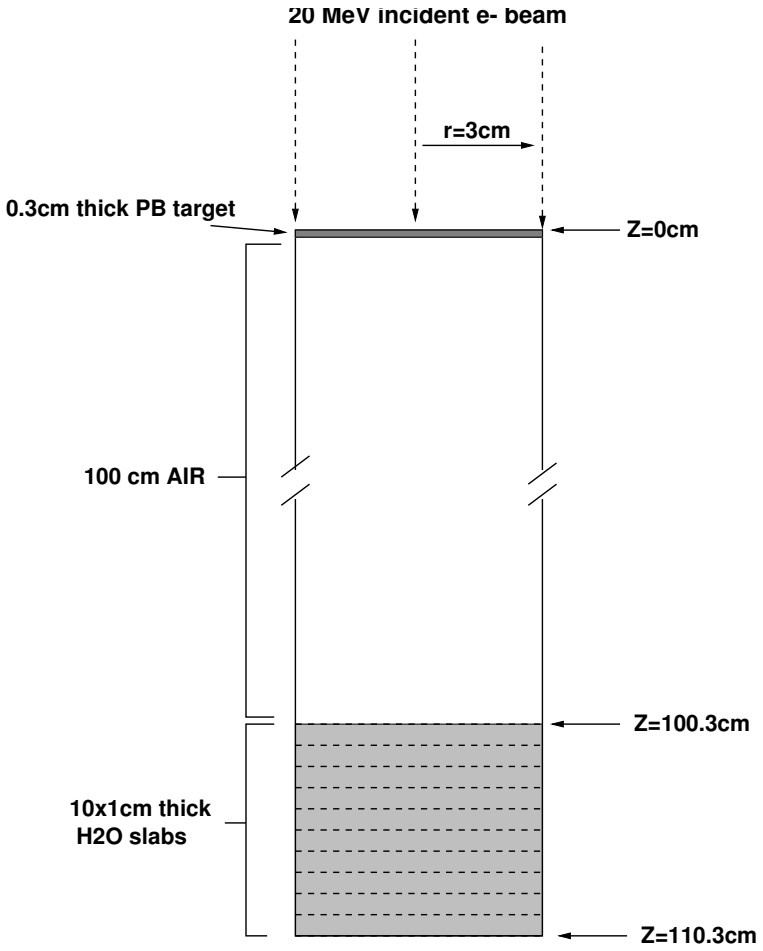

Figure 145: The geometry used for testing various of combinations of variance reduction options. Of primary interest was the depth dose curve in the water starting at Z=100.3 cm.

Figure **??** below show the ratios of the depth-dose curves in the water (starting at Z=100.3 cm) with indicated variance reduction options on to that with all options off.

Since FLURZnrc uses a different photon forcing scheme from DOSRZnrc, we also wanted to perform a quick QA of photon forcing in FLURZnrc. We used the geometry shown in Figure **??** and calculated the ratio of photon and electron fluence in the water with photon forcing on (with no other variance reduction options) to the photon and electron fluence with photon forcing off. The photon and electron fluence ratios vs depth are shown in Figure **??** below.

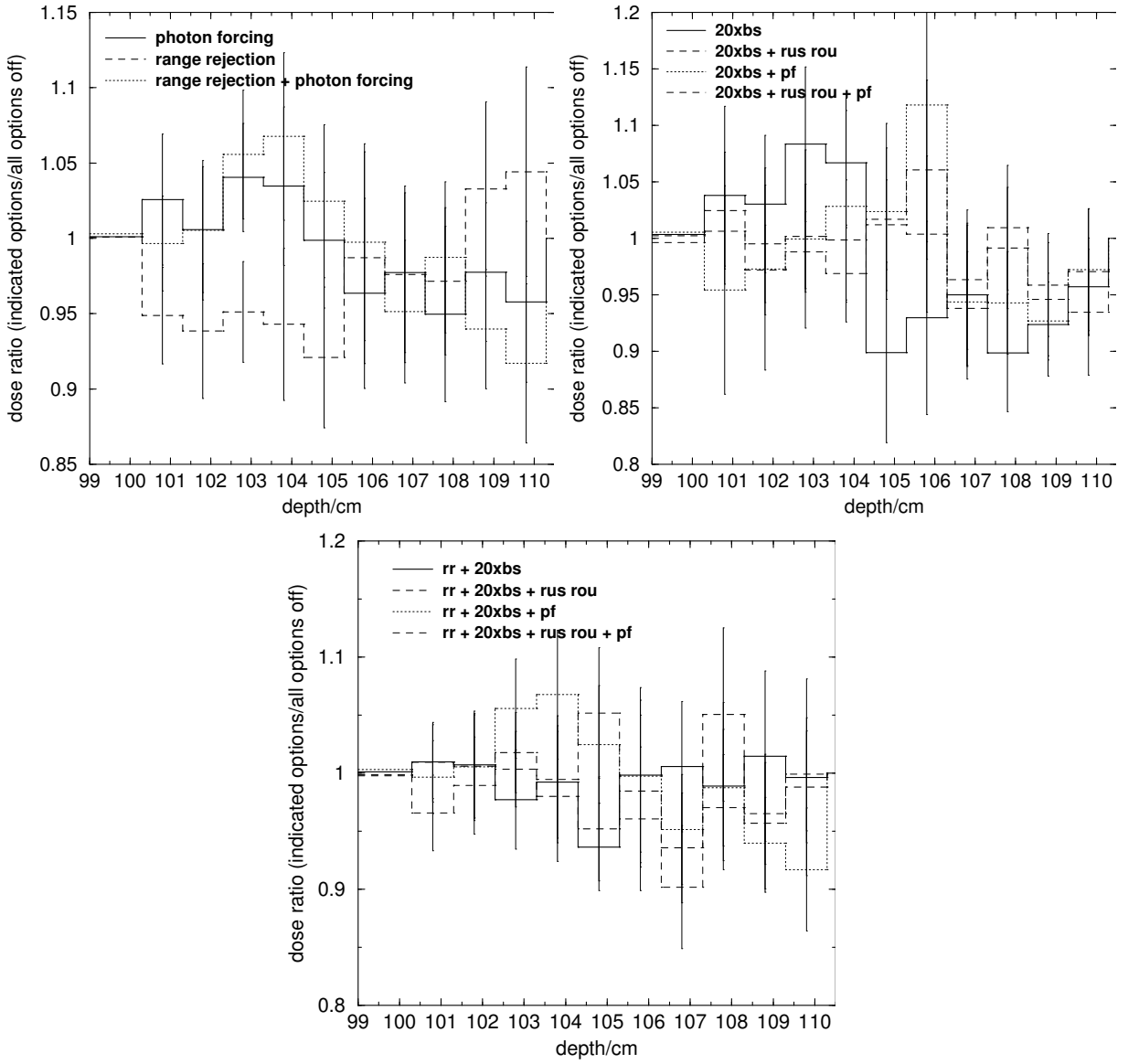

Figure 146: Ratio of depth dose curves in water with indicated variance reduction options on to the depth dose curve with no variance reduction options on. rr=range rejection (ESAVE=3 MeV), 20xbs=20 times bremsstrahlung splitting, rus rou=charged particle Russian Roulette, pf=photon forcing.

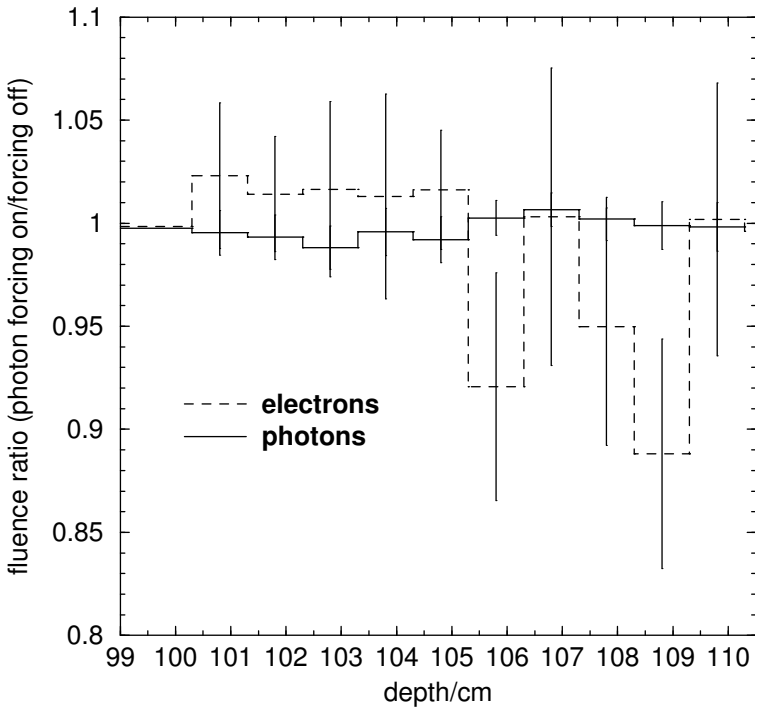

Figure 147: Ratio of photon and electron fluence in water calculated using FLURZnrc with photon forcing on (no other variance reduction options) to photon and electron fluence calculated with photon forcing off as a function of depth.

11 References